Order Number 8809941

Lateral effects in controlled source audiomagnetotellurics

MacInnes, Scott Charles, Ph.D.

The University of Arizona, 1988

U·M·I
300 N. Zeeb Rd.
Ann Arbor, MI 48106

LATERAL EFFECTS IN CONTROLLED SOURCE AUDIOMAGNETOTELLURICS

by

Scott Charles MacInnes

A Dissertation Submitted to the Faculty of the

DEPARTMENT OF GEOSCIENCES

In Partial Fulfillment of the Requirements

For the Degree of

DOCTOR OF PHILOSOPHY

In the Graduate College

THE UNIVERSITY OF ARIZONA

1 9 8 8

THE UNIVERSITY OF ARIZONA
GRADUATE COLLEGE

As members of the Final Examination Committee, we certify that we have read the dissertation prepared by Scott Charles MacInnes

entitled Lateral Effects in Controlled Source Audiomagnetotellurics

and recommend that it be accepted as fulfilling the dissertation requirement for the Degree of Doctor of Philosophy.

James R. Wait	17 Dec. 1987 Date
[signature]	12/17/87 Date
R F Sutton	17 Dec 1987 Date
Kenneth L Jones	17 Dec 1987 Date
Randall M. Richardson	17 Dec 1987 Date

Final approval and acceptance of this dissertation is contingent upon the candidate's submission of the final copy of the dissertation to the Graduate College.

I hereby certify that I have read this dissertation prepared under my direction and recommend that it be accepted as fulfilling the dissertation requirement.

James R. Wait	13 JAN. 1988
Dissertation Director	Date

STATEMENT BY AUTHOR

This dissertation has been submitted in partial fulfillment of requirements for an advanced degree at The University of Arizona and is deposited in the University Library to be made available to borrowers under rules of the Library.

Brief quotations from this dissertation are allowable without special permission, provided that accurate acknowledgement of source is made. Requests for permission for extended quotation from or reproduction of this manuscript in whole or in part may be granted by the head of the major department or the Dean of the Graduate College when in his or her judgment the proposed use of the material is in the interests of scholarship. In all other instances, however, permission must be obtained from the author.

SIGNED: 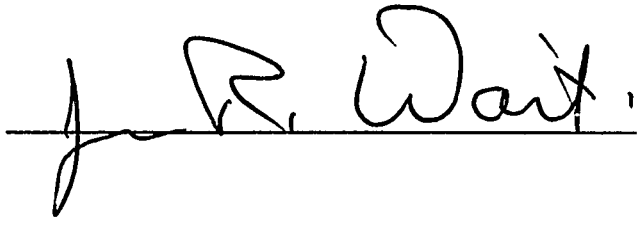

ACKNOWLEDGMENTS

Many people contributed advice and help to this dissertation project, I am grateful for their aid. I would like to especially thank the following people for their invaluable assistance.

Dr. James R. Wait was of major help in providing advice and direction during the theoretical development of this dissertation and in giving lucid and constructive criticism when evaluating the results.

Dr. Kenneth Zonge provided the motivation and inspiration for choosing the specific problem of modeling the effects of lateral variations in geology. Dr. Zonge provided the observational data which demanded a theoretical explanation. Dr. Zonge's encouragement and support facilitated the completion of this project.

The Amoco Foundation Doctoral Fellowship provided financial support for my graduate program, support which gave me the freedom to thoroughly explore the topic of lateral variations in controlled source audiomagnetotellurics.

TABLE OF CONTENTS

TABLE OF CONTENTS - Continued

LIST OF ILLUSTRATIONS

LIST OF ILLUSTRATIONS - Continued

LIST OF TABLES

ABSTRACT

A popular electrical exploration method is controlled source audiomagnetotellurics (CSAMT). Although the CSAMT method has had practical success, the theory used in CSAMT interpretation remains limited.

The controlled source in CSAMT is a grounded electric dipole placed as far as is practical from the survey area. When the source-receiver separation is large enough, source fields can be adequately modeled by a single plane wave and conventional magnetotelluric interpretation methods can be used. Quite often however, data collected at lower frequencies can not be interpreted with magnetotelluric algorithms. If the electrical distance between source and receiver is too small, mathematical models must explicitly include the dipolar nature of the source fields to accurately model the data.

Models which include a dipole source are limited. Most interpretation of CSAMT data is based upon horizontally layered models. In this dissertation, the model of plane layers excited by an arbitrary source is extended to include the effects of lateral changes in layer thickness. The method developed for modeling undulating interfaces mimics nature more accurately than plane-layered models, while

preserving the utility of quick evaluation and insight lost to more general numerical methods. While the main emphasis here is on CSAMT applications, the theoretical results are valid for any source type. Topographic effects are modeled for plane wave and magnetic dipole sources. The effects of relief in basement topography on the response of a horizontal loop-loop system are computed and compared with scale-model measurements. CSAMT field data which can not be adequately explained by plane-layered models are analyzed using models with variable layer thickness. The correctness of the theoretical development is verified by comparison with physical measurements. The utility of the theory is illustrated by application to problems which can not be explained by plane-layered models.

CHAPTER 1

INTRODUCTION

Controlled-source audiomagnetotellurics (CSAMT), an electromagnetic exploration method, is used in mineral, oil, and geothermal exploration, as well as in geological engineering and waste disposal investigations. The controlled source in CSAMT is either a grounded electric bipole antenna or an ungrounded horizontal loop antenna. Time varying electromagnetic signals are broadcast in the audio frequency range, from 1 Hz to 5 kHz. The source antenna is placed as far as practical from the area of geologic interest to allow magnetotelluric-like measurements of electromagnetic field components. Far from the source, the primary field behaves like a plane wave. Measurements of orthogonal field components can be combined into impedances which characterize the ground's electrical properties. Measured impedances are compared with predictions from theoretical models with the goal of inferring the electrical properties of the subsurface. Successful interpretation of CSAMT data depends upon sound theoretical models of the interaction between electromagnetic fields and geologic structure. The theoretical modeling of CSAMT is investigated in this

dissertation. Extensions to existing theory provide both a tool for refined interpretation and a guide for determining when traditional interpretation methods are invalid.

A Description of CSAMT

CSAMT evolved from the magnetotelluric method. In magnetotelluric surveys, orthogonal components of naturally excited electric and magnetic fields are measured. Filtering extracts information about impedances for a broad range of frequencies. Because high frequency electromagnetic energy penetrates less deeply than low frequency energy, a spectrum of measurements provides information about resistivity as a function of depth. For the depths of interest in most exploration surveys, the necessary frequencies are in the audio range.

There are problems associated with the use of natural sources in the audio frequency range. Absorption effects at 2 kHz limit field strengths available from natural sources. Because fields radiated by the tropical thunderstorm belt are attenuated too much to be useful, only local thunderstorms provide strong enough source fields near 2 kHz (Goldstein and Strangway, 1975; Wait, 1981). Local thunderstorms are an erratic source. The sporadic

presence of sufficiently strong source fields is a major drawback of natural source AMT.

Even with active natural sources, AMT data acquisition is slow. Since the polarizations of natural sources are unknown, multiple components of the electomagnetic fields $\underline{e}$ and $\underline{h}$ must be measured. Collecting two components of $\underline{e}$ and three components of $\underline{h}$ requires elaborate equipment and data analysis. The frequency content of natural sources is also uncontrolled. In order to obtain sufficient information for a broadband spectrum analysis, data must be collected for an extended period of time at each observation site.

Frustration with erratic natural sources lead to the idea of a controlled source for AMT surveys. Goldstein and Strangway (1975) proposed a grounded electric bipole for a source antenna. A bipole source provides a stable, known primary field. The geometry of a CSAMT survey is shown in Figure 1.1 The source antenna is a straight, insulated wire, often one or two kilometers long, grounded at each end with metal stakes. A constant current transmitter drives the selected waveform, usually a square wave. Measurements are typically made broadside to the transmitter bipole. Two components are measured at each station, the electric field parallel to the transmitter bipole, e_x, and the magnetic

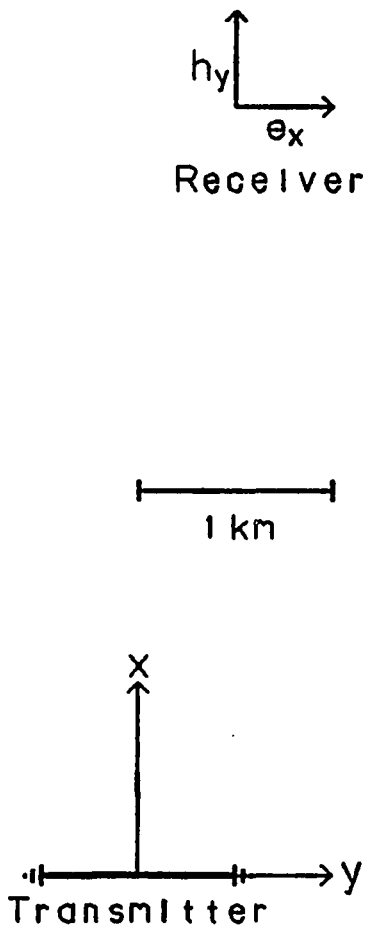

Figure 1.1 Map View of CSAMT Survey

The transmitter is placed as far as is practical from the survey area and is oriented so that e_x is perpendicular to regional strike.

field perpendicular to the transmitter, h_y. e_x is measured as a voltage gradient along a wire grounded at each end by non-polarizable electrodes. h_y is measured with a ferrite-cored coil. Controlling the polarization of the source field reduces the number of electromagnetic field components that must be measured. With fewer field components to measure at each observation location, equipment is lighter and data acquisition is faster.

An alternative source is a horizontal loop antenna, effectively a vertical magnetic dipole. Loop antennas do not have grounded endpoints, an advantage in highly resistive terrains. The disadvantage of large loop sources is that, unlike an electric bipole, their orientation can not be changed. The large loops must be horizontal. Ideally, the transmitter should be oriented so as to produce a broadcast pattern with an electric field oriented perpendicularly to geologic strike in the survey area. Lateral resistivity contrasts are most sharply defined if $\underline{e}$ is perpendicular to strike. Primary field orientations can be controlled with an electric bipole source, a virtue denied to the horizontal loop source.

As in magnetotellurics, CSAMT survey results are organized into frequency sounding curves for each observation location. A sounding curve is shown in Figure

1.2, a log-log plot of Cagniard apparent resistivity versus frequency, where the Cagniard apparent resistivity, ρ_a, is defined as $\rho_a = \frac{1}{\omega\mu}|e_x/h_y|^2$. The relationship between the frequency of a time-harmonic electromagnetic field and its depth-of-penetration is characterized by a measure of electrical distance, the skin depth (Figure 1.3). A plane wave propagating through a uniform media is attenuated by a factor of 0.37 or 8.7 db in one skin depth. In terms of resistivity and frequency, a skin depth, δ, is equal to $503\sqrt{\rho/f}$, where δ is skin depth in meters, ρ is complex resistivity amplitude in ohm-meters, and f is frequency in Hertz. Skin depths are proportional to the square root of resistivity and inversely proportional to the square root of frequency. At higher frequencies, electromagnetic fields attenuate rapidly with depth. Measurements at high frequencies reflect the earth's near-surface electrical properties. At low frequencies, electromagnetic fields penetrate more deeply into the ground. Measurements made at low frequencies reflect the electrical properties of a larger volume of the subsurface.

To investigate a range of depths, a broad band of frequencies must be sampled. With natural sources, a broad bandwidth is obtained by making measurements for an extended time at each station. With CSAMT, the frequency spectrum

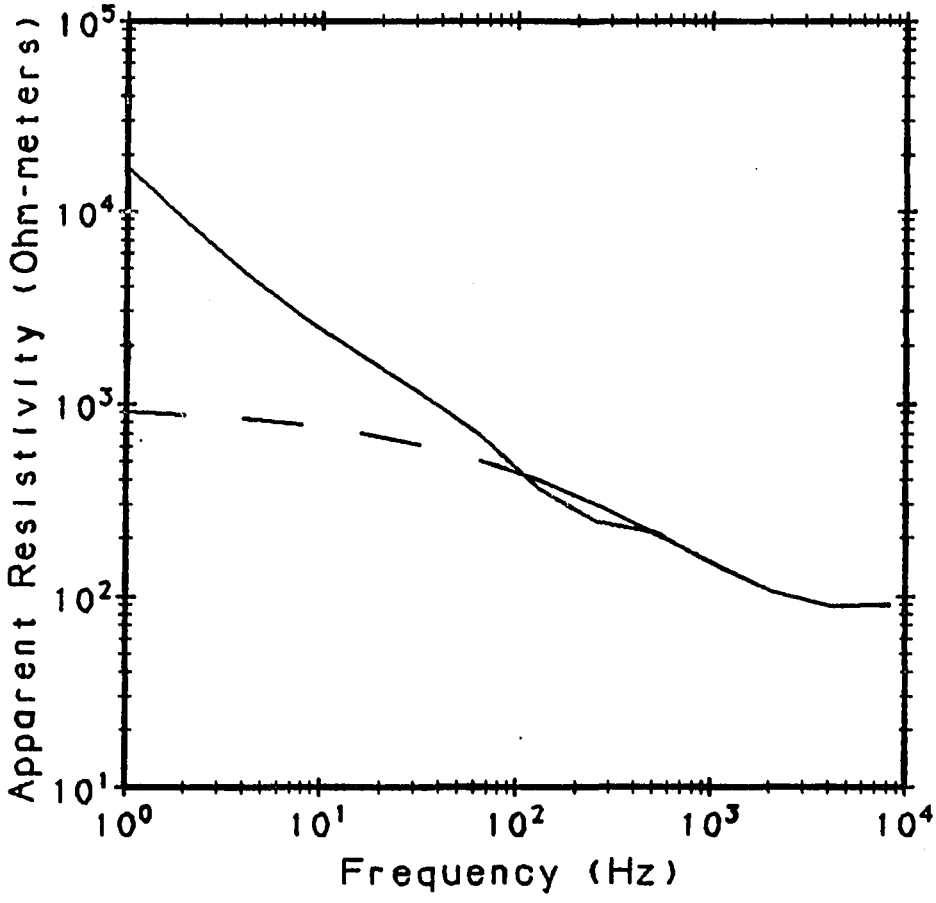

Figure 1.2 Frequency Sounding over Two-layer Earth.

A log-log plot of apparent resistivity vs frequency for a two-layer earth. The solid line is for a horizontal electric dipole (HED) source placed at (0,0) km relative to a receiver at (5,0.5) km. The x axis is parallel to the transmitter dipole and the y axis is perpedicular to the transmitter. The dashed line is for a plane-wave source. At low frequencies, apparent resistivities based on the plane-wave source model are inappropriate for a HED source.

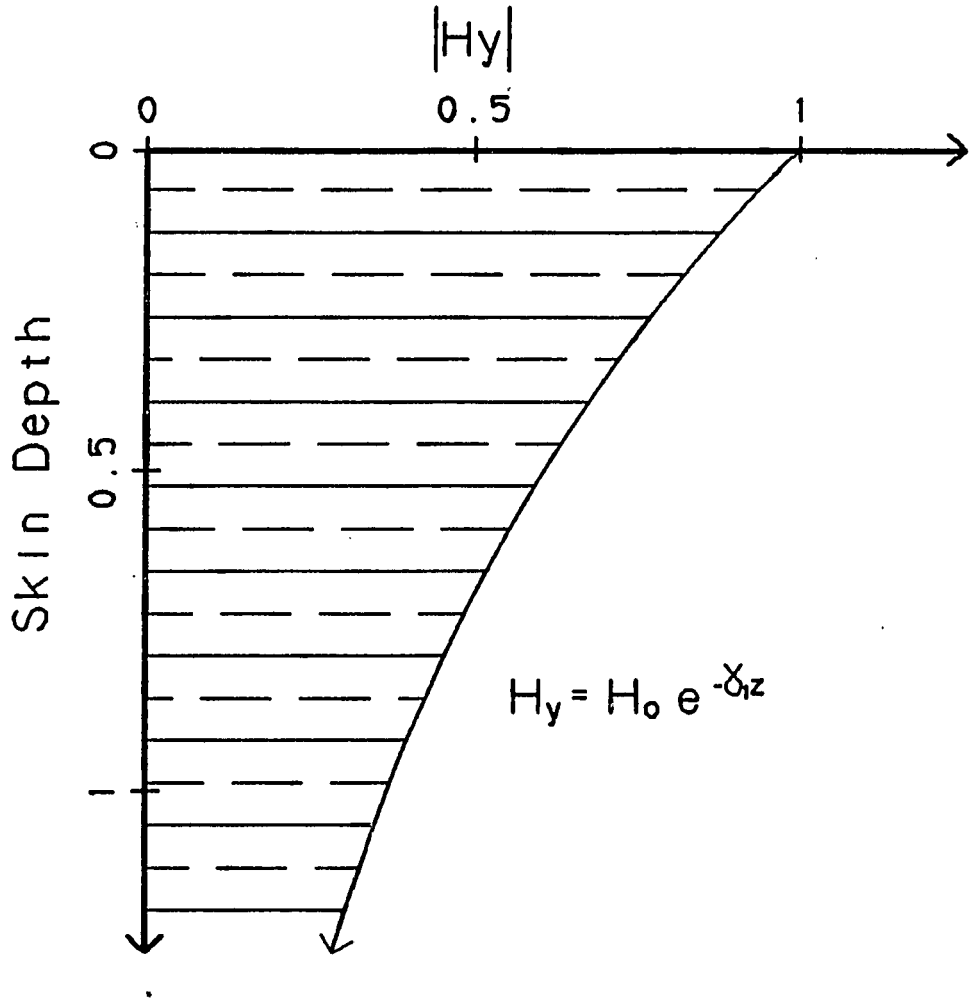

Figure 1.3 Skin Depths, a Measure of Electrical Distance

A normally incident plane wave is exponentially damped in a lossy material. The distance in which the field amplitude decreases by a factor of 1/e or 0.37 is defined to be one skin depth.

can be sampled in a more systematic way. By transmitting a square wave, several frequencies can be measured for each transmitted primary waveform. Fourier analysis of the measured data provides information at the primary frequency and at several odd harmonics. The transmitter can step through the frequency range in large increments, yet the spectrum is well filled with measurements.

Artificial sources provide control over signal strength, primary field polarization, and frequency content. The well-developed methods of magnetotelluric interpretation can be applied directly to CSAMT data for measurements made far enough from the transmitter. How far is far enough? By standard criteria, the transmitter should be more than three skin depths away from the measurement area for magnetotelluric-like, plane-wave field behavior. As shown in Figure 1.4, for a uniform half-space the Cagniard apparent resistivity is accurate if measurements are made broadside to the transmitter and are more than three skin depths away. The situation is not so simple however, for an earth model which includes a highly resistive lower layer. Wait and Spies (1973a, 1973b) investigate the dependence of surface impedance on source-receiver for a line source. The same effects are apparent for a electric bipole source. Figure 1.5 depicts

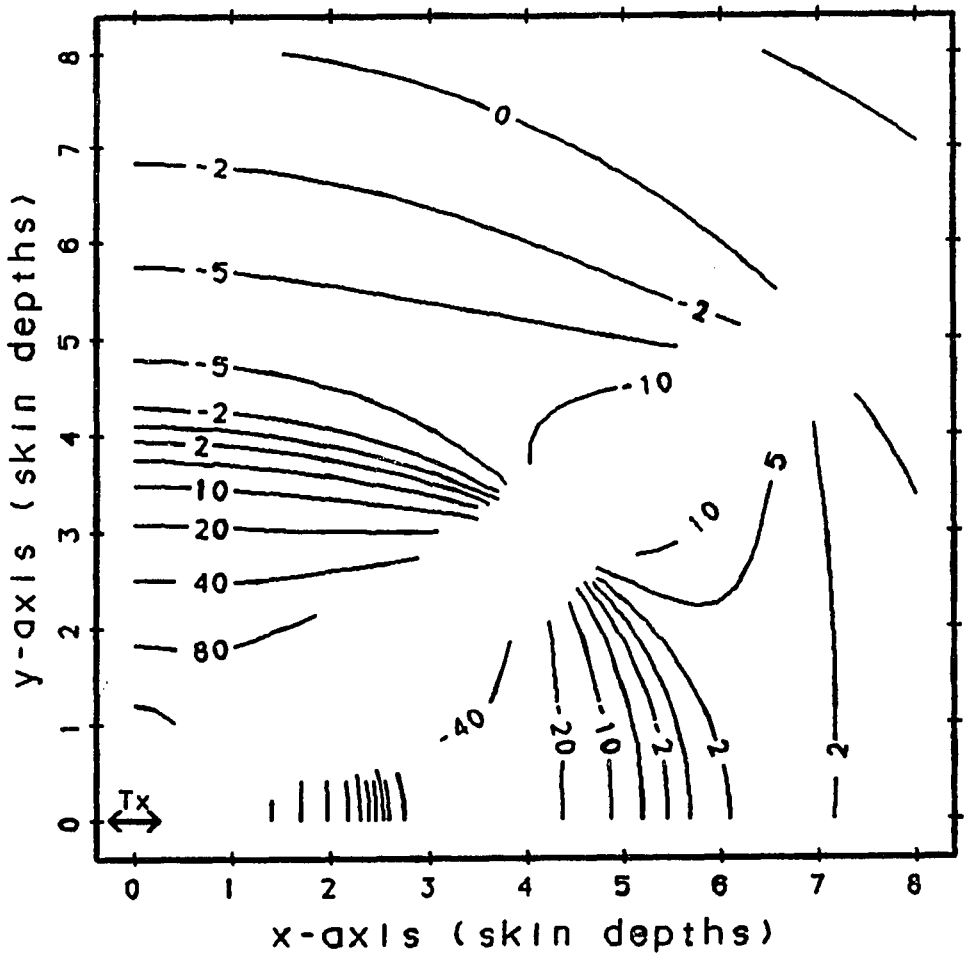

Figure 1.4 Error in Cagniard Apparent Resistivity over a Uniform Half-space.

The Cagniard apparent resistivity is not exact due to finite separation between source and receiver. Contours show percent deviation of apparent resistivity, ρ_a for fields excited by HED with respect to ρ_a for plane-wave excitation, where $\rho_a = \frac{1}{\omega\mu}|Z^2|$.

the Cagniard apparent resistivity for a low over high geometry. The two-layer model is a low resistivity, 100 ohm-meter overburden layer, 100 meters thick, overlaying a resistive basement of 1000 ohm-meters. The apparent resistivities deviate from "far-field" magnetotelluric values at a distance of 8 skin depths. The finite distance to the grounded source has an appreciable effect well beyond the three-skin-depth radius, when skin depths are calculated with the resistivity of the overburden layer. The three-skin-depth criteria is invalid, even for skin depths computed with apparent resistivities, rather than overburden resistivity. Only when the resistivity of the highly resistive basement is used in the skin depth formula is the three-skin-depth criteria correct. In areas with a resistive geologic unit, the separation between transmitter and receiver must be based upon the lowest frequency to be measured and the highest resistivity present in the local geology. Large enough separation between transmitter and receiver may be difficult to achieve.

The advantages of a controlled source are somewhat offset by the disadvantages of the effects that the source has on measurements made too close to the transmitter. Source effects or "near-field" measurements can be avoided by increasing the separation between the transmitter and

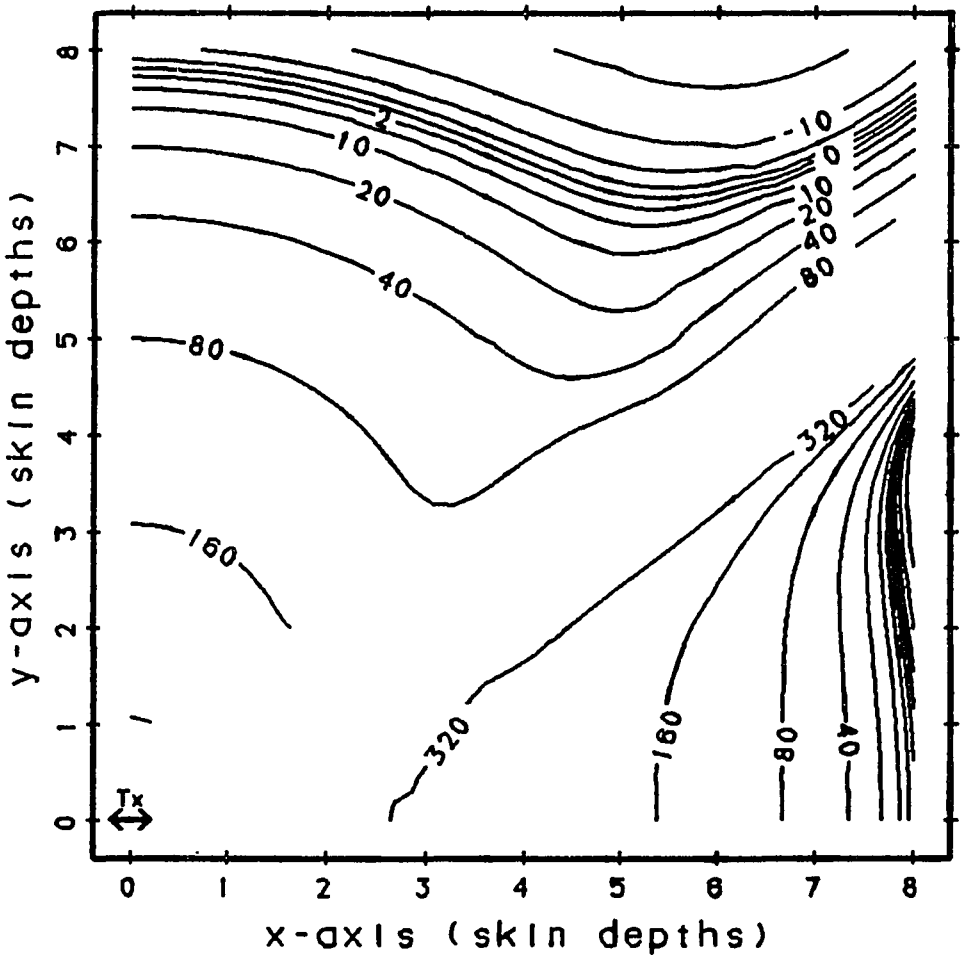

Figure 1.5 Error in Cagniard Apparent Resistivity over a Two-layer Earth.

Contours show percent deviation of ρ_a computed from fields excited by a HED with respect to ρ_a for plane-wave excitation.

receiver. Practical limitations on transmitter size and power, however, limit the maximum separation between the source and receiver. Low frequency measurements are often made in the near field, where fields are not well approximated by a single plane wave component and the Cagniard apparent resistivity does not model field behavior well. In the frequency sounding curve shown in Figure 1.2, low frequency apparent resistivities are inversely proportional to frequency, reflecting the inappropriateness of the Cagniard apparent resistivity for near-field data.

Existing Theoretical Models

Since CSAMT measurements often include near-field data, modeling programs used in CSAMT interpretation should explicitly include the artificial source. The catalog of available model types which include a grounded dipole source is quite limited.

The simplest earth model is a uniform half-space. Wait (1961) developed analytical expressions for fields about a horizontal electric dipole on the surface of a homogeneous earth. An immediate application for Wait's exact closed-form expressions is the computation of an improved apparent resistivity which explicitly includes both

the character of the transmitter field and the effects of finite separation between the transmitter and receiver. A second application of Wait's results is as an aid in computing numerical solutions to the plane-layered earth problem. By computing the effects of subsurface layers as a perturbation to a half-space, the amount of computation required for model evaluation is reduced.

A layered earth model is a logical extension to the uniform half space. Electromagnetic fields about a horizontal electric dipole on a layered earth can be computed by numerically evaluating an integral representation (Wait, 1966). Anderson (1974) documents an efficient computer program which evaluates layered earth models. The convergence of the integrals numerically evaluated by Anderson's routines is accelerated by subtracting a half-space response before integration, an improvement made possible by Wait's closed form expressions for half-space fields. Anderson's computer routines are efficient enough for use in routine interpretation and most CSAMT interpretation is based upon one-dimensional models. In reality, lateral variations are common and can make plane-layered models invalid.

Models which include both an electric bipole source and lateral variations are limited. A simple

two-dimensional shape which is amenable to mathematical analysis is a circular cylinder. Howard (1975a) describedinductive anomalies due to a circular cylinder embedded in a conductive half-space and excited by a magnetic dipole source. For vertical magnetic dipole (VMD) excitation, Tsubota and Wait (1980) derived equations for both frequency and time domain responses of a thin, cylindrical conductor. Wait (1959, 1986) included a discussion of plane-wave scattering from cylinders for oblique incidence. A spectrum of plane waves can be used to synthesize a three-dimensional source.

Another two-dimensional shape which invites analytical analysis is the wedge. Although a wedge-like body would be a good model for dipping contacts, the problem is surprisingly intractable and few solutions exist. Geyer (1972) addressed the issue of magnetotelluric anomalies over wedge shapes excited with a uniform and constant magnetic field parallel to strike by applying the Lebedev-Kontovovich transform. Geyer's results involve integrals with modified Bessel functions of fractional order and are of limited utility. Schlak and Wait (1967) used a geometrical ray approximation to determine fields over a sloping interface within a half-space excited by a vertical electric dipole. A ray tracing approximation seems to be the most promising

approach to modeling wedge-like structures.

A three-dimensional shape which yields analytical solutions is the sphere. Wait (1960) considered the effects of a sphere excited by a dipole source in a whole space. Ogunade, Ramsuany, and Dosso (1974) derived results for the response of a sphere in a conductive half-space excited by a magnetic dipole source. Lee (1983) also addressed the sphere problem and calculated the transient response to VMD excitation.

Numerical methods provide a more general approach to modeling, but at the cost of increased computational effort. Varentsov (1983) reviewed three-dimensional numerical modeling. For two-dimensional geology excited by a three-dimensional source, Lee and Morrison (1985a, 1985b) reported a finite element solution. Their model's source is a magnetic dipole. Three-dimensional finite element modeling is described by Pridmore, Hohmann, Ward, and Sill (1981). The finite element method can model almost any geological structure, but at a tremendous computational cost.

An alternative to finite elements is the integral equation approach. Wannamaker, Hohmann, and San Filipo (1984) used the integral equation method to compute the response of a brick-like shape in a layered earth. Newman,

Hohmann, and Anderson (1986) used Wannamaker, et al's, (1984) frequency domain algorithm to compute the transient response of a prism embedded in a layered earth and excited by a magnetic dipole source. For the transient response of the same model to horizontal electric dipole (HED) excitation, Gunderson, Newman, and Hohmann (1986) used the same algorithm. A hybrid combination of finite elements and integral equations was described by Best, Duncan, Jacobs, and Scheen (1985). The hybrid scheme combines the generality of finite elements with the numerical efficiency of integral equations. Inhomogeneities are restricted to a localized finite element mesh. Fields outside of the mesh are described by integral equations. By restricting the size of the mesh, solution matrix dimensions are kept under control.

For smooth, compact shapes, the T-matrix method can be applied. Kristensson and Strom (1982), Karlsson and Kristensson (1983), and Kristensson (1984) reviewed geophysical applications of the T-matrix method. The T-matrix approach is most suitable for objects such as elliptical cylinders or ellipsoids.

Although general numerical model schemes exist, they require huge computer resources. Finite element, finite difference, integral equation, hybrid, and T-matrix methods

have all been applied to the three-dimensional electromagnetic induction problem, but the computation required to evaluate a general model remains enormous. Analytical results require less computation, but are restricted to a limited class of shapes.

Extensions to Existing Theory

Most CSAMT interpretation is based upon one-dimensional modeling. The interpreter changes parameters of a horizontally layered earth until the computed model response matches observed data in terms of a statistical measure such as root mean square difference. Inversion programs automate selection of layer parameters, but the theoretical model is limited to layers of uniform thickness. To interpret two- or three-dimensional environments, one-dimensional models are pieced together. The more complicated effects of lateral variations are ignored, even though they can be important. An immediate extension to horizontal layering is to allow variations in layer thickness. The problem of modeling the electromagnetic effects of undulating interfaces excited by a general source is addressed in this dissertation.

The problem of modeling the lateral effects caused

by variations in layer thickness is best treated as a perturbation to a plane-layer model. The plane-layered model itself is evaluated by considering the effects of subsurface layering to be a modification to a half-space response. By splitting the problem into sections, the amount of numerical computation required to evaluate a model is minimized.

The theoretical development presented in this dissertation follows the strategy outlined above. The first section follows Weyl (1919), Weaver (1970, 1973), Lajoie, Alfonso-Roche, and West (1975), and Wait (1980a) in developing a representation for the six components of $\underline{e}$ and $\underline{h}$ in terms of two scalar Hertz vector potential components, π_z and π_z^*. A pair of rotation operators are derived, providing a useful utility for moving between representations with a vertical potential orientation and representations with an arbitrary Hertz potential representation. The rotation operators are a modification of results developed by Olsson (1983). Representations for half-space fields excited by HED and VMD sources are derived next. Half-space fields are presented in a two-dimensional Fourier transform domain, $[(x,y,z) \longleftrightarrow (k_x,k_y,z)]$. Whereas previous work has been limited to development of representations with just one Hertz potential orientation,

the link between Fourier and Hankel transform domains and between representations with different choices for Hertz potential orientation is demonstrated. The catalog of Fourier transform domain representations presented by Lajoie, et al. (1975) is extended to include a representation for a horizontal, rectangular loop of finite size. The analysis for plane layers is described and efficient methods for the computation of layered earth models are indicated. Previous work by Anderson (1974) for efficient evaluation of layered earth models is extended by developing an analytical correction term which improves the convergence of the required numerical integration. Finally, the primary extension developed in this dissertation is a first-order perturbation solution for the effects of lateral changes in layer thicknesses. Expressions for reflection from and transmission through an interface with three-dimensional undulations are derived. Several special cases of the general first-order solution are considered. Limiting undulations to two dimensions reduces the numerical work required for model evaluation. Assuming the same permeability for all materials eliminates many terms in the expressions for reflection and transmission. For the special case of two-dimensional undulations, uniform permeability, and TM or TE mode source fields, the general

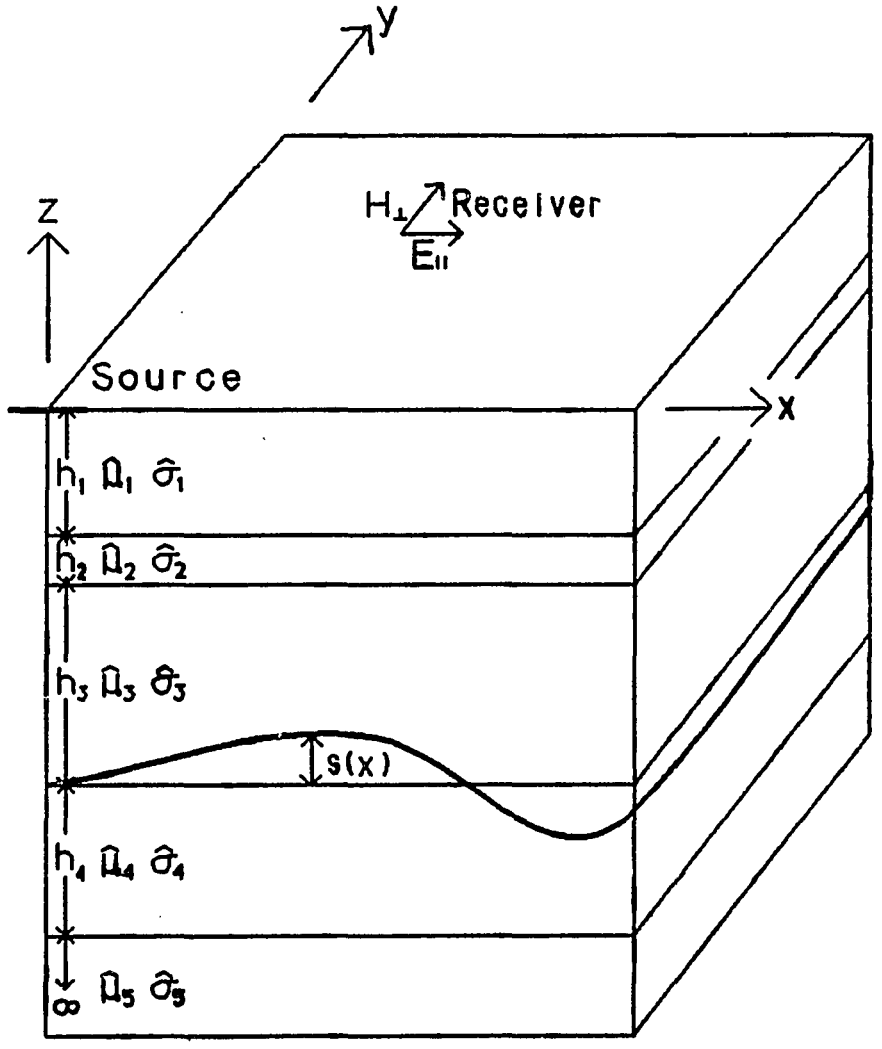

Figure 1.6 Block diagram of Undulating Interface Model

The plane-layered earth model is extended by allowing undulations on one interface. A three-dimensional source is placed at the origin and electomagnetic field components can be computed at any point on the surface.

solution reduces to previous results presented by Hughes and Wait (1975a).

Applications of the theory are included at each stage of the development. Closed-form solutions for half-space fields are useful for determining apparent resistivities. Plane-layered earth models lead to inversion routines which speed up interpretation and estimate model parameter statistics. The undulating interface model is applied to several problems. Placing undulations on the air-earth interface models topography. Topographic effects are examined for CSAMT and AMT measurements. The effects of variable depth-to-basement is modeled for two situations. Scale modeling results are duplicated for the response of a horizontal loop-loop system over steps in a conductive basement. The effects of variable depth-to-basement on CSAMT data is illustrated with data from Avra Valley, Arizona. The Avra Valley data can not be explained by plane-layer models, while a model with a sloping subsurface interface successfully matches the measurements in terms of squared differences.

CHAPTER 2

FIELD REPRESENTATIONS

The first task in solving the problem of modeling the electromagnetic effects of non-uniformly layered earths is to present a basis for representing electromagnetic fields. A Hertz vector potential representation is developed in this chapter. Within homogeneous regions the six components of $\underline{e}$ and $\underline{h}$ can be represented in terms of an electric Hertz potential, $\underline{\pi}$, and a magnetic Hertz potential, $\underline{\pi}^*$ as follows (Stratton, 1941):

$$\underline{e} = \nabla \times \nabla \times \underline{\pi} + \hat{\mu} \nabla \times \underline{\pi}^* \qquad (2.1)$$

$$\underline{h} = \nabla \times \nabla \times \underline{\pi}^* + \hat{\sigma} \nabla \times \underline{\pi} \qquad (2.2)$$

where $\hat{\mu} = -i\omega\mu$, $\hat{\sigma} = \sigma + i\omega\epsilon$, with $\exp(i\omega t)$ time dependence. The definitions of $\hat{\mu}$ and $\hat{\sigma}$ are chosen so as to produce symmetry between $\underline{e}$ and $\underline{h}$ with respect to $\underline{\pi}$ and $\underline{\pi}^*$.The vector potentials themselves are solutions of the vector wave equation, viz:

$$\nabla \times \nabla \times \underline{\pi} - \nabla\nabla\underline{\pi} - \gamma^2\underline{\pi} = -\underline{P}\,\delta(x-x')\delta(y-y')\delta(z-z') \qquad (2.3)$$

$$\nabla \times \nabla \times \underline{\pi}^* - \nabla\nabla\underline{\pi}^* - \gamma^2\underline{\pi}^* = 0 \qquad (2.4)$$

where $\underline{P} = \underline{p}\ Idl$, $\gamma^2 = -\hat{\mu}\hat{\sigma}$, $Real(\gamma) > 0$, and $Imag(\gamma) > 0$.

Table 2.1 Mathematical Notation

$\underline{e} = \begin{bmatrix} e_x \\ e_y \\ e_z \end{bmatrix}$	Electric field vector (volts/meter). Lower case indicates space domain. Upper case → Fourier transform domain.
$g(\lambda)$, $g^*(\lambda)$	Reflectance functions. * indicates TE mode.
$\underline{h} = \begin{bmatrix} h_x \\ h_y \\ h_z \end{bmatrix}$	Magnetic field vector (amperes/meter). Lower case indicates space domain. Upper case → Fourier transform domain.
$\underline{J} = \begin{bmatrix} J_x \\ J_y \\ J_z \end{bmatrix}$	Electric current density (amperes/meter^2). Upper case → Fourier transform domain.
$K = \frac{u}{\hat{\sigma}}$	Intrinsic impedance (ohms).
k_x, k_y	Spacial wavenumbers (1/meters).
$\underline{M} = \begin{bmatrix} M_x \\ M_y \\ M_z \end{bmatrix}$	Magnetic current density (tesla/meter^2). Upper case → Fourier transform domain.
$N = \frac{u}{\hat{\mu}}$	Negative of intrinsic admittance (-mhos).
$\underline{P} = \begin{bmatrix} P_x \\ P_y \\ P_z \end{bmatrix}$	Electric dipole moment per meter^3. Upper case → Fourier transform domain.
R_j, R_j^*	Reflection coefficients. * indicates TM mode.
T_j, T_j^*	Transmission coefficients. * indicates TM mode.
$u = \sqrt{\gamma^2 + \lambda^2}$	Vertical propagation constant. Re(u) > 0, Im(u) > 0, (1/meters).
Y	Negative of admittance (mhos).
Z	Impedance (ohms).

Table 2.1 (continued)

$\gamma = \sqrt{-\hat{\mu}\hat{\sigma}}$	Propagation constant (1/meters). $Re(\gamma) > 0$, $Im(\gamma) > 0$.
$\delta = 1/Re(\gamma)$	Skin depth (meters).
ϵ	Permitivity (farads/meter).
$\lambda = \sqrt{k_x^2 + k_y^2}$	Radial wavenumber (1/meters).
μ	Permeability (henries/meter).
$\hat{\mu} = i\omega\mu$	Complex permeability (henries/meter-second).
$\underline{\pi} = \begin{bmatrix}\pi_x \\ \pi_y \\ \pi_z\end{bmatrix}$	Electric Hertz vector potential. Lower case indicates space domain. Upper case → Fourier transform domain.
$\underline{\pi}^* = \begin{bmatrix}\pi_x^* \\ \pi_y^* \\ \pi_z^*\end{bmatrix}$	Magnetic Hertz vector potential. Lower case indicates space domain. Upper case → Fourier transform domain.
ρ	Resistivity (ohm-meters).
σ	Conductivity (siemens).
$\hat{\sigma} = \sigma + i\omega\epsilon$	Complex conductivity (siemens).
ω	Radial frequency (radians/second).
∂_x, ∂_y, ∂_z	Derivative operators (1/meters).

$\underline{P}$ represents an grounded electric dipole source. A grounded dipole source is a short insulated wire carrying a time-varying current of $Re(Ie^{i\omega t})$ amperes and grounded at each end. The dipole is oriented parallel to the unit vector $\underline{p}$ and has a infinitesimal length, dl. Since the wire is very conductive and is relatively short, the current is assumed to be uniform along the length of the wire. Dirac impulse functions, $\delta(x-x')\delta(y-y')\delta(z-z')$, fix the location of the dipole source at (x',y',z'). The electric dipole source represents segments in a transmitter antenna. To obtain the response due to a finite length source, the response due to a dipole source must be integrated over the length of the transmitter antenna. In general, there is no requirement that the transmitter antenna be straight or that the current along the length of the transmitter antenna be uniform, although both assumptions are often made for CSAMT source antennas.

Vertically Oriented Hertz Potentials

The choice of orientation for $\underline{\pi}$ and $\underline{\pi}^*$ is not unique, and the choice of which orientations to use has a major impact on the simplicity of solutions to the problem at hand. For matching boundary conditions in a layered earth problem, a good choice is vertically oriented Hertz

potentials, $\underline{\pi} = (0,0,\pi_z)$ and $\underline{\pi}^* = (0,0,\pi_z^*)$. All six electromagnetic field components can be derived from vertically oriented $\underline{\pi}$ and $\underline{\pi}^*$. As pointed out by Lajoie, Alfonso-Roche, and West (1975), the induction theorem presented by Harrington (1961) guaranties the uniqueness of fields represented by vertically oriented Hertz potentials or vertical electric and magnetic currents distributed on a horizontal surface. Any source can be represented by a horizontal distribution of vertically oriented Hertz potentials. Choosing π_z and π_z^* as a basis will give a complete representation and leads to simple expressions for interactions with layered earth models. Writing out the relationship between $\underline{e}$, $\underline{h}$ and $\underline{\pi}_z$ in matrix form gives the compact notation:

$$\begin{bmatrix} e_x \\ e_y \\ e_z \end{bmatrix} = \begin{bmatrix} \partial_{xz} & \hat{\mu}\partial_y \\ \partial_{yz} & -\hat{\mu}\partial_x \\ \partial_{zz}-\gamma^2 & 0 \end{bmatrix} \begin{bmatrix} \pi_z \\ \pi_z^* \end{bmatrix} \tag{2.5}$$

$$\begin{bmatrix} h_x \\ h_y \\ h_z \end{bmatrix} = \begin{bmatrix} \hat{\sigma}\partial_y & \partial_{xz} \\ -\hat{\sigma}\partial_x & \partial_{yz} \\ 0 & \partial_{zz}-\gamma^2 \end{bmatrix} \begin{bmatrix} \pi_z \\ \pi_z^* \end{bmatrix} \tag{2.6}$$

where

$$\underline{e} = \begin{bmatrix} e_x \\ e_y \\ e_z \end{bmatrix} \qquad \underline{h} = \begin{bmatrix} h_x \\ h_y \\ h_z \end{bmatrix} \qquad \underline{\pi}_z = \begin{bmatrix} \pi_z \\ \pi_z^* \end{bmatrix}$$

To make mathematical expressions more concise, partial derivatives are symbolized with an operator notation, $\partial_y = \frac{\partial}{\partial y}$ and $\partial_{yz} = \frac{\partial^2}{\partial y \partial z}$. The notation anticipates the use of Fourier and Hankel transforms. In the space domain, ∂_y implies differentiation. In the Fourier and Hankel transform domains used later in this theoretical development, terms like ∂_y can be handled algebraically. For Fourier transforms with respect to x and y, $\partial_x \leftrightarrow ik_x$ and $\partial_y \leftrightarrow ik_y$. In the (k_x, k_y, z) Fourier transform domain an expression like

$$(\partial_{xx} + \partial_{yy})^{-1} = \frac{1}{(\partial_{xx} + \partial_{yy})} \text{ is valid.}$$

Rotation of Potential Orientation

Vertically oriented Hertz potentials are a natural representation for vertical dipole sources. Vertically oriented potentials can also represent horizontal dipole sources, but the representations are more complicated. To represent a horizontal electric dipole with a vertical potential orientation requires a combination of both magnetic and electric Hertz potentials. Horizontal source representation is more complicated with a vertical potential orientation, but interactions with horizontal layers are simplified.

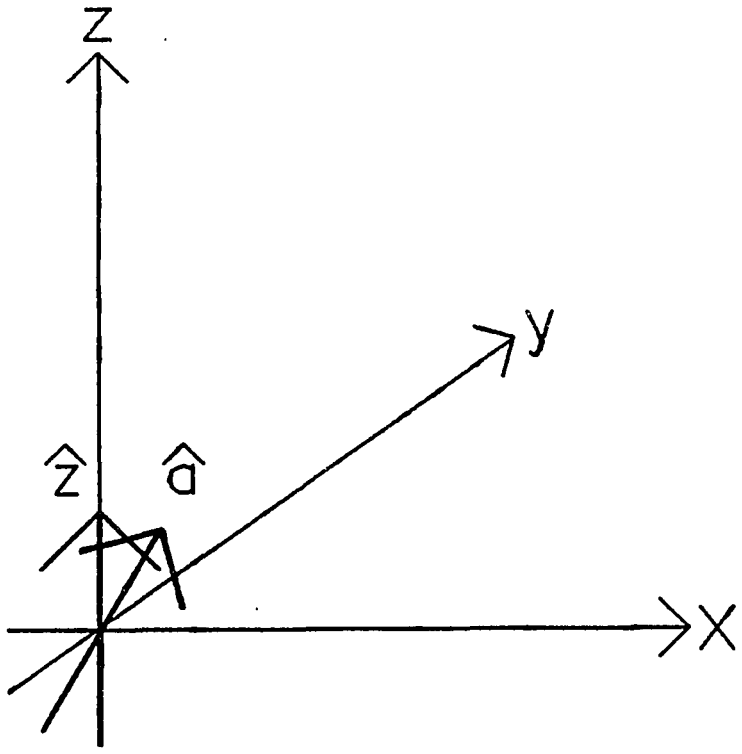

Figure 2.1 Hertz Potential Rotation

A distribution of vertically oriented Hertz potentials in the x-y plane uniquely determines electromagnetic field components. The rotation operator, $\underline{V}$, can transform a vertically oriented representation into an equivalent representation with potentials oriented parallel to an arbitrary unit vector $\hat{a}$. A second rotation operator, $\underline{U}_{\hat{a}}$ rotates representations back, from an $\hat{a}$ orientation to a $\hat{z}$ orientation.

Fortunately it is not necessary to remain with one choice of potential orientation throughout the development of a problem's solution. It is possible to rotate Hertz potentials from one orientation to another, choosing the orientation which is most convenient for solving each separate part of the problem. Simple representations of horizontal dipoles by horizontally oriented potentials can be rotated to vertically oriented Hertz potentials. After determining the effect of interaction with horizontal layers, a vertically oriented Hertz potential representation can be rotated to a horizontal direction, parallel to strike, to deal with interactions with two-dimensional objects. Rotation of potential orientation can be applied to the problem of reflection from sloping interfaces. By rotating potential representations to an orientation normal to a sloping interface reflection coefficients are easily calculated. Rotation back to the original orientation creates the more complicated expression for reflection coefficients in the original orientation.

Rotation operators can be constructed to change Hertz potential representations from one arbitrary orientation to another. As pointed out by Olsen (1983), field components must be invariant no matter what potential orientation is used, allowing the construction of rotation

operators to change representations from one Hertz potential orientation to another. For example, e_z can be represented by either π_z or $\underline{\pi}$ and $\underline{\pi}^*$ as follows:

$$e_z = (\partial_{zz}-\gamma^2)\pi_z = \hat{z}\cdot[\nabla(\nabla\cdot\underline{\pi}) + \hat{\mu}(\nabla \times \underline{\pi}^*)] \qquad (2.7)$$

where $\underline{\pi}$ and $\underline{\pi}^*$ are Hertz potentials oriented parallel to the arbitrarily oriented unit vector $\hat{a}$ and $\hat{z}$ is a unit vector oriented vertically. Since e_z must be the same for either representation, π_z must be related to $\underline{\pi}$ and $\underline{\pi}^*$ by the relation

$$\pi_z = \frac{1}{(\partial_{zz}-\gamma^2)}\left[\partial_z(\nabla\cdot\hat{a})\pi_a + \beta(\nabla \times \hat{a})_z\pi_a^*\right] \qquad (2.8)$$

where π_a and π_a^* are the amplitudes of $\underline{\pi}$ and $\underline{\pi}^*$ respectively and $(\nabla \times \hat{a})_z$ represents the z component of the curl($\hat{a}$). Division by the term $(\partial_{zz}-\gamma^2)$ requires a Hankel or Fourier transform representation of π_z. To continue the example, h_z can be represented either by π_z^* or by $\underline{\pi}$ and $\underline{\pi}^*$ as follows:

$$h_z = (\partial_{zz}-\gamma^2)\pi_z^* = \hat{z}\cdot[\nabla(\nabla\cdot\underline{\pi}^*) + \partial(\nabla \times \underline{\pi})] \qquad (2.9)$$

Since h_z must be the same regardless of the choice of potential orientation, equation 2.9 implies that:

$$\pi_z^* = \frac{1}{(\partial_{zz}-\gamma^2)}\left[\partial(\nabla \times \hat{a})_z\pi_a + \partial_z(\nabla\cdot\hat{a})\pi_a^*\right] \qquad (2.10)$$

Equations 2.8 and 2.10 can be combined into a matrix to form a single rotation operator:

$$\underline{\pi}_z = \underline{U}\,\underline{\pi}_a \tag{2.11}$$

where

$$\underline{\pi}_z = \begin{bmatrix} \pi_z \\ \pi_z^* \end{bmatrix}, \qquad \underline{U} = \frac{1}{(\partial_{zz}-\gamma^2)} \begin{bmatrix} \partial_z(\nabla\cdot\hat{a}) & \beta(\nabla \times \hat{a})_z \\ \partial(\nabla \times \hat{a})_z & \partial_z(\nabla\cdot\hat{a}) \end{bmatrix}$$

and

$$\underline{\pi}_a = \begin{bmatrix} \pi_a \\ \pi_a^* \end{bmatrix}$$

To obtain a operator for rotation from $\hat{z}$ to $\hat{a}$, the same reasoning can be applied to the field components e_a and h_a, the electric and magnetic field components aligned parallel to the unit vector $\hat{a}$. Following the same steps as used in deriving equation 2.11 and using the fact that $(\nabla \times \hat{z})_a = -(\nabla \times \hat{a})_z$ gives the result:

$$\underline{\pi}_z = \underline{V}\,\underline{\pi}_a, \tag{2.12}$$

where

$$\underline{V} = \frac{1}{((\nabla\cdot\hat{a})^2-\gamma^2)} \begin{bmatrix} \partial_z(\nabla\cdot\hat{a}) & -\beta(\nabla \times \hat{a})_z \\ -\partial(\nabla \times \hat{a})_z & \partial_z(\nabla\cdot\hat{a}) \end{bmatrix}$$

Olsson (1983) presents a similar result for the rotation of potentials between arbitrary orientations. Equations 2.11 and 2.12 are in a slightly different notation than used by Olsson and are for a slightly different potential representation. Potential rotation operators allow the option of changing from one potential orientation to another

at any stage in a problem's solution. Different parts of each problem may be most easily done with different potential orientations. The first application of the potential rotation operators will be to change the representation of an x-directed electric dipole from its simple form using π_x to a form using π_z and π_z^*.

Chapter 3

SOURCE REPRESENTATIONS

Two types of sources used in CSAMT surveys are horizontal electric bipoles and horizontal loop sources. Both source types can be uniquely represented by distributions of the vertical components of electric and magnetic currents. In anticipation of application to the non-planar interface problem, source representations are developed here in a two-dimensional Fourier transform domain ($(x,y,z) \leftrightarrow (k_x,k_y,z)$).

This approach most closely follows the development by Weaver (1970) and by Lajoie, Alfonso-Roche, and West (1975), who present expressions for a horizontal electric dipole (HED) source on the surface of a layered earth in terms of Π_z and Π_z^*. Lajoie, et al. (1975) include Fourier transform domain expressions for finite length bipole and infinite length line sources. Their results are extended here to include Fourier transform representations for rectangular loop sources of finite size. Wait and Hill (1980) discuss rectangular and circular loops of finite size, but their development is in the Hankel transform domain. Howard (1975b) considers the problem of

three-dimensional scattering from a buried cylinder excited by a vertical magnetic dipole (VMD) source. Howard's analysis of the problem is within a two-dimensional Fourier transform domain. Howard (1975a, 1975b) also includes in his analysis a method for choosing sampling windows and spacing so as to minimize errors due to aliasing when Fourier integrals are approximated by fast Fourier transforms. Wait (1980a), in analyzing a layered earth problem, includes some discussion of the Fourier transform representation of a general sheet current source using Π_z and Π_z^*.

For laterally varying layered earth models, the two-dimensional Fourier transform domain (k_x,k_y,z) is the most appropriate. To reduce the amount of computation needed to evaluate a model, the effects of curved interfaces are treated as perturbations to horizontal layering. Horizontal layering is treated as a modification to a uniform half-space.

For the plane-layered problem, sources must be presented in the Hankel transform domain. The third part of this section relates the Fourier transform results using (Π_z,Π_z^*) to Hankel transform representation using (Π_z,Π_z^*) (Wait, 1985) and to Hankel transform results using (Π_x,Π_z) (Wait, 1961, 1985, Hill and Wait, 1973a, 1973b).

Closed form equations for half-space fields are also possible. Wait (1961) and Hill and Wait (1973a, 1973b) derive closed form expressions for the surface and subsurface fields of a HED on the surface of an uniform half-space.

Whole-space Source Fields

An electric dipole source in an unbounded, homogeneous region is best represented by an electric Hertz potential aligned in the same direction. For a vertical electric dipole source (Figure 3.1a), the most natural representation is a vertically oriented Hertz potential. For vertically oriented potentials the vector wave equation simplifies to a scalar relationship:

$$(\nabla^2-\gamma^2)\begin{bmatrix}\pi_z\\ \pi_z^*\end{bmatrix} = \begin{bmatrix}-P_z\delta(x-x')\delta(y-y')\delta(z-z')\\ 0\end{bmatrix} \qquad (3.1)$$

where $P_z = \underline{p} \cdot \hat{z}\ I\ dl$. By taking the Fourier transform with respect to x and y using the Fourier transform pair,

$$F(k_x,k_y,z) = \int_{-\infty}^{\infty}\int f(x,y,z)\ \exp(-i(k_x x + k_y y))\ dx\ dy \qquad (3.2)$$

$$f(x,y,z) = \frac{1}{4\pi^2}\int_{-\infty}^{\infty}\int F(k_x,k_y,z)\exp(\ i(k_x x + k_y y))dk_x dk_y \qquad (3.3)$$

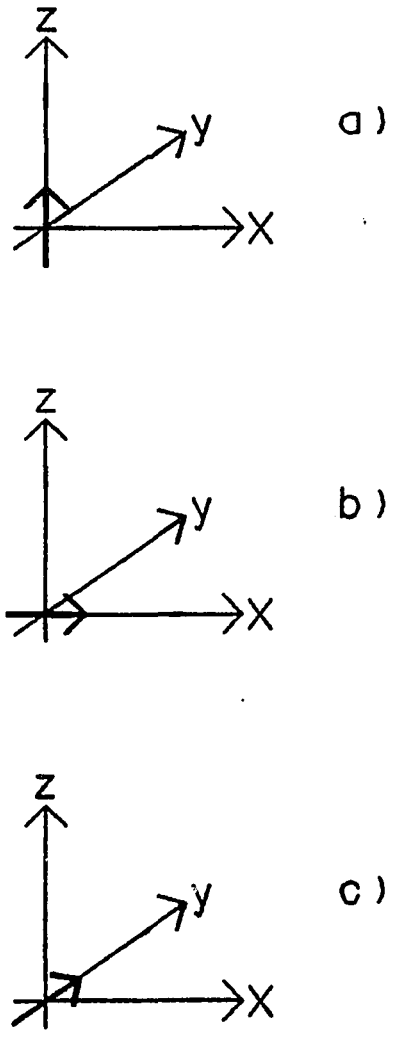

Figure 3.1 Cartesian Orientations of an Electric Dipole

Source representation of an arbitrarily oriented electric dipole can be generated by combining the representations of a vertical electric dipole (a), an x-directed, horizontal electric dipole (b), and a y-directed, horizontal electric dipole (c).

the partial differential equations in equation 3.1 become the ordinary differential equations

$$(d_{zz}-u^2)\begin{bmatrix}\Pi_z\\ \Pi_z^*\end{bmatrix} = \begin{bmatrix}-P_z\delta(z-z')\exp(-i(k_x x' + k_y y'))\\ 0\end{bmatrix} \qquad (3.4)$$

where $u^2 = \gamma^2 + k_x^2 + k_y^2$, with $\mathrm{Re}(u) > 0$, and $\mathrm{Im}(u) > 0$. Equation 3.4 has the solution

$$\begin{bmatrix}\Pi_z\\ \Pi_z^*\end{bmatrix} = \begin{bmatrix}P_z\dfrac{\exp(-u|z-h|)}{2u\partial}\\ 0\end{bmatrix} \qquad (3.5)$$

where the multiplier $\exp(-ik_x x' - ik_y y' + i\omega t)$ is suppressed. Equation 3.5 is called the Weyl solution (Stratton, 1941, Weyl, 1919). The Fourier transformed representation of a vertical electric dipole (equation 3.5) is a spectrum of plane waves traveling in all directions. Individually, each plane wave component satisfies the wave equation. By summing the spectrum with the inverse Fourier transform (equation 3.3), we recover the spatial potential distribution.

The vertically oriented Hertz potential representation of a vertical dipole source is straightforward. Representation of a horizontal electric dipole source is only slightly more complicated. By analogy with equation 3.5, the $\underline{\Pi}_x$ representation of a x-directed dipole source in an unbounded, homogeneous region is

$$\begin{bmatrix} \Pi_x \\ \Pi_x^* \end{bmatrix} = \begin{bmatrix} P_x \dfrac{\exp(-u|z-h|)}{2u\hat{\sigma}} \\ 0 \end{bmatrix} \tag{3.6}$$

with the multiplier $\exp(-ik_x x' - ik_y y' + i\omega t)$ suppressed. Using the rotation operator $\underline{U}$ (equation 2.11) we find the vertically oriented potential representation of an x-directed source to be

$$\begin{bmatrix} \Pi_z \\ \Pi_z^* \end{bmatrix} = \begin{bmatrix} \dfrac{\delta_z}{\lambda^2} \dfrac{\exp(-u|z-h|)}{2u\hat{\sigma}} (\partial_x P_x) \\ \dfrac{1}{\lambda^2} \dfrac{\exp(-u|z-h|)}{2u} (-\partial_y P_x) \end{bmatrix} \tag{3.7}$$

where $\lambda^2 = k_x^2 + k_y^2$.

Similarly, by rotating the y-directed potential representation of a y-directed source using the rotation operator $\underline{U}$ (equation 2.11), we find the vertically oriented potential representation of a y-directed source to be

$$\begin{bmatrix} \Pi_z \\ \Pi_z^* \end{bmatrix} = \begin{bmatrix} \dfrac{\delta_z}{\lambda^2} \dfrac{\exp(-u|z-h|)}{2u\hat{\sigma}} (\partial_y P_y) \\ \dfrac{1}{\lambda^2} \dfrac{\exp(-u|z-h|)}{2u} (\partial_x P_y) \end{bmatrix} \tag{3.8}$$

For representation of an arbitrarily oriented, horizontal electric dipole (HED), equations 3.7 and 3.8 can be combined to give

$$\begin{bmatrix} \Pi_z \\ \Pi_z^* \end{bmatrix} = \begin{bmatrix} \frac{\delta_z}{\lambda^2} \frac{\exp(-u|z-h|)}{2u\hat{\sigma}} (\partial_x P_x + \partial_y P_y) \\ \frac{1}{\lambda^2} \frac{\exp(-u|z-h|)}{2u} (-\partial_y P_x + \partial_x P_y) \end{bmatrix} \tag{3.9}$$

In Fourier transform space there is a close relationship between vertically oriented Hertz potentials and the vertical components of electric and magnetic current, viz

$$\begin{bmatrix} J_z \\ M_z \end{bmatrix} = \begin{bmatrix} \hat{\sigma} \lambda^2 \Pi_z \\ \hat{\mu} \lambda^2 \Pi_z^* \end{bmatrix} \tag{3.10}$$

where

$\lambda^2 = k_x^2 + k_y^2$.

Using the relation between vertically oriented potentials and the vertical components of current (equation 3.10) allows representation of a HED source by

$$\begin{bmatrix} J_p \\ M_p \end{bmatrix} = \begin{bmatrix} \mp \frac{\exp(-u|z-h|)}{2} \operatorname{div}(\underline{P}) \\ \hat{\mu} \frac{\exp(-u|z-h|)}{2u} \operatorname{curl}(\underline{P}) \end{bmatrix} \quad \begin{array}{l} - \text{ for } z > h \\ + \text{ for } z < h \end{array} \tag{3.11}$$

where

$$\underline{P} = \begin{bmatrix} P_x \\ P_y \end{bmatrix}$$

$P_x = \hat{x} \; I \; dl$

$P_y = \hat{y} \; I \; dl$

The vertical component of electric current, J_p, is driven by divergence of the source, corresponding to injection of current from the grounded ends of the source dipole. The vertical component of magnetic current, M_p, is driven by curl of the source, corresponding to the inductive effects of currents loops at the source dipole.

Integration over a finite-length line source can be carried out on the Fourier transformed source representations. Figure 3.2 depicts an arbitrarily oriented bipole source of finite length. The position dependent part of the source representation is carried in the multiplier $\exp(-ik_x x' - ik_y y')$. Integrating over the length of the source wire creates a multiplier holding the effects of source length and position, viz

$$L = \int_{-\frac{l}{2}}^{\frac{l}{2}} \exp(-is(k_x \cos\theta + k_y \sin\theta))ds \qquad (3.12)$$

where l = bipole length and θ = angle w.r.t. x axis. Evaluating the integral in equation 3.12 gives

$$L = l \, \mathrm{sinc}\left[\frac{k_s}{2} \right] \qquad (3.13)$$

where

$$\mathrm{sinc}(z) = \frac{\sin(z)}{z}$$

and

$$k_s = k_x \cos\theta + k_y \sin\theta$$

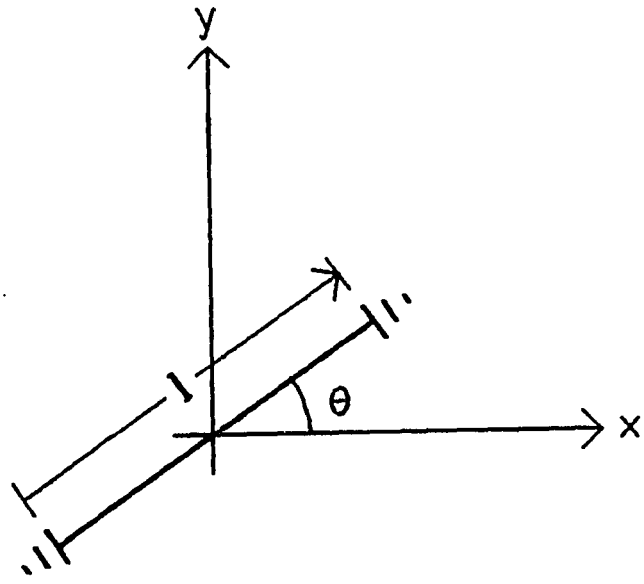

Figure 3.2 Map View of Electric Bipole Source

Bipole has a finite length, l, and makes an angle of θ with respect to x axis.

In the limit as $l \to \infty$, $L = \delta(k_s)$, the result expected for an infinitely long wire source. For l small enough, $L = l \exp(-ik_x x' - ik_y y')$, which is the shift operator predicted by Fourier transform theory.

A rectangular loop can also be represented analytically. Figure 3.3 shows a rectangular source loop with sides of length 2a in the x-direction and 2b in the y-direction. Using equation 3.13 and the shift operator for each side gives

$$J_p = \exp(-u|z-h|)\begin{bmatrix} - ik_x a(e^{ik_y b} - e^{-ik_y b})\ \mathrm{sinc}(k_x a) \\ + ik_y b(e^{ik_x a} - e^{-ik_x a})\ \mathrm{sinc}(k_y b) \end{bmatrix} \qquad (3.14)$$

which can be simplified to

$$J_p = 2\exp(-u|z-h|)\begin{bmatrix} - \sin(k_y b)\ \mathrm{sinc}(k_x a) \\ + \sin(k_x a)\ \mathrm{sinc}(k_y b) \end{bmatrix} \qquad (3.15)$$

The two terms inside the brackets are equal and opposite in sign, so $J_p = 0$. As expected, a horizontal loop source with a uniform current does not drive vertical electric currents. Solving for the vertical component of magnetic current gives

$$M_p = \hat{\mu}\,\frac{\exp(-u|z-h|)}{2u}\begin{bmatrix} ik_y a(e^{ik_y b} - e^{-ik_y b})\ \mathrm{sinc}(k_x a) \\ +ik_y b(e^{ik_x a} - e^{-ik_x a})\ \mathrm{sinc}(k_y b) \end{bmatrix} \qquad (3.16)$$

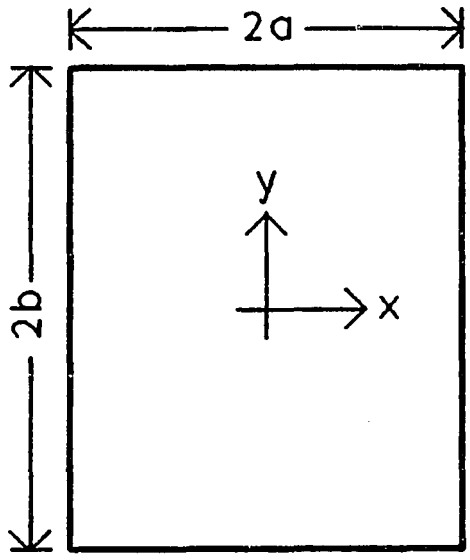

Figure 3.3 Map View of Horizontal Loop Source

The rectangular loop source has sides of 2a parallel to the x axis and sides of length 2b parallel to the y axis.

Exponential terms in equation 3.16 can be combined to give

$$M_p = \hat{\mu}\,\lambda^2\,\frac{\exp(-u|z-h|)}{2u}\left[4ab\ \mathrm{sinc}(k_x a)\ \mathrm{sinc}(k_y b)\right] \qquad (3.17)$$

A horizontal loop source carrying a uniform current drives a vertical magnetic current and no vertical electric current. In the limit of small loop we obtain

$$M_p = \frac{\hat{\mu}\lambda^2}{2u}\,(4ab)\,\exp(-u|z-h|) \qquad (3.18)$$

which is the result expected for a vertical magnetic dipole of moment IdA = 4ab.

Analytical expressions have been developed for both finite-length, grounded electric bipole and horizontal loop sources. Both source types are used in CSAMT surveys. The grounded electric bipole source represents a straight insulated wire lying on the earth's surface. The ends of the wire are grounded and it is assumed that the current along the length of the wire is constant. An assumption of constant current is justified because $|\gamma_e l| \ll 1$ where γ_e is the effective propagation constant along the antenna wire and l is the length of the bipole (Chang and Wait, 1974). The effect of finite length is expressed by equation 3.13. A horizontal loop source is a loop of insulated wire carrying a current which is assumed to be constant around the circumference of the loop. The effect of finite loop

size is shown, for a rectangular loop, by equation 3.17. Expressions for more complicated transmitter configurations can be constructed by linking dipole segments together. Integration over arbitrarily complicated source configurations can be carried out within the Fourier transform domain, minimizing the number of double Fourier transforms needed to determine electromagnetic field components in the space domain.

Dipole sources are useful for modeling controlled source magnetotelluric survey configurations. For magnetotellurics, natural sources can be represented by a spectrum of down-going plane waves impinging upon the earth's surface. In magnetotelluric modeling a single homogeneous plane wave component is often an adequate representation of the source. Having only one plane wave component eliminates the need to evaluate a double integral in transforming results from the (k_x,k_y,z) Fourier transform domain to the (x,y,z) space domain. A single plane-wave component is a simple special case which is often an adequate representation of natural sources.

Half-space Source Fields

The source representations derived in the previous section apply to fields in a whole space. In CSAMT surveys, sources are placed right on the air-earth interface. The

effect of a source on an interface can be determined by first solving the problem of a source above the interface and then taking the limit as the source approaches the interface from above. By first solving the problem with the source away from the interface, we can apply boundary conditions in a straightforward manner.

Interaction between the vertical components of current and horizontal boundaries is simple. Both J_z and M_z are continuous across horizontal boundaries. The condition that tangential $\underline{E}$ and $\underline{H}$ be continuous across interfaces requires that

$$E_x = \frac{1}{\lambda^2}\left[\frac{\partial_{xz}}{\hat{\sigma}} J_z + \partial_y M_z\right] \tag{3.19}$$

and

$$H_x = \frac{1}{\lambda^2}\left[\frac{\partial_{xz}}{\hat{\mu}} M_z + \partial_y J_z\right] \tag{3.20}$$

be continuous. Continuity of J_z and M_z force continuity of $\partial_y J_z$ and $\partial_y M_z$, with the implication that $\frac{\partial_{xz}}{\hat{\sigma}} J_z$ and $\frac{\partial_{xz}}{\hat{\mu}} M_z$ must be continuous across horizontal interfaces as well. The additional requirement that J_z and M_z go to zero at large distances from the source forces the condition that $\frac{\partial_z}{\hat{\sigma}} J_z$ and $\frac{\partial_z}{\hat{\mu}} M_z$ are continuous. The boundary conditions for vertical components of $\underline{J}$ and $\underline{M}$ on horizontal boundaries do not couple J_z and M_z.

The plane-wave representation of the source on a half-space is

$$\begin{bmatrix} J_z \\ M_z \end{bmatrix} = \begin{bmatrix} J_p[\exp(u_0 z) + R \exp(-u_0 z)] \\ M_p[\exp(u_0 z) + R^* \exp(-u_0 z)] \end{bmatrix} \quad \text{for } 0 < z < h \qquad (3.21)$$

$$\begin{bmatrix} J_z \\ M_z \end{bmatrix} = \begin{bmatrix} J_p\, T \exp(-u_1 z) \\ M_p\, T^* \exp(-u_1 z) \end{bmatrix} \quad \text{for } z < 0 < h \qquad (3.22)$$

where

$$\begin{bmatrix} J_p \\ M_p \end{bmatrix} = \begin{bmatrix} \frac{1}{2} \operatorname{div}(\underline{P}) \exp(-u_0 h) \\ \frac{\hat{\mu}_0}{2u_0} \operatorname{curl}(\underline{P}) \exp(-u_0 h) \end{bmatrix}$$

in the limit as $h \to z \to 0+$. Allowing the source to approach the air-earth interface from above merely eliminates the exponential factor in the expression for for J_p and M_p in equations 3.21 and 3.22. Applying the boundary conditions at the interface $z = 0$ gives

$$\begin{bmatrix} 1 + R \\ K_0(1 - R) \end{bmatrix} = \begin{bmatrix} T \\ K_1 T \end{bmatrix} \qquad (3.23)$$

and

$$\begin{bmatrix} 1 + R^* \\ N_0(1 - R^*) \end{bmatrix} = \begin{bmatrix} T^* \\ N_1 T^* \end{bmatrix}$$

where $K_j = \frac{u_j}{\hat{\sigma}_j}$ and $N_j = \frac{u_j}{\hat{\mu}_j}$.

Solving for half-space R, R^*, T, and T^* results in

$$\begin{bmatrix} R \\ T \end{bmatrix} = \begin{bmatrix} \frac{K_0 - K_1}{K_0 + K_1} \\ \frac{2K_0}{K_0 + K_1} \end{bmatrix} \qquad (3.24)$$

and

$$\begin{bmatrix} R^* \\ T^* \end{bmatrix} = \begin{bmatrix} \frac{N_0 - N_1}{N_0 + N_1} \\ \frac{2N_0}{N_0 + N_1} \end{bmatrix}$$

Reflection and transmission coefficients for the vertical components of current interacting with horizontal layers are the same coefficients as for transverse electric and magnetic component representations. The coefficients in equation 3.24 are identical to results presented by Wait (1985, p148-158) for reflection and transmission of plane waves in layered structures. The same symbols used by Wait (1985) are used in equations 3.23 and 3.24 to emphasize the similarity between the two results. Wait's recursive relationships for reflection and transmission in multiple layers follow directly from the single interface results for the vertical components of current shown by equation 3.24. By using the vertical components of current rather than vertically oriented Hertz potentials, we find that the transmission coefficients in equation 3.24 do not have to be modified from their usual transverse electric and magnetic

field form. Using vertically oriented Hertz potentials introduces additional factors of $\hat{\sigma}_j$ and $\hat{\mu}_j$ in transmission coefficients.

Making the quasi-static assumption ($\hat{\sigma}_0 = 0$) further simplifies equation 3.22 to give an expression for the vertical components of source current at the earth's surface as follows:

$$\begin{bmatrix} J_s \\ M_s \end{bmatrix} = \begin{bmatrix} T\ J_p \\ T^* M_p \end{bmatrix} = \begin{bmatrix} \text{div}(\underline{P}) \\ \hline \text{curl}(P) \\ \hline N_0 + N_1 \end{bmatrix} \tag{3.25}$$

The HED source representation summarized by equation 3.25 has one shortcoming. For the special case of $\lambda = 0$, representations using the vertical components of current or vertically oriented Hertz potentials fail. There is a singularity at $\lambda = 0$ for vertically oriented representations. The difficulty is easily avoided however, by switching to an alternative representation for the special case of $\partial_y = 0$. For $\partial_y = 0$, J_z and M_z are simply related to E_y and H_y by

$$\begin{bmatrix} J_z \\ M_z \end{bmatrix} = \partial_x \begin{bmatrix} H_y \\ E_y \end{bmatrix} \tag{3.26}$$

The simple relationship in equation 3.26 suggests that for $\partial_y = 0$, a HED source is well represented as follows:

$$\begin{bmatrix} E_s \\ H_s \end{bmatrix} = \begin{bmatrix} P_x \\ \dfrac{P_y}{N_0 + N_1} \end{bmatrix} \quad \text{for } \partial_y = 0. \tag{3.27}$$

This special case representation is useful for the later development of theory for interactions with undulating interfaces.

As intuition would suggest, the vertical component of electric current on the earth's surface is zero everywhere except at the grounded ends of the dipole source in the quasi-static limit and is driven directly by the divergence of the source dipole. The vertical component of magnetic current on the earth's surface is driven by the swirling pattern of surface currents around the dipole source. J_s represents direct current coupling of the source and M_s represents inductive coupling. As frequency approaches zero, the inductive component of the source disappears. Vertical magnetic source currents vanish at low frequencies. The vertical component current representation provides a clear separation between direct current coupling and inductive current coupling of sources and layered earth models. The relative importance of each mode of source coupling can be investigated by examining the effects of J_s and M_s separately.

Hankel Transform Representation

A further check of the methodology of source representation in the Fourier transform domain and of the validity of Hertz vector rotation is to compare the results presented by Wait (1982, 1985) for the same problem, but using (Π_z,Π_z^*) or (Π_z,Π_x) in the Hankel transform domain. To begin this demonstration, it is convenient to revert to vertically oriented Hertz potentials. Specializing the source to an x-directed HED gives

$$\begin{bmatrix}\Pi_z \\ \Pi_z^*\end{bmatrix} = \begin{bmatrix}\dfrac{\exp(-u_0 h)}{2\,\lambda^2\hat{\sigma}_0}(\,\partial_x P_x)\left[\exp(u_0 z) + R\exp(-u_0 z)\right] \\ \dfrac{\exp(-u_0 h)}{2\,\lambda^2 u_0}(-\partial_y P_x)\left[\exp(u_0 z) + R^*\exp(-u_0 z)\right]\end{bmatrix} \qquad (3.28)$$

for $0 < z < h$.

For functions with no angular dependence on $\theta = \arctan(k_y/k_x)$, the double Fourier transform is related to the Hankel transform by (from Bracewell, 1978, p247)

$$\frac{1}{4\Pi^2}\int_{-\infty}^{\infty}\int F\left[\sqrt{k_x^2 + k_y^2}\,,z\right]\exp[i(k_x x + k_y y)]\,dk_x\,dk_y \qquad (3.29)$$

$$= \frac{1}{2\Pi}\int_0^{\infty}\lambda\,F(\lambda,z)\,J_0(\lambda r)\,d\lambda$$

where $\lambda^2 = (k_x^2 + k_y^2)$ and $r^2 = (x^2 + y^2)$

The Hankel transform representation of equation 3.28 is

$$\begin{bmatrix} \pi_z(r,z) \\ \pi_z^*(r,z) \end{bmatrix} =$$

$$\begin{bmatrix} \frac{Idl}{4\Pi\hat{\sigma}_0}\,\partial_x \int_0^\infty \frac{1}{\lambda}\left[e^{u_0 z} + R\, e^{-u_0 z}\right] e^{-u_0 h}\, J_0(\lambda r)\, d\lambda \\ -\frac{Idl}{4\Pi}\,\partial_y \int_0^\infty \frac{1}{\lambda u_0}\left[e^{u_0 z} + R^* e^{-u_0 z}\right] e^{-u_0 h}\, J_0(\lambda r)\, d\lambda \end{bmatrix} \qquad (3.30)$$

for $0 < z < h$.

Equation 3.30 is the Debye potential result presented by Wait (1985, equations 6.135 and 6.136) for the half space problem. The link between a Fourier transform representation (equation 3.28) and independent results in the Hankel transform domain (equation 3.30) validates the Fourier transform solution.

To check the correctness of potential rotations, Debye potential results can be rotated to a (π_x, π_z) representation. The Hankel transform Π_x representation of a x-directed source can be obtained by using the relation between Fourier transforms and Hankel transforms (equation 3.29) on the Fourier transform Π_x source representation (equation 3.6) to obtain

$$\pi_x^s(r,z) = \frac{Idl}{4\Pi\hat{\sigma}_0} \int_0^\infty \frac{\lambda}{u_0}\, e^{u_0(z-h)}\, J_0(\lambda r)\, d\lambda \qquad (3.31)$$

for $0 < z < h$.

The reflected components are given in equation 3.30 in terms of Π_z and Π_z^* as follows:

$$\begin{bmatrix} \Pi_z^r(\lambda,z) \\ \Pi_z^{r*}(\lambda,z) \end{bmatrix} = \frac{\partial_x u_0}{\lambda^2} \begin{bmatrix} R\ \Pi_x^s \\ 0 \end{bmatrix} \tag{3.32}$$

To obtain Π_x^r from Π_z^{r*}, Π_z^{r*} is rotated to Π_x^r and Π_x^{r*} using the $\underline{V}$ operator (equation 2.12), with the following result:

$$\begin{bmatrix} \Pi_x^r(\lambda,z) \\ \Pi_x^{r*}(\lambda,z) \end{bmatrix} = \frac{R^*\Pi_x^s}{(\partial_{xx}-\gamma^2)\lambda^2} \begin{bmatrix} \gamma^2\partial_y^2 \\ -\hat{\sigma}\partial_x\partial_y\partial_z \end{bmatrix} \tag{3.33}$$

To obtain a complete (Π_x,Π_z) representation, part of Π_x^r and all of Π_x^{r*} must be rotated back to Π_z. Using the fact that

$$1 = \frac{u^2\partial_x^2 + \gamma^2\partial_y^2}{(\partial_{xx}-\gamma^2)\lambda^2} \tag{3.34}$$

gives

$$\begin{bmatrix} \Pi_x^r(\lambda,z) \\ \Pi_x^{r*}(\lambda,z) \end{bmatrix} = \begin{bmatrix} R^*\Pi_x^s \\ 0 \end{bmatrix} + \frac{R^*\Pi_x^s}{(\partial_{xx}-\gamma^2)\lambda^2} \begin{bmatrix} -u^2\partial_x^2 \\ -\hat{\sigma}\partial_x\partial_y\partial_z \end{bmatrix} \tag{3.35}$$

Rotating the second term on the right-hand-side of equation 3.35 back to vertical and combining the reflected Π_z terms results in

$$\begin{bmatrix} \Pi_x^r(\lambda,z) \\ \Pi_x^{r*}(\lambda,z) \end{bmatrix} = \begin{bmatrix} R^*\Pi_x^s \\ 0 \end{bmatrix} \tag{3.36}$$

$$\begin{bmatrix} \Pi_z^r(\lambda,z) \\ \Pi_z^{r*}(\lambda,z) \end{bmatrix} = \frac{\partial_x u_0}{\lambda^2} \begin{bmatrix} (R + R^*)\Pi_x^s \\ 0 \end{bmatrix} \tag{3.37}$$

By combining the source and reflected terms in the full

integral expression we obtain

$$\begin{bmatrix}\pi_x(r,z)\\ \pi_z(r,z)\end{bmatrix} =$$

$$\begin{bmatrix} \frac{Idl}{4\Pi\hat{\sigma}_0} & \int_0^\infty \frac{\lambda}{u_0}\left[e^{u_0 z} + R^* e^{-u_0 z}\right]e^{-u_0 h} J_0(\lambda r)d\lambda \\ \frac{-Idl}{4\Pi\hat{\sigma}_0}\,\partial_x & \int_0^\infty \frac{R + R^*}{\lambda} e^{-u_0(z+h)} J_0(\lambda r)d\lambda \end{bmatrix} \qquad (3.38)$$

for $0 < z < h$.

which is the complete expression for (π_x,π_z) potentials over a half space (Wait, 1982). By showing the relationships between differing representations, we demonstrate the utility and correctness of the rotation operators. Potential representations can be transformed from one orientation to another directly without having to rederive expressions from first principles.

The source representations developed in this chapter include all of the source types used in CSAMT. Fourier transform representations for electric bipole, line, and rectangular loop sources have been presented, using the HED as a basic building block. Naturally excited fields can be represented by magnetic dipole or line sources elevated above the earth's surface or by a single down-going plane-wave component. Although the theme of this

theoretical development is CSAMT, the results are general and can be applied to other electromagnetic exploration techniques. A catalog of source representations has been derived. The next step is to describe the interaction of electromagnetic fields with a plane-layered earth.

CHAPTER 4

HORIZONTAL LAYERING

The source representations developed in the previous chapter model half-space fields. Grounded electric bipole, horizontal loop, and natural field sources are presented in terms of their plane-wave spectrum in the Fourier transform (k_x,k_y,z) domain. Chapter 3 also includes source representations in the Hankel transform domain and in closed form, results which will be applied in this section. Interaction with a uniform half-space is explicitly included in the source representations presented in chapter 3. The next step in developing a representative model is to add the effects of subsurface layering as a modification to a homogeneous half-space.

The amount of numerical computation needed for model evaluation is reduced by treating the effects of subsurface layering as a modification to a uniform half-space. The effects of subsurface layering have been described by Wait (1953, 1970, 1980a, 1982, 1985) in terms of a recursive expression. Wait's recursive form is rederived here in terms of vertical electric and magnetic currents. Wait's recursive solution can be rearranged into a form which is useful both for evaluation of the effects of known

subsurface layering and for directly inverting magnetotelluric data to obtain parameter estimates for layering when the subsurface geology is unknown. Ideas presented by Koefoed (1979) for direct interpretation of resistivity data and by Keceli (1983) for the direct interpretation of magnetotelluric data are combined and extended to treat the case of direct interpretation of magnetotelluric and far-field CSAMT measurements over a multiply layered earth.

For the single plane-wave source usually used for magnetotelluric modeling, plane layered earths are easily evaluated. For a general excitation however, the modification introduced by horizontal layering must be evaluated by integrating a Hankel transform. Efficient convolution methods (Anderson, 1974, 1982, 1984, and Johansen and Sorenson, 1979) exist for evaluation of Hankel transforms. Anderson (1974) documents a computer program for evaluating electromagnetic fields around a finite length HED source on or above the surface of a layered earth.

There are many other approaches to evaluation of the Sommerfeld integral which results from a Hankel transform representation of a plane-layered earth excited by a dipole source. The configuration of source, receiver, frequency, and material properties determine the applicability of each

method. Habashy, Kong, and Tsang (1985) compare several methods for computing fields due to a dipole source on or within a layered earth. Habashy, et al. (1985), compare brute force numerical integration, mode evaluation, source-image representation, and a hybrid method combining modes and source-images. For CSAMT-like geometries, Habashy, et al. (1985), conclude that modal or hybrid modal-image methods are the best approaches. The idea of hybrid representations is also advanced in a paper by Kan and Clay (1979). Kan and Clay split a Hankel transform representation for a HED on a layered earth into surface wave part and a source-image part. For CSAMT configurations, the idea of a hybrid representation can be combined with Wait's (1961) and Hill and Wait's (1973a, 1973b) closed-form solutions for half-space fields to develop an efficient algorithm for the computation of fields about an HED source exciting a layered earth. In an extension to previous work, an efficient hybrid form for computation of electromagnetic fields excited by a HED on the surface of a plane-layered earth is presented here.

Reflection and Transmission from Horizontal Layers

Horizontal layering is the simplest extension to a uniform earth. The choice of vertical currents for field

representation allows a straight-forward solution to the plane layered problem. The boundary conditions at interfaces are the same as for the air-earth interface described in the development of reflection and transmission coefficients for a half-space. J_z, $\frac{\partial_z J_z}{\hat{\sigma}}$, M_z, and $\frac{\partial_z M_z}{\hat{\mu}}$ are continuous across horizontal interfaces. For horizontal layers there is no coupling between the vertical components of electric and magnetic current. Reflection and transmission coefficients for J_z and M_z are independent and can be solved for separately.

A two-layer geometry is depicted in Figure 4.1. The model has three regions. Air fills the upper half space ($z > 0$) and has electrical properties denoted by a zero subscript, complex conductivity ($\hat{\sigma}_0 = i\omega\varepsilon_0$) and complex permeability ($\hat{\mu}_0 = -i\omega\mu_0$). Region 1 represents an overburden layer with a complex conductivity of $\hat{\sigma}_1 = \sigma_1 + i\omega\varepsilon_1$, a complex permeability of $\hat{\mu}_1 = -i\omega\mu_1$, and a thickness of h. The lower half space has a complex conductivity of $\hat{\sigma}_2$ and a complex permeability of $\hat{\mu}_2$.

Applying the boundary conditions at the air-earth interface ($z = 0$) and at the bottom of the overburden layer ($z = -h$) gives four equations for J_z

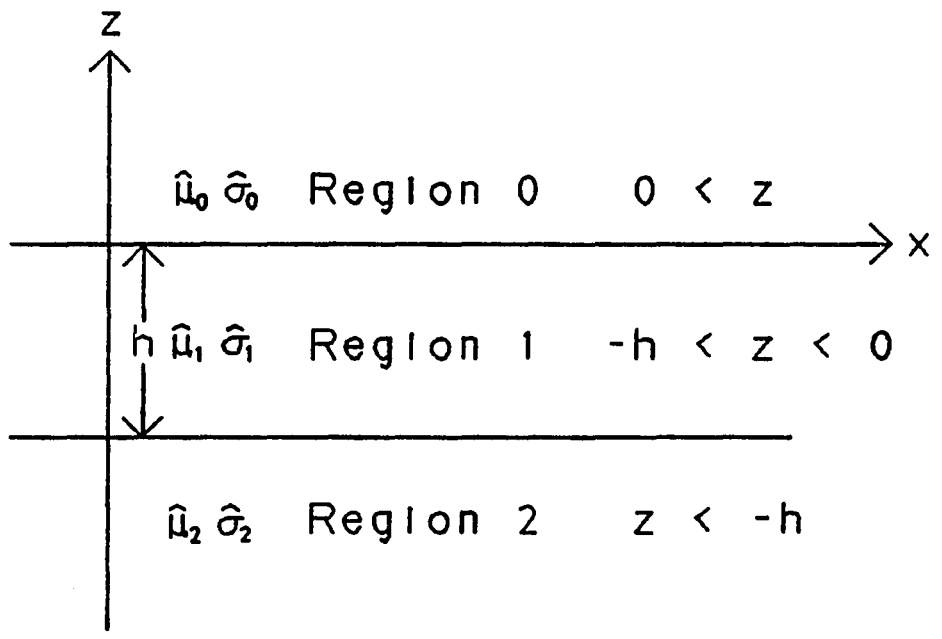

Figure 4.1 Cross-section of Two-layer Model

Three regions are separated by two horizontal, plane interfaces, one at at z = 0 and one at z = -h. The z axis is vertical with z positive upwards.

$$J_{z0}\Big|_{z=0} = J_{z1}\Big|_{z=0} \rightarrow (1 + g_0) = a(1 + g_1) \qquad (4.1)$$

$$\frac{\partial_z}{\partial_0} J_{z0}\Big|_{z=0} = \frac{\partial_z}{\partial_1} J_{z1}\Big|_{z=0} \rightarrow K_0(1 - g_0) = aK_1(1 - g_1) \qquad (4.2)$$

$$J_{z1}\Big|_{z=h} = J_{z2}\Big|_{z=h} \rightarrow a(e^{-u_1h} + g_1e^{u_1h}) = T^{\downarrow} \qquad (4.3)$$

$$\frac{\partial_z}{\partial_1} J_{z1}\Big|_{z=h} = \frac{\partial_z}{\partial_2} J_{z2}\Big|_{z=h} \rightarrow aK_1(e^{-u_1h} - g_1e^{u_1h}) = K_2T^{\downarrow} \qquad (4.4)$$

with the four unknowns, g_0, a, g_1, and $T^{\downarrow}$. Dividing equation 4.4 by equation 4.3 gives an impedance boundary condition at the lower interface, viz

$$K_2 = K_1 \frac{1 + g_1\exp(2u_1h)}{1 - g_1\exp(2u_1h)} \qquad (4.5)$$

K_2 is the impedance at the top of the lower half-space. Solving for g_1 in equation 4.5 gives

$$g_1 = R_1\exp(-2u_1h) \qquad (4.6)$$

where

$$R_1 = \frac{K_1 - K_2}{K_1 + K_2}$$

As shown in Figure 4.2, the reflectance function, g_1, represents plane-wave propagation from the surface down to the lower interface ($\exp(-u_1h)$), reflection from the lower interface (R_1), and propagation back to the surface ($\exp(-u_1h)$).

To solve for the surface reflection coefficient, g_0, the impedance boundary condition is applied at the

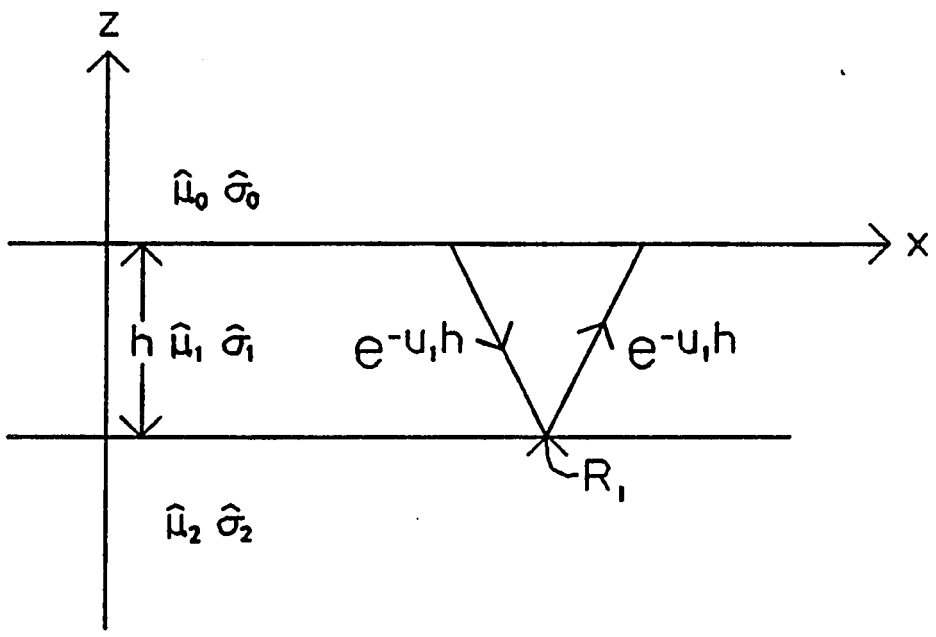

Figure 4.2 Geometric Interpretation of Reflectance

The two-layer reflectance function, $g(\lambda) = R_1 e^{-2u_1 h}$, represents transmission from the surface down to an interface at $z = -h$, $\exp(-u_1 h)$, reflection off of the interface, R_1, and transmission back up to the surface, $\exp(-u_1 h)$.

air-earth interface (z = 0). Dividing equation 4.2 by equation 4.1 gives surface impedance, Z_1, as

$$Z_1 = K_0\frac{(1 - g_0)}{(1 + g_0)} = K_1\frac{(1 - g_1)}{(1 + g_1)} \tag{4.7}$$

The right-hand side of equation 4.7 is an expression of Z_1 in terms of the known function g_1. Rearranging the right-hand side of equation 4.7 gives the familiar transmission-line relationship for Z_j (Wait, 1985)

$$Z_1 = K_1\frac{(1 - g_1)}{(1 + g_1)} = K_1\frac{(K_2 + K_1 \tanh(u_1h))}{(K_1 + K_2 \tanh(u_1h))} \tag{4.8}$$

The middle term in equation 4.7 can be solved for the surface reflection coefficient, g_0, in terms of Z_1

$$g_0 = \frac{(K_0 - Z_1)}{(K_0 + Z_1)} \tag{4.9}$$

To solve for the transmission coefficient, $T^{\downarrow}$, g_1 can be eliminated by adding equations 4.1 and 4.2 to get

$$T^{\downarrow} = aT_1^{\downarrow}\exp(-u_1h) \tag{4.10}$$

where

$$T_1^{\downarrow} = \frac{2K_1}{K_1 + K_2}$$

To isolate the layer source term, a, equation 4.1 and equation 4.2 are added and solved for a to get

$$a = \frac{T_0^{\downarrow}}{1 - R_0^{\uparrow} g_1} \tag{4.11}$$

where

$$T_0^{\downarrow} = \frac{2K_0}{K_0 + K_1}$$

and

$$R_0^{\uparrow} = \frac{K_1 - K_0}{K_1 + K_0}$$

which gives a complete expression for the total transmission coefficient

$$T^{\downarrow} = \frac{T_0^{\downarrow} T_1^{\downarrow}}{1 - R_0^{\uparrow} g_1} \exp(-u_1 h) \tag{4.12}$$

For a physical interpretation of $T^{\downarrow}$, the denominator, $1 - R_0^{\uparrow} g_1$, can be expanded in a series to give

$$T^{\downarrow} = T_0^{\downarrow} T_1^{\downarrow} \exp(-u_1 h)[1 + R_0^{\uparrow} g_1 + (R_0^{\uparrow} g_1)^2 + \text{h.o.t.}] \tag{4.13}$$

The transmission coefficient includes transmission through the air-earth interface, $T_0^{\downarrow}$, propagation through the overburden layer, $\exp(-u_1 h)$, and transmission through the lower interface, $T_1^{\downarrow}$. The series in $R_0^{\uparrow} g_1$ represents multiple reflections within the overburden layer. $R_0^{\uparrow}$ is the reflection off the underside of the air-earth interface, while $g_1 = R_1 \exp(-2u_1 h)$ includes the effects of two-way travel through the overburden layer and reflection off the top of the lower interface.

The extension of results from the two layer case to multiple layers is straightforward because of the recursive

form of the expression for surface impedance, equation 4.8 (Wait, 1953, 1970, 1982, 1985). Multiple layer problems can be solved from the bottom up. Figure 4.3 represents an earth model with M layers. The impedance at the top of the lower half-space is $Z_m = K_m$. Equation 4.8 gives the impedance at the top of the next layer as

$$Z_{m-1} = K_{m-1}\frac{(Z_m + K_{m-1}\tanh(u_{m-1}h_{m-1}))}{(K_{m-1} + Z_m \tanh(u_{m-1}h_{m-1}))} \qquad (4.14)$$

The impedance at the top of layer m-2 can be calculated by replacing m with m-1 and m-1 with m-2 in equation 4.14. The impedance at the surface of an earth with arbitrarily many subsurface layers can be computed by working recursively from bottom to top.

Solutions to the multiple layer problem for vertical electric currents are concisely stated in the classic transmission line form. Solutions for vertical magnetic currents can also be cast in the transmission line format. The reflection coefficient for vertical magnetic currents over a horizontally layered earth is

$$g_0^* = \frac{(N_0 - Y_1)}{(N_0 + Y_1)} \qquad (4.15)$$

Where the surface admittance, Y, is given recursively in transmission line form as

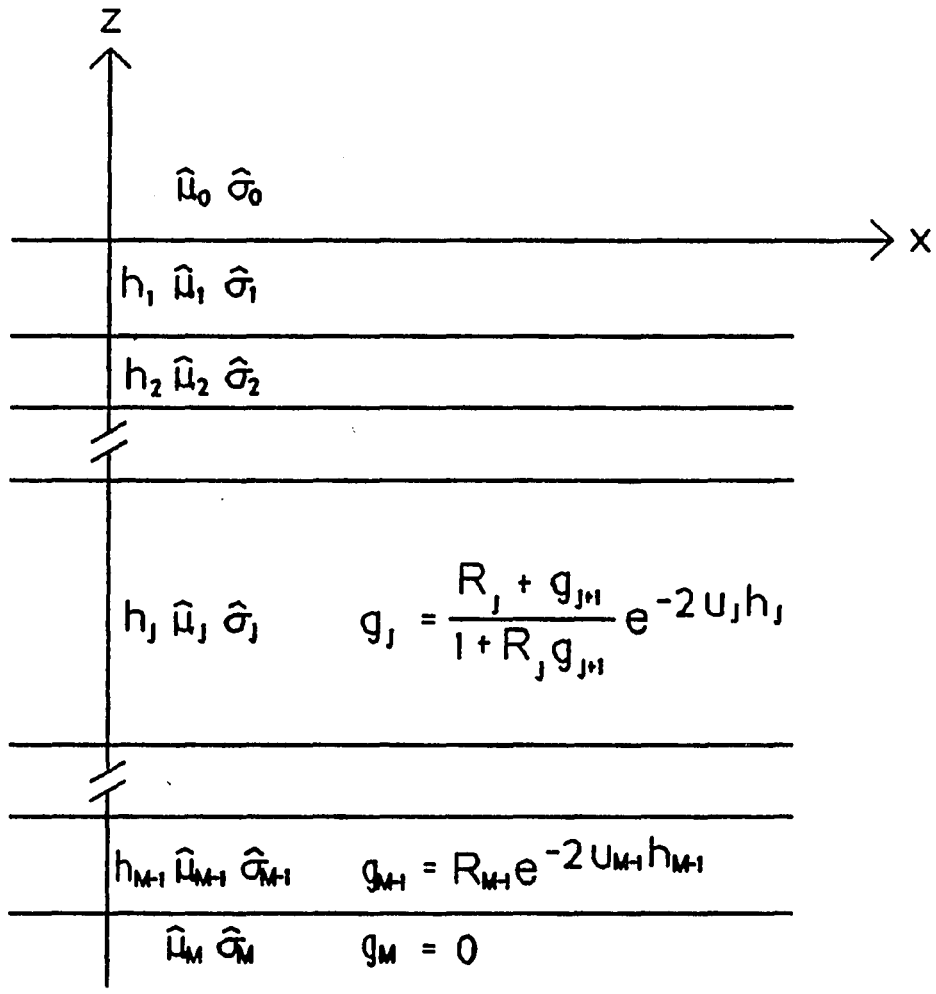

Figure 4.3 Cross-section of M-layer Model.

Recursive relationships for $g_j(\lambda)$ allow easy computation of reflection from an entire stack of plane-layers.

$$Y_1 = N_1 \frac{(Y_2 + N_1 \tanh(u_1 h))}{(N_1 + Y_2 \tanh(u_1 h))} \qquad (4.16)$$

with

$$N_j = \frac{u_j}{\hat{\mu}_j}$$

All of the results derived for vertical electric currents can be applied directly to vertical magnetic currents with g^* replacing g, R^* replacing R, $T^{\downarrow *}$ replacing $T^{\downarrow}$, Y_j replacing Z_j, N_j replacing K_j, and $\hat{\mu}_j$ replacing $\hat{\sigma}_j$. The vertical components of electric and magnetic currents are decoupled in horizontally layered geometries. Horizontal layers do not mix direct current and inductive source effects.

The recursive transmission-line form for solutions to layered earth problems is not new (Wait, 1953). The resistivity transform kernel is formed by taking the low frequency limit ($\omega \rightarrow 0$) of equation 4.8 which gives

$$Z_1 = \lambda \rho_1 \frac{(\rho_2 + \rho_1 \tanh(\lambda h))}{(\rho_1 + \rho_2 \tanh(\lambda h))} \qquad (4.17)$$

Koefoed (1979) describes the transmission line solution for the direct current resistivity kernel as the Pekeris recurrence relationship, and credits Pekeris (1940) with developing it for modeling direct current resistivity.

Another special case of practical interest in magnetotellurics is the limit as $\lambda \rightarrow 0$, indicating a

normally incident plane wave. Normal incidence is often assumed in magnetotelluric interpretation. With $\mu_j = \mu_0$, the transmission line impedance relationship simplifies to

$$Z_1 = \sqrt{i\omega\mu\rho_1}\,\frac{(Z_2 + \sqrt{i\omega\mu\rho_1}\,\tanh(\gamma_1 h))}{(\sqrt{i\omega\mu\rho_1} + Z_2\,\tanh(\gamma_1 h))} \qquad (4.18)$$

As pointed out by Keceli (1983), the ideas developed by Koefoed (1979) for the direct interpretation of resistivity data can be applied to magnetotelluric data.

Direct Interpretation of Plane-wave Data

A scheme for the direct inversion of magnetotelluric data into layered earth parameters evolves from the properties of the reflectance function $g_1(\omega) = R_1\exp(-2\gamma_1 h)$. Taking the log of $g_1(\omega)$ gives

$$\mathrm{Re}(\ln(g_1(\omega))) = \ln|R_1| - \sqrt{2\omega\mu}\,h_1/\sqrt{\rho_1} \qquad (4.19)$$

$$\mathrm{Im}(\ln(g_1(\omega))) = \mathrm{phase}(R_1) - \sqrt{2\omega\mu}\,h_1/\sqrt{\rho_1} \qquad (4.20)$$

As Keceli (1983) points out, for the two layer-case, a plot of $\mathrm{Re}(\ln(g_1(\omega)))$ vs $\sqrt{\omega}$ is a straight line with an intercept of $\ln|R_1|$ and a slope of $-\sqrt{2\mu_0}\,h/\sqrt{\rho_1}$ (Figure 4.4). The reflectance function $g_1(\omega)$ can be directly calculated from magnetotelluric observations.

Observed data from magnetotelluric surveys is a set of surface impedances, $Z(\omega)$, measured over a range of

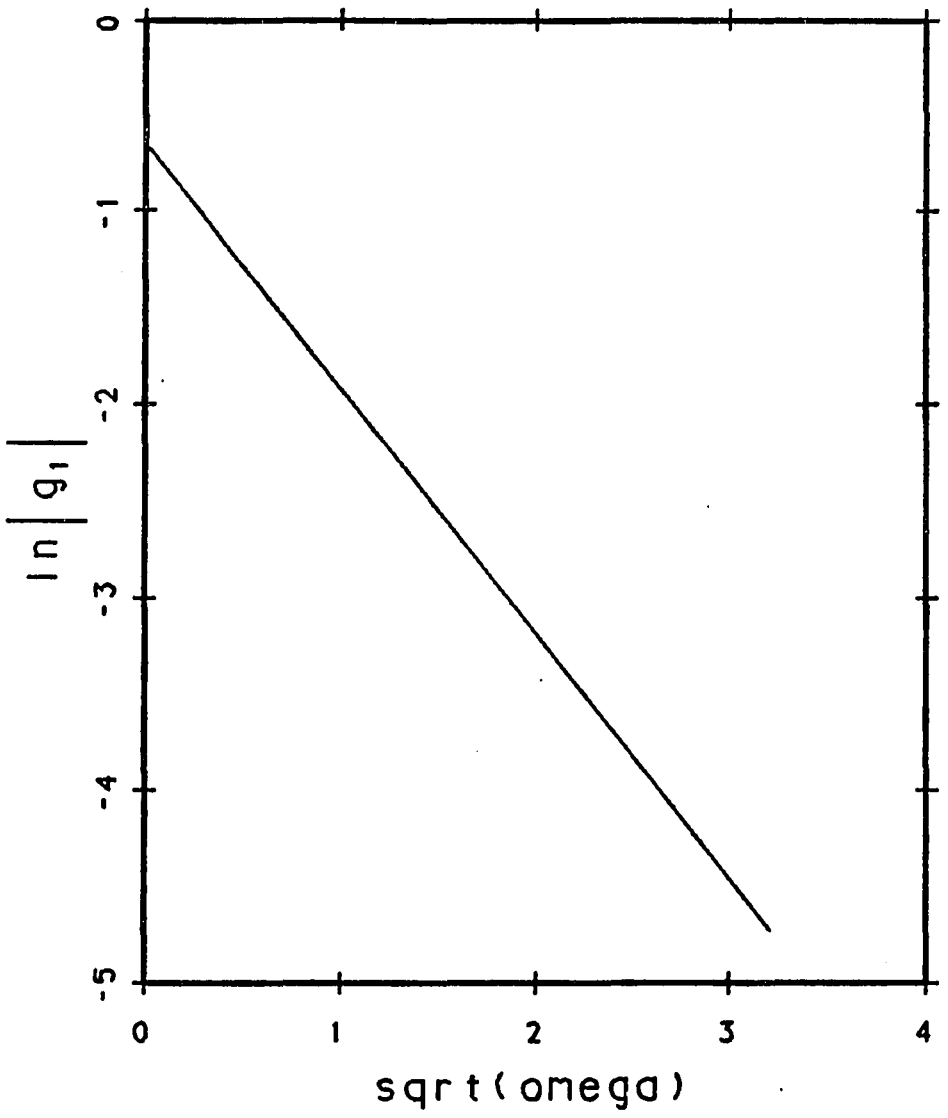

Figure 4.4 Direct Interpretation from Reflectance

For the two-layer case, a plot of $\ln(g_1)$ vs $\sqrt{\omega}$ is a straight line. For more than two layers, fitting a straight line to higher frequency measurements gives parameters of top-most layer.

frequencies. Using the three highest frequencies, an accurate estimate of ρ_1 can be made. Knowing ρ_1, the reflectance function $g_1(\omega)$ can be calculated from observed data

$$g_1(\omega) = \frac{1 - Q}{1 + Q} \tag{4.21}$$

where

$$Q = \frac{Z(\omega)}{K_1}$$

and

$$K_1 = \gamma_1 \rho_1$$

An estimate of layer parameters $h_1/\sqrt{\rho_1}$ and R_1 can be made by fitting a straight line to $\mathrm{Re}(\ln(g_1(\omega)))$ vs $\sqrt{\omega}$. Redundant information about layer thickness is obtained by extending Keceli's suggestion to include fitting a second line to $\mathrm{Im}(\ln(g_1(\omega)))$ vs $\sqrt{\omega}$. Using redundant information increases the robustness of parameter estimation.

Data measured for the highest frequencies can always be fitted by a two-layer model. If the data are obtained over a two-layer geologic environment, measured impedances for all frequencies will be fit by a two-layer model. Deviation of $\ln(g_1(\omega))$ vs $\sqrt{\omega}$ from a straight line at lower frequencies indicates the influence of a deeper subsurface layer, and the need for adding a third layer to the model.

In view of the utility of the reflectance function $g_1(\omega)$ for direct interpretation of the two layer case, it is

useful to recast the classic transmission line formula in terms of reflectance functions. For a M-layer problem, the reflectance function at the M'th interface is zero.

$$g_{m+1} = 0 \qquad (4.22)$$

The reflectance function at the top of layer m-1 is

$$g_m = \frac{(R_m + g_{m+1})}{(1 + R_m g_{m+1})} \exp(-2\gamma_m h_m) \qquad (4.23)$$

where

$$R_m = \frac{\sqrt{\rho_m} - \sqrt{\rho_{m+1}}}{\sqrt{\rho_m} + \sqrt{\rho_{m+1}}}$$

As for the transmission line formula for impedances, equation 4.23 can be evaluated recursively from the bottom half-space to the top of a stack of arbitrarily many layers. This recursive relationship for g_m is computationally efficient, R_m is computed with real arithmetic and only one exponential term per layer must be evaluated.

For recursion from the top down, equation 4.23 can be inverted to yield

$$g_{m+1} = \frac{(R_a - R_m)}{(1 - R_m R_a)} \qquad (4.24)$$

where

$$R_a = g_m \exp(2\gamma_m h_m)$$

For the interpretation of magnetotelluric data, equation 4.24 allows direct inversion of impedance measurements to multiple layer models. Since $g_1(\omega)$, $h_1/\sqrt{\rho_1}$, and R_1 are known from higher frequency measurements, equation 4.24 can

be used to "strip off" the effects of the top-most layer. With the new $g_2(\omega)$, two-layer interpretation can be continued until either $g_j(\omega)$ has been fit for all remaining frequencies or deviation from a straight line indicates the influence of yet another layer. An entire sequence of layer parameters can be inferred by fitting $g_j(\omega)$ from the highest measured frequencies to the lowest.

Direct interpretation can give good estimates of layered model parameters. A drawback however, is instability of the stripping procedure. Small errors in estimates of ρ_1, $h_1/\sqrt{\rho_1}$, and R_1 are amplified during stripping and can cause large errors in estimations of $g_2(\omega)$ (Figure 4.5). A second stripping amplifies errors even further. Koefoed (1979) describes a procedure for keeping track of error amplification during stripping. Monitoring error amplification is a crucial key to the successful application of direct interpretation methods.

Direct interpretation is strengthened by use in conjunction with iterative inversion methods. Direct methods can be used to compute layered-earth models which are approximately correct. Iterative inversion methods are very good at improving the fit of approximate models. Iterative inversion techniques can also be used to explore the range of model parameters which give an adequate fit to

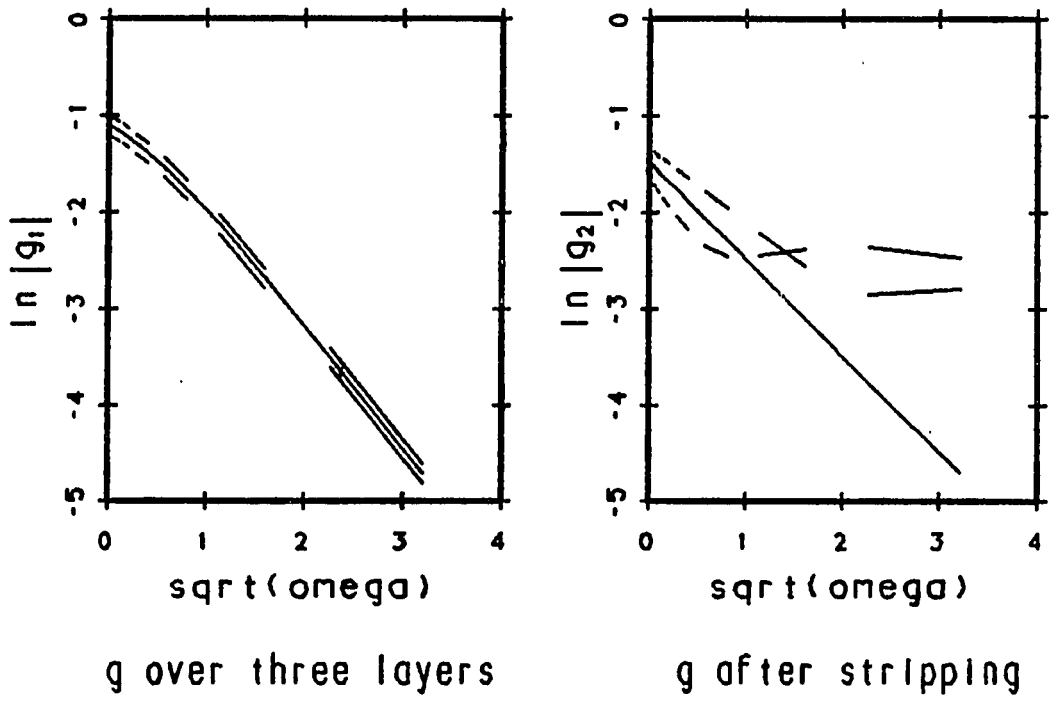

Figure 4.5 Error Amplification due to Layer Stripping

The top-to-bottom recursion form for g_j amplifies errors. Parameter estimates for the second layer must include the effects of amplified error bounds.

the data.

Assal and Mahmoud (1987) describe an inversion technique for direct-current resistivity. Their method uses the reflectance function, $g(\lambda)$, form of the resistivity kernel to obtain a linear system for multiple-layer models. Their results for direct-current resistivity can be extended directly to the inversion of magnetotelluric data.

Interpretation methods for magnetotelluric data depend upon the simplifying assumption that the source is well represented by a single, normally incident, homogeneous plane wave. In general this may not be true (Wait, 1954, 1982). For CSAMT surveys much of the data which is actually collected can not be accurately modeled using magnetotelluric algorithms. For general excitation of a plane-layered earth, a Hankel transform must be inverted.

Computer Evaluation of Plane-layered Models

For excitation by a HED source, the effect of horizontal layering must be evaluated by integrating a Hankel transform. A Hankel transform representation for surface fields generated by a HED on the surface of an earth with M horizontal layers is given in terms of $\underline{\pi}_z$ by

$$\begin{bmatrix} \pi_z(r) \\ \pi_z^*(r) \end{bmatrix} = \begin{bmatrix} \frac{Idl}{4\Pi\partial_1}\,\partial_x \int_0^\infty \frac{T_0^{\downarrow}}{\lambda}\left[1 + g_0'\right]J_0(\lambda r)d\lambda \\ -\frac{Idl}{4\Pi}\,\partial_y \int_0^\infty \frac{T_0^{\downarrow *}}{\lambda^2}\left[1 + g_0^{*\prime}\right]J_0(\lambda r)d\lambda \end{bmatrix} \qquad (4.25)$$

where

$$g_0' = T_0^{\uparrow}\frac{g_1}{1 + R_0 g_1} \qquad g_0^{*\prime} = T_0^{\uparrow *}\frac{g_1^*}{1 + R_0^* g_1^*}$$

$$g_m = \frac{R_m + g_{m1}}{1 + R_m g_{m+1}}\,e^{-2u_m h_m} \qquad g_m^* = \frac{R_m^* + g_{m1}^*}{1 + R_m^* g_{m+1}^*}\,e^{-2u_m h_m}$$

$$g_M = 0 \qquad g_M^* = 0$$

$$T_0^{\downarrow} = \frac{2K_0}{K_0 + K_1} \qquad T_0^{\downarrow *} = \frac{2N_0}{N_0 + N_1}$$

$$T_0^{\uparrow} = \frac{2K_1}{K_0 + K_1} \qquad T_0^{\uparrow *} = \frac{2N_1}{N_0 + N_1}$$

and

$$R_m = \frac{K_m - K_{m+1}}{K_m + K_{m+1}} \qquad R_m^* = \frac{N_m - N_{m+1}}{N_m + N_{m+1}}$$

The kernels, g_0' and $g_0^{*\prime}$, in equation 4.25 represent a modification to half-space fields caused by subsurface layers. To minimize computational effort, as much as possible of equation 4.25 should be evaluated analytically. Wait's (1961) closed-form expressions for half-space fields can be used to reduce the numerical work involved in evaluating equation 4.25. Wait's solutions assume that the complex conductivity of air is zero, $\partial_0 = 0$, and that

permeability is uniform everywhere, $\mu_0 = \mu_1$. Both assumptions are valid for typical CSAMT applications. Subtracting the half-space contribution from equation 4.25 and substituting the quasi-static forms for $T_0^{\downarrow}$ and $T_0^{\downarrow *}$ creates an expression which treats subsurface layering as a modification to a half-space. Writing the modification contribution as $\underline{\pi_z}'$, the integral equation becomes

$$\begin{bmatrix} \pi_z'(r) \\ \pi_z^{*\prime}(r) \end{bmatrix} = \begin{bmatrix} \frac{Idl}{2\pi\partial_1}\,\partial_x \int_0^{\infty} \frac{g_0'}{\lambda} J_0(\lambda r)\,d\lambda \\ -\frac{Idl}{2\pi}\,\partial_y \int_0^{\infty} \frac{g_0^{*\prime}}{\lambda(\lambda+u_1)} J_0(\lambda r)\,d\lambda \end{bmatrix} \qquad (4.26)$$

The modified kernels, g_0' and $g_0^{*\prime}$, in equation 4.26 include an exponential term of $e^{-2u_1 h}$, which drives both kernels to zero exponentially for large values of λ. The modified kernels also include the upward transmission coefficients $T_0^{\uparrow}$ and $T_0^{\uparrow *}$. The transmission coefficients in the quasi-static limit and with $\mu_0 = \mu_1$ are

$$T_0^{\uparrow} = 1 - R_0 = 0 \qquad (4.27)$$

$$T_0^{\uparrow *} = 1 - R_0^{*} = \frac{2u_1}{\lambda + u_1} \qquad (4.28)$$

In the presence of the differential operator ∂_z, the upward transmission coefficients are modified to

$$\partial_z T_0^{\uparrow} = -u_1(1 + R_0) = -2u_1 \tag{4.29}$$

$$\partial_z T_0^{\uparrow *} = -u_1(1 + R_0^*) = \frac{-2u_1\lambda}{\lambda + u_1} \tag{4.30}$$

Equations 4.27 through 4.30 have interesting consequences. The layering modification carried in the electric Hertz potential component π_z' only effects electromagnetic field components related to $\partial_z\pi_z$, i.e. e_x and e_y. π_z' is zero and does not contribute to any component of $\underline{h}$ in the quasi-static limit. The magnetic Hertz potential component $\pi_z^{*\prime}$ affects both $\underline{e}$ and $\underline{h}$ for nonzero frequencies. In the static limit π_z^* is zero. Static magnetic fields are not perturbed by horizontal subsurface layering, an observation made by Stefanesu (1929, 1963) in a description of magnetometric resistivity theory.

Layered earth fields can be computed using equation 4.26 and analytical expressions for half-space fields. The modifications to half-space field components caused by horizontal subsurface layering are expressed by

$$e_x' = \frac{Idl}{\Pi\partial_1}\left\{\frac{x^2-y^2}{r^3}\int_0^\infty (f-f^*)J_1(\lambda r)d\lambda - \int_0^\infty\left[\frac{x^2}{r^2}f + \frac{y^2}{r^2}f^*\right]\lambda J_0(\lambda r)d\lambda\right\} \tag{4.31}$$

$$e_y' = \frac{Idl}{\Pi\partial_1}\frac{xy}{r^2}\left\{\frac{2}{r}\int_0^\infty (f-f^*)J_1(\lambda r)d\lambda - \int_0^\infty (f-f^*)\lambda J_0(\lambda r)d\lambda\right\} \tag{4.32}$$

$$h_x' = \frac{Idl}{\Pi\gamma_1^2}\frac{xy}{r^2}\left\{\frac{2}{r}\int_0^\infty f^*\,\lambda J_1(\lambda r)d\lambda - \int_0^\infty f^*\,\lambda^2 J_0(\lambda r)d\lambda\right\} \tag{4.33}$$

$$h_y' = \frac{Idl}{\Pi\gamma_1^2}\left\{\frac{y^2-x^2}{r^3}\int_0^\infty f^*\,\lambda J_1(\lambda r)d\lambda - \frac{y^2}{r^2}\int_0^\infty f^*\,\lambda^2 J_0(\lambda r)d\lambda\right\} \tag{4.34}$$

and finally

$$h_z' = \frac{Idl}{\Pi\gamma_1^2}\frac{y}{r}\int_0^\infty f^*\lambda^2 J_1(\lambda r)d\lambda \tag{4.35}$$

where

$$f(\lambda) = \frac{u_1 R_1}{1 + g_1} e^{-2u_1 h_1}$$

and

$$f^*(\lambda) = \frac{u_1 R_0^* R_1^*}{1 + R_1^* g_1} e^{-2u_1 h_1}$$

Anderson's (1974) program EMFIN evaluates Wait's (1961) expressions for half-space fields and expressions equivalent to equations 4.31 through 4.35 to compute fields generated by a HED on the surface of a plane-layered earth. However, the modified kernels $f(\lambda)$ and $f^*(\lambda)$ can be reduced even further.

Far-field data from CSAMT surveys can be modeled successfully with magnetotelluric algorithms. For measurements made at a large electrical distance from the transmitter, most of the source energy is propagating as a surface wave. The direct, through-the-earth signal is insignificant. Since most of the interaction with subsurface layers in the far field is by energy traveling almost vertically, it can be anticipated that the behavior of $f(\lambda)$ and $f^*(\lambda)$ for small values of λ controls electromagnetic far-field behavior. The modified kernels $f(\lambda)$ and $f^*(\lambda)$ are well approximated at small values of λ by

$$f(\lambda) \cong (f_0 + \lambda f_1)e^{-2\lambda h_1} \tag{4.36}$$

$$f^*(\lambda) \cong (f_0^* + \lambda f_1^*)e^{-2\lambda h_1} \tag{4.37}$$

where the constants f_0, f_0^*, f_1, and f_1^* are determined by

$$f_0 = f(0) = f_0^* = f^*(0)$$

and

$$f_1 = \frac{f(\lambda_1)e^{2\lambda_1 h_1} - f_0}{\lambda_1} \quad \text{and} \quad f_1^* = \frac{f^*(\lambda_1)e^{2\lambda_1 h_1} - f_0^*}{\lambda_1}$$

where $\lambda_1 = \delta_1/50$

Equations 4.36 and 4.37 capture the behavior of $f(\lambda)$ and $f^*(\lambda)$ for small values of λ with a linear term. The exponential damping in equations 4.36 and 4.37 captures the behavior of $f(\lambda)$ and $f^*(\lambda)$ for large values of λ. Substituting the approximations for $f(\lambda)$ and $f^*(\lambda)$ into equations 4.31 through 4.35 results in a set of integrals which can be evaluated analytically using solutions of the form

$$\frac{1}{R} = \int_0^\infty e^{-\lambda z} J_0(\lambda r) d\lambda \qquad (4.38)$$

and

$$\frac{1}{r}\left[1 - \frac{z}{R}\right] = \int_0^\infty e^{-\lambda z} J_1(\lambda r) d\lambda \qquad (4.39)$$

where $R = \left[x^2 + y^2 + z^2\right]^{0.5}$.

after Wait (1982). Polynomials in λ in the integrands of equations 4.38 and 4.39 can be created by differentiation with respect to z. The results when evaluated with $z = 2h_1$ are relatively simple functions of R^{-n}. The equality $f_0 = f_0^*$ allows a series of cancellations which further simplify the analytical results. The closed-form expressions for field components are valid for large separations between transmitter and receiver. Defining the remainder kernels as

$$\Delta f(\lambda) = f(\lambda) - (f_0 + \lambda f_1)e^{-2\lambda h_1} \qquad (4.40)$$

$$\Delta f^*(\lambda) = f^*(\lambda) - (f_0^* + \lambda f_1^*)e^{-2\lambda h_1} \qquad (4.41)$$

the modifications to half-space fields caused by planar subsurface layering are expressed by

$$e'_x = \frac{Idl}{\Pi\hat{\sigma}_1}\left\{\frac{1}{R^3}\left[-zf_0 + \left[\frac{3x^2}{R^2} - 1\right]f_1 + \left[\frac{3y^2}{R^2} - 1\right]f_1^*\right]\Bigg|_{z\,=\,2h_1}\right. \tag{4.42}$$

$$\left. + \frac{x^2 - y^2}{r^3}\int_0^\infty(\Delta f - \Delta f^*)J_1(\lambda r)d\lambda - \int_0^\infty\left[\frac{x^2}{r^2}\Delta f + \frac{y^2}{r^2}\Delta f^*\right]\lambda J_0(\lambda r)d\lambda\right\},$$

$$e'_y = \frac{Idl}{\Pi\hat{\sigma}_1}\left\{\frac{1}{R^3}\left[\frac{3xy}{R^2}\right]\left[f_1 - f_1^*\right]\Bigg|_{z\,=\,2h_1}\right. \tag{4.43}$$

$$\left. + \frac{xy}{r^2}\left[\frac{2}{r}\int_0^\infty(\Delta f - \Delta f^*)J_1(\lambda r)d\lambda - \int_0^\infty(\Delta f - \Delta f^*)\lambda J_0(\lambda r)d\lambda\right]\right\}$$

$$h'_x = \frac{Idl}{\Pi\gamma_1^2}\left\{\frac{1}{R^3}\left[\left[\frac{xy}{R^2}\right]f_0^* + \left[\frac{8xyz}{R^4}\right]f_1^*\right]\Bigg|_{z\,=\,2h_1}\right. \tag{4.44}$$

$$\left. + \frac{xy}{r^2}\left[\frac{2}{r}\int_0^\infty\Delta f^*\lambda J_1(\lambda r)d\lambda - \int_0^\infty\Delta f^*\lambda^2 J_0(\lambda r)d\lambda\right]\right\}$$

$$h'_y = \frac{Idl}{\Pi\gamma_1^2}\left\{\frac{1}{R^3}\left[\left[\frac{3x^2}{R^2} - 1\right]f_0^* + \frac{z}{R^2}\left[\frac{8x^2}{R^2} - 1\right]f_1^*\right]\Bigg|_{z\,=\,2h_1}\right. \tag{4.45}$$

$$\left. + \frac{y^2 - x^2}{r^3}\int_0^\infty\Delta f^*\lambda J_1(\lambda r)d\lambda - \frac{y^2}{r^2}\int_0^\infty\Delta f^*\lambda^2 J_0(\lambda r)d\lambda\right\}$$

and finally

$$h'_z = \frac{Idl}{\Pi\gamma_1^2}\left\{\frac{3x}{R^5}\left[zf_0^* + \left[\frac{5z^2}{R^2} - 1\right]f_1^*\right]\Bigg|_{z\,=\,2h_1} + \frac{y}{r}\int_0^\infty\Delta f^*\lambda^2 J_1(\lambda r)d\lambda\right\} \tag{4.46}$$

Equations 4.41 through 4.46 are hybrid expressions for the modifications to half-space field components caused by horizontal subsurface layering. The analytical terms are valid in the far field while the remaining integrals represent correction terms which are important in the transition zone and near field.

Plots of the magnitude of the near-field correction term kernels, $\Delta f(\lambda)$ and $\Delta f^*(\lambda)$ show a reduced basis relative to the original kernels $f(\lambda)$ and $f^*(\lambda)$. Figure 4.6 diplays log-log plots of $|\Delta f(\lambda)|$ vs λ as a solid line and $|f(\lambda)|$ vs λ as a dashed line. The correction-term kernel is driven to zero at both limits of integration. The correction-term kernel, $\Delta f(\lambda)$, has a maximum amplitude near $\lambda = \delta_1$, indicating that the near-field correction terms will make a significant contribution to the modified field components in the transition zone, where $r \cong \delta_1$. Plots of $|\Delta f^*(\lambda)|$ and $|f^*(\lambda)|$ show a similar result (Figure 4.7). The numerical correction terms represented as integrals in equations 4.42 through 4.46 do not make a significant contribution at large transmitter-receiver separations. The correction terms can be neglected in the far field. When numerical integration of the correction terms is required, in the transition zone and near-field, the reduced bases of the kernels $\Delta f(\lambda)$ and $\Delta f^*(\lambda)$ eases the computational effort required for

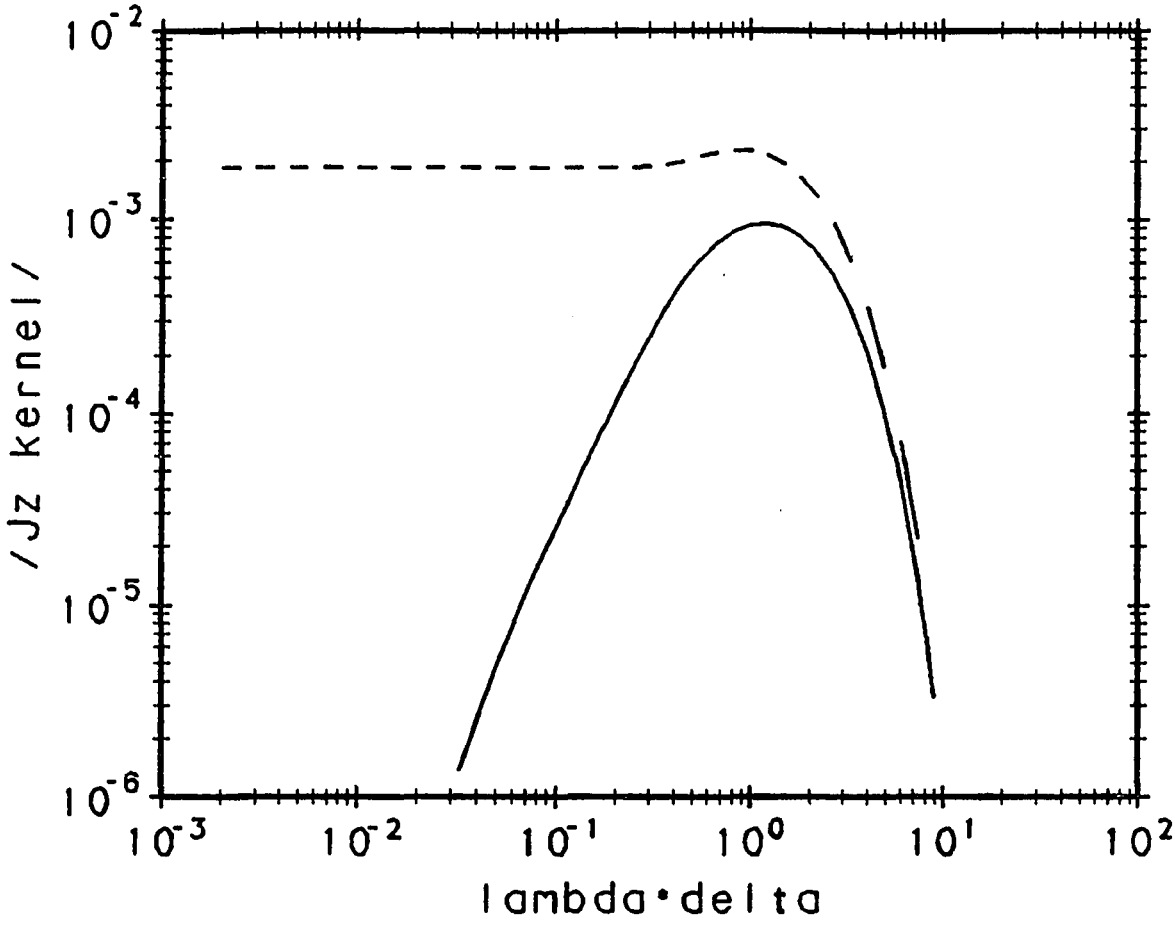

Figure 4.6 J_z Kernel for Correction Term in Hybrid Layered-earth Algorithm.

The convergence of the Hankel transform is greatly improved by subtracting a subsurface source-image from integral representation. The solid line is the modified kernel, $\Delta f(\lambda)$, the dashed line is the kernel $f(\lambda)$, for computing the modification to half-space fields necessary for multiple plane-layers.

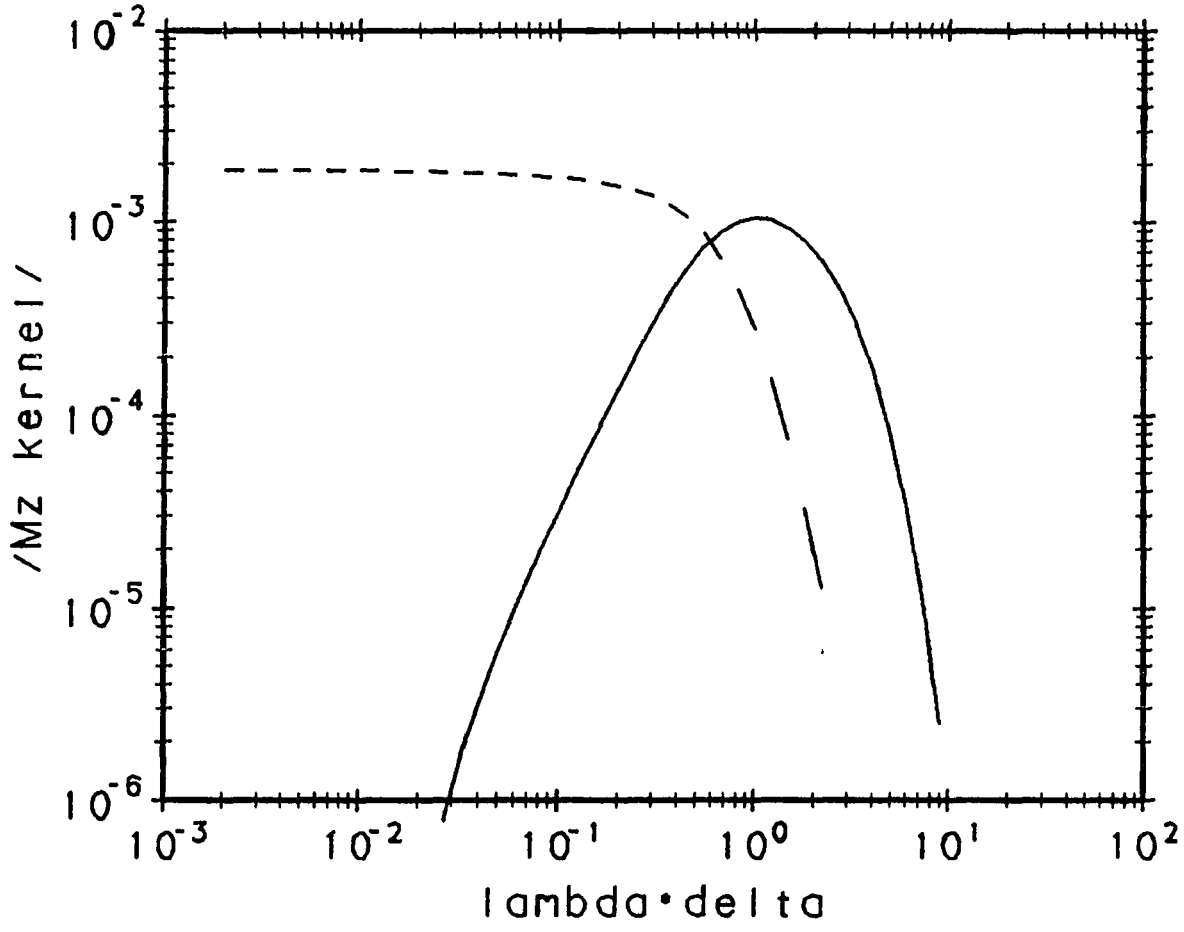

Figure 4.7 M_z Kernel for Correction Term in Hybrid Layered-earth Algorithm.

The convergence of the Hankel transform is greatly improved by subtracting a subsurface source-image from integral representation. The solid line is the modified kernel, $\Delta f^*(\lambda)$, the dashed line is the kernel $f^*(\lambda)$, for computing the modification to half-space fields necessary for multiple plane-layers.

evaluation.

Treating horizontal subsurface layers as a modification to a homogeneous half-space leads to efficient algorithms for the computation of fields excited by a HED source. In a similar manner, the problem of electromagnetic induction over a nonplanar interface can be treated as a perturbation to horizontal layering.

Chapter 5

UNDULATING INTERFACE

A logical extension to plane layered models is to compute the effects of undulations in layer thickness. The plane layered models developed in the previous section have the advantage of simplicity. Simple models allow the development of automated interpretation techniques. Layer thicknesses, however, often vary between observation sites. In routine CSAMT interpretation, the plane layered model is assumed to be an adequate representation of the geology under each observation site. The actual effects of changing layer thickness and of sloping interfaces are not considered. In this section, expressions for reflection from and transmission through an undulating interface are developed. The analysis includes closed-form expressions for first-order reflection and transmission coefficients, as well as a discussion of the errors involved in the approximate solution.

A relatively simple result is obtained for reflection from a non-planar interface by treating the problem as a perturbation to reflection from a flat, horizontal interface. Closed-form expressions are possible in a first-order approximation to reflection and

transmission from an undulating interface by a general plane wave with an arbitrary angle of incidence. There is an extensive literature dealing with the problem of electromagnetic scattering from rough surfaces. For the TE and TM plane waves used in magnetotelluric modeling, a well-developed theory exists for the undulating interface problem. Mann (1964) considers the case of two layers separated by a sinusoidal interface. Using a perturbation scheme, Mann derives a set of integral equations which can be solved exactly. Hughes (1973, 1974), Hughes and Wait (1975a), Wait and Chang (1976), and Hill and Wait (1982) investigate the effects of two-dimensional structures on TE and TM plane-wave fields. Geyer (1976) also examines the effects of subsurface structure on magnetotelluric measurements. Rosich and Wait (1977) consider perturbation solutions of all orders for the TM polarization. For fields generated by a line source, Hughes and Wait (1975b) estimate the effect of a sinusoidal interface between a overburden layer and basement. Perturbation solutions are relatively simple, but require that the amplitude and slope of undulations in the interface be small in terms of skin depths in the surrounding media. More general methods have been developed which are less restricted.

Waterman (1975), Karlsson (1981), Kristensson and

Strom (1982), and Karlson and Kristensson (1983) treat the problem of scattering from non-planar interfaces in terms of the T-matrix method. Although the approach is very general, it requires a considerable amount of numerical computation. Chuang and Kong (1982) investigate the scattering of microwaves from plowed fields using an approach similar to the T-matrix method. Chuang and Kong's (1982) results apply to a general angle of incidence, but require numerical integration along the interface to obtain reflection and transmission coefficients. A Fourier transformed, point-matching algorithm for computing the scattering of plane waves is developed by Jiracek (1972, 1973). Jiracek's "Rayleigh-FFT" method requires the numerical inversion of a large linear system of equations. Jiracek and co-workers have applied the Rayleigh-FFT approach to magnetotelluric modeling (Reddig, 1984, Reddig and Jiracek, 1984, Kojima, 1985, and Jiracek, Reddig, and Kojima, 1986). An iterative numerical approach for plane-wave scattering from surfaces with three-dimensional bumps is presented by van den Berg and DeHoop (1984). They describe a conjugate gradient method which, again, involves extensive numerical work. Numerical approaches to the problem allow solutions to more general problems, but at the cost of increased computation and, often, loss of insight.

Fields excited by a three-dimensional source can be represented as a spectrum of plane waves, as the Fourier transform source representations developed in chapter 3 show. For a practical solution to the problem of interaction of three-dimension source fields with an undulating interface, the reflection and transmission of each plane-wave component must be treated succinctly. Numerical solutions allow the treatment of more general problems, but at the cost of increased computational effort. Perturbation solutions are in closed form, but the undulations allowed in the model must be small in amplitude and slope. For a usable solution, the limitations of small slope and amplitude must be accepted. The approach chosen here extends the earlier work of Hughes (1973, 1974), Hughes and Wait (1975a, 1975b), Wait and Chang (1976), Rosich and Wait (1977), and Hill and Wait (1982) for TE and TM polarizations. The extension is from reflection of TE and TM modes only to a first-order perturbation solution for reflection and transmission of plane waves with an arbitrary, complex angle of incidence. The problem is first solved for surfaces with two-dimensional undulations and then extended to include three-dimensional undulations. An analysis of errors involved in the first-order approximation is included to give guidelines for the range of valid models.

Two-dimensional Undulations

Plane wave source representations and an analysis of reflection from plane layers are presented in the preceding sections. The problem of electromagnetic interaction with an undulating interface is reduced to the reflection and transmission of fields excited by a single plane wave component by using plane wave source representations. The geometry of the problem is depicted in Figure 5.1. An outline of the derivation procedure is presented in Table 5.1

For two-dimensional undulations, the interface is described by a finite Fourier series

$$s(x) = \sum_{j=-M}^{M} d_j \, e^{ik_j x} \tag{5.1}$$

where $d_0 = 0$ and $k_j = \Delta j$. The interface is a real-valued function, $s(x)$, which varies in the x direction and is uniform in the y direction. The slope of $s(x)$ is

$$\frac{ds}{dx}(x) = \sum_{j=-M}^{M} ik_j \, d_j \, e^{ik_j x} \tag{5.2}$$

The undulating interface, $s(x)$, separates two regions. The medium above the interface is characterized by a complex conductivity, $\hat{\sigma}_1 = \sigma_1 + i\omega\varepsilon_1$, and a complex permeability, $\hat{\mu}_1 = -i\omega\mu_1$. The region below the interface has the medium properties $\hat{\sigma}_2$ and $\hat{\mu}_2$. In many geological environments

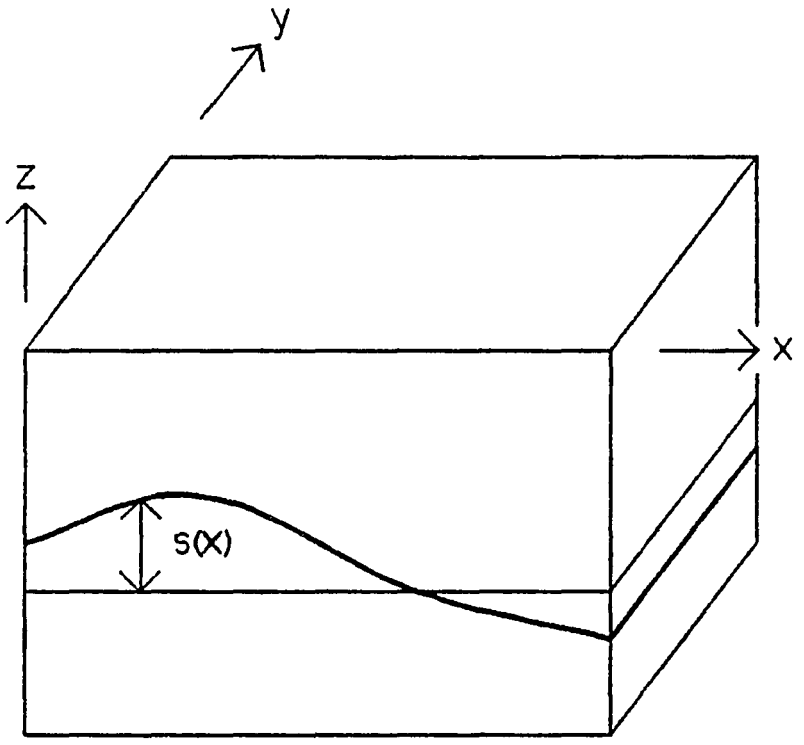

Figure 5.1 Block diagram of Two-dimensional Undulating Interface Model

The interface is described by a real-valued function, s(x), which has gentle slope and has small amplitude in terms of skin depths.

Table 5.1 Outline of Derivation Procedure

1 Define electromagnetic field expansion in J_z and M_z.
Fourier series an approximation to Fourier transform.
Upgoing plane waves above interface and downgoing plane waves below interface, Rayleigh (1896) hypothesis.

2 Match boundary conditions across undulating interface.
Tangential $\underline{E}$ and $\underline{H}$ are continuous.
Normal $\underline{J}$ and $\underline{M}$ are continuous.

3 Expand exponential terms in Taylor series.

4 Make first-order approximation.
Save terms which are zero- or first-order with respect to $u_j s$ and ds/dx.
First-order approximation → $|\gamma_j s|$ and $|ds/dx| < 0.3$

5 Express s and ds/dx in Fourier series.
Fourier series an approximation to Fourier transform.

6 Use orthogonality of exponential basis functions to isolate terms with $\exp(ik_n x)$ dependence.

7 Solve linear system of equations for $\underline{R}_n$ and $\underline{T}_n$.

$\beta_1 = \beta_2 = \beta_0$, but constant permeability will not be assumed during the development of this problem.

The incident field is a plane wave traveling downward towards the interface. The incident plane wave is traveling at an arbitrary angle and represents both J_z and M_z components. A single incident wave will be scattered into plane waves traveling in all directions. For the gentle slopes considered in this perturbation approach, the scattered field is adequately represented by upgoing plane waves above the interface and by downgoing plane waves below the interface. This assumption, the Rayleigh hypothesis (Rayleigh, 1896, 1907), limits the maximum slope of the interface to 31 degrees. The limit on slope imposed by using the Rayleigh hypothesis is less restrictive than the limit which is imposed by using a first-order perturbation method. Using the Rayleigh hypothesis, fields above the interface are described by

$$\begin{bmatrix} J_{z1} \\ M_{z1} \end{bmatrix} = \left[\underline{I}\, e^{u_{1m}z}\, e^{ik_m x} + \sum_{n=-\infty}^{\infty} \underline{R_n}\, e^{-u_{1n}z}\, e^{ik_n x} \right] \begin{bmatrix} J_s \\ M_s \end{bmatrix} \qquad (5.3)$$

$z > s(x)$, where the multiplier $e^{ik_y y}$ is suppressed, and

$u_{1j} = \sqrt{\gamma_1^2 + k_j^2 + k_y^2}$, Real$(u_{1j})$ and Imag$(u_{1j}) > 0$.

The down-going source fields are represented by $e^{u_{1m}z}\, e^{ik_m x}\, \underline{J_s}$, while $\sum \underline{R_n}\, e^{-u_{1n}z}\, e^{ik_n x}\, \underline{J_s}$ represents a

discrete spectrum of reflected, upgoing waves. As the matrix character of $\underline{R_n}$ suggests, J_z and M_z are coupled by their interaction with an undulating interface. The discrete spectrum represented by $\sum \underline{R_n}\, e^{-u_{1n}z}\, e^{ik_n x}$ is an approximation to the continuous spectrum of a Fourier integral. The approximation can be improved by decreasing the spacing between consecutive k_n.

Electromagnetic fields below the interface can also be approximated by a discrete spectrum of plane waves

$$\begin{bmatrix} J_{z2} \\ M_{z2} \end{bmatrix} = \left[\sum_{n=-\infty}^{\infty} \underline{T_n}\, e^{\,u_{2n}z}\, e^{ik_n x} \right] \begin{bmatrix} J_s \\ M_s \end{bmatrix} \qquad \text{for } z < s(x) \qquad (5.4)$$

As with reflected fields, $\underline{T_n}$ couples J_z and M_z together.

To solve for the unknown coefficients $\underline{R_n}$ and $\underline{T_n}$, equations 5.3 and 5.4 must be linked by boundary conditions. The three boundary conditions linking $\underline{J_{z1}}$ and $\underline{J_{z2}}$ together across the interface s(x) are continuity of tangential $\underline{E}$ and $\underline{H}$

$$\begin{bmatrix} E_x \\ H_x \end{bmatrix} + \frac{ds}{dx} \begin{bmatrix} E_z \\ H_z \end{bmatrix} = \left(\frac{-1}{\partial_x^2 + \partial_y^2} \begin{bmatrix} \frac{\partial_{xz}}{\hat{\sigma}} & \partial_y \\ \partial_y & \frac{\partial_{xz}}{\hat{\mu}} \end{bmatrix} + \frac{ds}{dx} \begin{bmatrix} \frac{1}{\hat{\sigma}} & 0 \\ 0 & \frac{1}{\hat{\mu}} \end{bmatrix} \right) \begin{bmatrix} J_z \\ M_z \end{bmatrix} \qquad (5.5)$$

$$\begin{bmatrix} E_y \\ H_y \end{bmatrix} = \frac{-1}{\partial_x^2 + \partial_y^2} \begin{bmatrix} \frac{\partial_{yz}}{\hat{\sigma}} & -\partial_x \\ -\partial_x & \frac{\partial_{yz}}{\hat{\mu}} \end{bmatrix} \begin{bmatrix} J_z \\ M_z \end{bmatrix} \qquad (5.6)$$

and continuity of currents normal to the interface

$$\begin{bmatrix} J_z \\ M_z \end{bmatrix} - \frac{ds}{dx}\begin{bmatrix} J_x \\ M_x \end{bmatrix} = \left[\underline{I} + \frac{\frac{ds}{dx}}{\partial_x^2+\partial_y^2}\begin{bmatrix} \partial_{xz} & \partial\partial_y \\ \hat{\mu}\partial_y & \partial_{xz} \end{bmatrix}\right]\begin{bmatrix} J_z \\ M_z \end{bmatrix} \tag{5.7}$$

Any two of the three boundary conditions are sufficient to uniquely determine field quantities, but all three are consistent and are helpful in reducing the complexity of the algebra involved in solving for $\underline{R_n}$ and $\underline{T_n}$.

Enforcing the boundary conditions along the interface s(x) creates a set of equations linking $\underline{J_{z1}}$ and $\underline{J_{z2}}$. To reduce the equations to a form which can be solved algebraically for $\underline{R_n}$ and $\underline{T_n}$, some simplifying approximations must be made to the way in which the fields are represented. Examining the representation of one component in detail gives

$$J_{z1} = J_s e^{u_{1m}s+ik_mx} + \sum_{n=-\infty}^{\infty}(J_sR_{11n} + M_sR_{12n})e^{-u_{1n}s+ik_nx} \tag{5.8}$$

The exponential terms $\exp(\pm u_{1j}s)$ are not constant and must be simplified to allow algebraic reduction of field representations. Exponential terms in $\pm u_{1j}s$ can be expanded in a Taylor series as follows:

$$J_{z1} = J_s\left(1 + u_{1m}s + \frac{(u_{1m}s)^2}{2} + \text{h.o.t.}\right) e^{ik_mx} \tag{5.9}$$

$$+ \sum_{n=-\infty}^{\infty}(J_sR_{11n} + M_sR_{12n})\left(1 - u_{1n}s + \frac{(u_{1n}s)^2}{2} - \text{h.o.t.}\right)e^{ik_nx}$$

For interfaces where $|s|$ is small in terms of skin depths in

the surrounding media, approximations to equation 5.9 can be made by truncating the Taylor series.

A zero-order approximation results from truncating the Taylor series after the first term. The zero-order approximation is equivalent to $s(x) = 0$, a planar interface. Rewriting the results derived for plane layers in matrix form gives

$$\underline{R_m} = \begin{bmatrix} \frac{K_1-K_2}{K_1+K_2} & 0 \\ 0 & \frac{N_1-N_2}{N_1+N_2} \end{bmatrix} \tag{5.10}$$

and

$$\underline{R_n} = \underline{0} \quad \text{for } n \neq m$$

$$\underline{T_m} = \begin{bmatrix} \frac{2K_1}{K_1+K_2} & 0 \\ 0 & \frac{2N_1}{N_1+N_2} \end{bmatrix} \tag{5.11}$$

and

$$\underline{T_n} = \underline{0} \quad \text{for } n \neq m$$

A first-order approximation can be made by truncating the Taylor series expansions of $e^{\pm us}$ after two terms. With $s(x)$ replaced by its series representation, a first-order approximation to equation 5.9 is

$$J_{z1} = J_e\left[e^{ik_m x} + u_{1m}\sum d_j\, e^{i(k_j + k_m)x}\right] \tag{5.12}$$

$$+ \sum_{n=-\infty}^{\infty} (J_e R_{11n} + M_e R_{12n})\left[e^{ik_m x} - u_{1m}\sum d_j\, e^{i(k_j + k_n)x}\right]$$

Equation 5.12 can be simplified further on the basis of its

dependence on x. Terms containing d_0 disappear, since $d_0 = 0$. The zero-order reflection coefficient R_{12m} is zero, and since R_{11n} and R_{12n} are first-order quantities for $n \neq m$, terms containing $u_{1n}s\ R_{11n}$ and $u_{1n}s\ R_{12n}$ can be neglected. For $e^{ik_m x}$ dependence, equation 5.12 becomes

$$J_{z1} = J_s(1 + R_{11m}) \tag{5.13}$$

For $e^{ik_n x}$ dependence, equation 5.12 becomes

$$J_{z1} = J_s(1 - R_{11m})\ u_{1m}\ d_{n-m} + J_s\ R_{11n} + M_s\ R_{12n} \tag{5.14}$$

The same first-order approximations can be applied to $\frac{ds}{dx}\ J_{x1}$. Since $\frac{ds}{dx}$ is a first-order quantity, J_{z1} must be represented by its zero-order approximation, which results in

$$\frac{ds}{dx}\ J_{x1} = 0 \tag{5.15}$$

for $e^{ik_m x}$ dependence, while for $e^{ik_n x}$ dependence we have

$$\frac{ds}{dx}\ J_{x1} = \frac{(ik_{n-m}\ d_{n-m})}{\lambda_m^2}\begin{bmatrix} J_s\ ik_m\ u_{1m}(1 - R_{11m}) \\ + M_s\ \partial_1\ ik_y(1 + R_{22m}) \end{bmatrix} \tag{5.16}$$

where $k_{n-m} = k_n - k_m$ and $\lambda_m^2 = k_m^2 + k_y^2$.

Substituting first-order, $e^{ik_m x}$ representations into the boundary conditions for the source condition $J_s = 1$ and $M_s = 0$ gives

$$J_n = 1 + R_{11m} = T_{11m} \tag{5.17}$$

$$M_n = R_{21m} = T_{21m} \tag{5.18}$$

$$E_x = A_m K_{1m}(1 - R_{11m}) + B_m R_{21m} = A_m K_{2m} T_{11m} + B_m T_{21m} \tag{5.19}$$

$$E_y = B_m K_{1m}(1 - R_{11m}) - A_m R_{21m} = B_m K_{2m} T_{11m} - A_m T_{21m} \tag{5.20}$$

$$H_x = A_m N_{1m}(1 - R_{21m}) + B_m R_{11m} = A_m N_{2m} T_{21m} + B_m T_{11m} \tag{5.21}$$

$$H_y = B_m N_{1m}(1 - R_{21m}) - A_m R_{11m} = B_m N_{2m} T_{21m} - A_m T_{11m} \tag{5.22}$$

where

$$A_j = \frac{ik_j}{k_j^2 + k_y^2}$$

$$B_j = \frac{ik_y}{k_j^2 + k_y^2}$$

$$K_{jm} = \frac{u_{jm}}{\hat{\sigma}_j}$$

$$N_{jm} = \frac{u_{jm}}{\hat{\mu}_j}$$

and

$$u_{jm} = \sqrt{\gamma_j^2 + k_m^2 + k_y^2} \quad \text{Real(u) and Imag(u)} > 0.$$

The electric current reflection coefficients R_{11m} and T_{11m} can be decoupled from the magnetic current reflection coefficients, R_{21m} and T_{21m}, by adding E_x/B_m to E_y/A_m and by adding H_x/B_m to H_y/A_m, which after clearing common factors results in

$$K_{1m}(1 - R_{11m}) = K_{1m} R_{11m} \tag{5.23}$$

$$-N_{1m} R_{21m} = N_{2m} T_{21m} \tag{5.24}$$

Equations 5.18 and 5.24 imply that $R_{21m} = T_{21m} = 0$. Equations 5.17 and 5.23 are the same equations as

encountered in the plane-layer problem. Doing the same steps for the source condition $J_s = 0$ and $M_s = 1$ gives the results

$$R_{12m} = T_{12m} = 0 \tag{5.25}$$

$$1 + R_{22m} = T_{22m} \tag{5.26}$$

$$N_{1m}(1 - R_{22m}) = N_{2m}T_{22m} \tag{5.27}$$

For a first-order approximation, the reflection operators $\underline{R_m}$ and $\underline{T_m}$ are the same as for a planar interface (equations 5.10 and 5.11).

An extension to the plane-layer results comes from considering terms with e^{ik_nx} dependence, which represent scattering at an arbitrary angle. Substituting first-order approximations for e^{ik_nx} dependence into the boundary conditions gives a more complicated set of equations. For the source condition $J_s = 1$ and $M_s = 0$ the resultant equations are as follows

$$J_n = -ik_{nm}d_{nm}A_m u_{1m}(1-R_{11m}) + R_{11n} + u_{1m}d_{nm}(1-R_{11m})$$
$$= -ik_{nm}d_{nm}A_m u_{2m}T_{11m} + T_{11n} + u_{1m}d_{nm}T_{11m} \quad (5.28)$$

$$M_n = -ik_{nm}d_{nm}B_m\beta_1 T_{11m}+R_{21n} = -ik_{nm}d_{nm}B_m\beta_2 T_{11m}+T_{21n} \quad (5.29)$$

$$E_t = -A_nK_{1n}R_{11n} + A_{1m}K_{1m}T_{11m} + B_nR_{21n} + \frac{ik_{nm}}{\hat{\sigma}_1}d_{nm}T_{11m}$$
$$= A_nK_{2n}T_{11n} + A_{2m}K_{2m}T_{11m} + B_nT_{21n} + \frac{ik_{nm}}{\hat{\sigma}_2}d_{nm}T_{11m} \quad (5.30)$$

$$E_y = -B_nK_{1n}R_{11n} + B_{1m}K_{1m}T_{11m} - A_nR_{21n}$$
$$= B_nK_{2n}T_{11n} + B_{2m}K_{2m}T_{11m} - A_nT_{21n} \quad (5.31)$$

$$H_t = -A_nN_{1n}R_{21n} + B_nR_{11n} + B_{1m}(1 - R_{11m})$$
$$= A_nN_{2n}T_{21n} + B_nT_{11n} + B_{1m}T_{11m} \quad (5.32)$$

$$H_y = -B_nN_{1n}R_{21n} - A_nR_{11n} + A_{1m}(1 - R_{11m})$$
$$= B_nN_{2n}T_{21n} - A_nT_{11n} + A_{1m}T_{11m} \quad (5.33)$$

where $A_{1m} = A_m d_{nm} u_{1m}$ and $B_{1m} = B_m d_{nm} u_{1m}$.

The pattern of unknowns in equations 5.28 through 5.33 is similar to the pattern in equations 5.17 through 5.22. The extra complication comes from known terms involving elements of $\underline{R_m}$ and $\underline{T_m}$. The same operation of adding $E_x/B_n + E_y/A_n$ and $E_x/B_n + E_y/A_n$ simplifies the algebra. Using the simplified equations along with the normal current boundary conditions (equations 5.24 and 5.25) makes two separate two by two systems of equations to be solved for the top row elements of $\underline{R_n}$ and $\underline{T_n}$. To solve for elements in the bottom row of R_n and T_n, the same procedure is followed with the source condition $J_s = 0$ and $M_s = 1$. The final result simplifies to

the following:

$$R_{11n} = A\ T_m\left[B(\Delta\hat{\mu} + K_{2n}K_{2m}\Delta\hat{\sigma}) + C\right] \tag{5.34}$$

$$R_{21n} = A^*T_mD(N_{2n}\Delta\hat{\mu} - K_{2m}\Delta\hat{\sigma}) \tag{5.35}$$

$$R_{12n} = A\ T_m^*D(K_{2n}\Delta\hat{\sigma} - N_{2m}\Delta\hat{\mu}) \tag{5.36}$$

$$R_{22n} = A^*T_m^*\left[B(\Delta\hat{\sigma} + N_{2n}N_{2m}\Delta\hat{\mu}) + C^*\right] \tag{5.37}$$

While solving for $\underline{T_n}$ results in:

$$T_{11n} = A\ T_m\left[B(\Delta\hat{\mu} - K_{1n}K_{2m}\Delta\hat{\sigma}) + C\right] \tag{5.38}$$

$$T_{21n} = A^*T_mD(-N_{1n}\Delta\hat{\mu} - K_{2m}\Delta\hat{\sigma}) \tag{5.39}$$

$$T_{12n} = A\ T_m^*D(-K_{1n}\Delta\hat{\sigma} - N_{2m}\Delta\hat{\mu}) \tag{5.40}$$

$$T_{22n} = A^*T_m^*\left[B(\Delta\hat{\sigma} - N_{1n}N_{2m}\Delta\hat{\mu}) + C^*\right] \tag{5.41}$$

where

$$A = \frac{d_{n-m}}{K_{1n} + K_{2n}} \qquad B = \frac{k_mk_n + k_y^2}{\lambda_m^2} \qquad C = \lambda_n^2\left[\frac{1}{\hat{\sigma}_1} - \frac{1}{\hat{\sigma}_2}\right]$$

$$A^* = \frac{d_{n-m}}{N_{1n} + N_{2n}} \qquad D = \frac{(k_n-k_m)k_y}{\lambda_m^2} \qquad C^* = \lambda_n^2\left[\frac{1}{\hat{\mu}_1} - \frac{1}{\hat{\mu}_2}\right]$$

$$\Delta\hat{\sigma} = \hat{\sigma}_2 - \hat{\sigma}_1 \qquad \Delta\hat{\mu} = \hat{\mu}_2 - \hat{\mu}_1$$

The resulting reflection and transmission coefficients are remarkably simple considering the extensive algebra required to obtain them.

A limitation of the results in equations 5.34 through 5.41 is the presence of a singularity as λ_m

approaches zero. For λ_m near zero, the coefficients B and D diverge. The singularity is fundamental to a vertical current or vertically oriented potential representation. However, the problems introduced by the singularity at normal incidence can be avoided by switching to an alternative representation. For the special case of $\partial_y = 0$, the source is best represented in terms of E_y and H_y, as described by equation 3.27. For $\partial_y = 0$ the coefficients B, C, C*, and D in equations 5.34 through 5.41 are modified to

$$B = 1 \tag{5.42}$$

$$C = k_n k_m \lambda_n^2 \left[\frac{1}{\hat{\sigma}_1} - \frac{1}{\hat{\sigma}_2}\right] \tag{5.43}$$

$$C^* = k_n k_m \lambda_n^2 \left[\frac{1}{\hat{\mu}_1} - \frac{1}{\hat{\mu}_2}\right] \tag{5.44}$$

$$D = 0 \tag{5.45}$$

The coefficients in $\underline{R}_n$ and $\underline{T}_n$ represent a perturbation to plane-layer reflection and transmission caused by undulations of the interface s(x). Because of the first-order approximations made in deriving $\underline{R}_n$ and $\underline{T}_n$, the amplitude and slope of s(x) must be small in terms of skin depths in the surrounding media.

The special case of constant permeability reduces the complexity of $\underline{R}_n$ and $\underline{T}_n$ even further. For most rock types permeability does not change from its free-space

value, μ_0; therefore $\hat{\mu}_j = \hat{\mu}_0$. A constant permeability eliminates almost half of the terms in equations 5.34 through 5.41. For $\hat{\mu}_j = \hat{\mu}_0$ the elements of $\underline{R_n}$ reduce to the following:

$$R_{11n} = A\, T_m \left[C + B\, K_{2n} K_{2m}\, \Delta\hat{\sigma}\right] \tag{5.46}$$

$$R_{21n} = -A^* T_m\, D\, K_{2m}\, \Delta\hat{\sigma} \tag{5.47}$$

$$R_{12n} = A\, T_m^*\, D\, K_{2n}\, \Delta\hat{\sigma} \tag{5.48}$$

$$R_{22n} = A^* T_m^*\, B\, \Delta\hat{\sigma} \tag{5.49}$$

while $\underline{T_n}$ simplifies to

$$T_{11n} = A\, T_m \left[C - B\, K_{1n} K_{2m}\, \Delta\hat{\sigma}\right] \tag{5.50}$$

$$T_{21n} = -A^* T_m\, D\, K_{2m}\, \Delta\hat{\sigma} \tag{5.51}$$

$$T_{12n} = -A\, T_m^*\, D\, K_{1n}\, \Delta\hat{\sigma} \tag{5.52}$$

$$T_{22n} = A^* T_m^*\, B\, \Delta\hat{\sigma} \tag{5.53}$$

where the definitions of A, A^*, B, C, D, and $\Delta\hat{\sigma}$ are unchanged. For $\partial_y = 0$, the coefficients B, C, and D are modified to the definitions given by equations 5.43 through 5.45. With $\partial_y = 0$, equation 5.46 and 5.49 are the same as the reflection coefficients published by Hughes and Wait (1975a) for TE and TM mode plane waves.

The first-order reflection and transmission coefficients describing plane-wave interaction with a

two-dimension undulating interface are fairly simple. A second-order approximation to $\underline{R}_n$ and $\underline{T}_n$ can be derived, but it involves cross-correlations of the Fourier transform of s(x). The second-order approximation is more cumbersome computationally, but allows less restrictive limits on $|s(x)|$ and $|ds/dx|$. Wait (1974) notes that for forward scattering from sea waves at grazing incidence, first-order reflection terms disappear and second-order terms become important. For the geophysical applications considered in this dissertation, the first-order solution is sufficient. The simple first-order result for two-dimensional undulations suggests that the three-dimensional problem should be tractable.

Three-dimensional Undulations

The development of first-order reflection and transmission coefficients for three-dimensional undulations is only slightly more complicated than for two-dimensional undulations. For three-dimensional undulations, the interface is described by a double finite Fourier series

$$s(x,y) = \sum_{k=-P}^{P} \sum_{j=-M}^{M} d_j f_k \, e^{ik_j x} \, e^{ik_k y} \tag{5.54}$$

where $d_0 = 0$, $f_0 = 0$, $k_j = \Delta j$, and $k_k = \Delta k$. The interface is a real-valued function, $s(x,y)$, which varies in the x and y directions. The slope of $s(x,y)$ in the x direction is

$$\frac{\partial s(x,y)}{\partial x} = \sum_{k=-P}^{P} \sum_{j=-M}^{M} ik_j \, d_j f_k \, e^{ik_j x} \, e^{ik_k y} \tag{5.55}$$

While the slope of $s(x,y)$ in the y direction is

$$\frac{\partial s(x,y)}{\partial y} = \sum_{k=-P}^{P} \sum_{j=-M}^{M} ik_k \, d_j f_k \, e^{ik_j x} \, e^{ik_k y} \tag{5.56}$$

Figure 5.2 illustrates the geometry of the problem. The undulating interface, $s(x,y)$, separates two regions. The medium above the interface is characterized by a complex conductivity, $\partial_1 = \sigma_1 + i\omega\varepsilon_1$, and a complex permeability, $\beta_1 = -i\omega\mu_1$. The region below the interface has the medium properties ∂_2 and β_2. The incident field is a single downward-travelling plane wave. The incident plane wave is

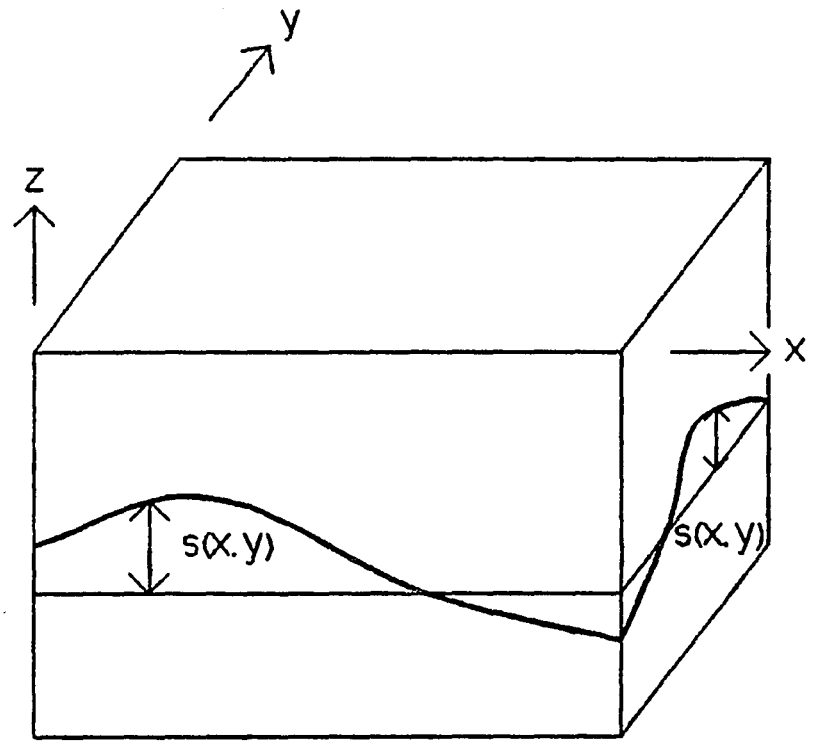

Figure 5.2 Block diagram of Three-dimensional Undulating Interface Model

The interface is described by a real-valued function, s(x,y), which has gentle slope and has small amplitude in terms of skin depths.

traveling at an arbitrary angle and represents both J_z and M_z components. A single incident wave will be scattered into plane waves travelling in all directions with both J_z and M_z components. Using the Rayleigh hypothesis, fields above the interface are described by the equation

$$\begin{bmatrix} J_{z1} \\ M_{z1} \end{bmatrix} = \tag{5.57}$$

$$\left[\underline{I}\, e^{u_{1mp}z}\, e^{ik_m x}\, e^{ik_p y} + \sum_{q=-\infty}^{\infty} \sum_{n=-\infty}^{\infty} \underline{R}_{nq}\, e^{-u_{1nq}z}\, e^{ik_n x}\, e^{ik_q y} \right] \begin{bmatrix} J_s \\ M_s \end{bmatrix}$$

for $z > s(x,y)$ and $u_{1jk} = \sqrt{\gamma_1^2 + k_j^2 + k_k^2}$, Real(u) > 0 and Imag(u) >0. The field representation for this three-dimensional problem is the same as for the two-dimensional problem, with the addition of an extra set of subscripts to keep track of oblique reflections in the y direction. J_z and M_z are coupled by their interaction with an undulating interface and oblique reflections will occur in both x and y directions. Electromagnetic fields below the interface can be approximated by a discrete spectrum of plane waves, viz

$$\begin{bmatrix} J_{z2} \\ M_{z2} \end{bmatrix} = \left[\sum_{q=-\infty}^{\infty} \sum_{n=-\infty}^{\infty} \underline{T_{nq}} \; e^{-u_{2nq}z} \; e^{ik_n x} \; e^{ik_q y} \right] \begin{bmatrix} J_e \\ M_e \end{bmatrix} \qquad (5.58)$$

for $z < s(x,y)$ and $u_{2jk} = \sqrt{\gamma_2^2 + k_j^2 + k_k^2}$, Real(u) > 0 and Imag(u) > 0. As for reflected fields, $\underline{T_{nq}}$ couples J_z and M_z together.

To solve for the unknown coefficients in $\underline{R_{nq}}$ and $\underline{T_{nq}}$, equations 5.57 and 5.58 must be linked by boundary conditions. The boundary conditions for the three-dimensional case are a slight extension to the two-dimensional problem in that the y-direction slope, $\frac{\partial s}{\partial y}$, is not zero everywhere. The three boundary conditions linking $\underline{J_{z1}}$ and $\underline{J_{z2}}$ together across the interface s(x,y) are continuity of tangential $\underline{E}$ and $\underline{H}$, viz

$$\begin{bmatrix} E_x \\ H_x \end{bmatrix} + \frac{\partial s}{\partial x} \begin{bmatrix} E_z \\ H_z \end{bmatrix} = \left(\frac{-1}{\partial_x^2 + \partial_y^2} \begin{bmatrix} \frac{\partial_{xz}}{\hat{\sigma}} & \partial_y \\ \partial_y & \frac{\partial_{xz}}{\hat{\mu}} \end{bmatrix} + \frac{\partial s}{\partial x} \begin{bmatrix} \frac{1}{\hat{\sigma}} & 0 \\ 0 & \frac{1}{\hat{\mu}} \end{bmatrix} \right) \begin{bmatrix} J_z \\ M_z \end{bmatrix} \qquad (5.59)$$

$$\begin{bmatrix} E_y \\ H_y \end{bmatrix} + \frac{\partial s}{\partial y} \begin{bmatrix} E_z \\ H_z \end{bmatrix} = \left(\frac{-1}{\partial_x^2 + \partial_y^2} \begin{bmatrix} \frac{\partial_{yz}}{\hat{\sigma}} & -\partial_x \\ -\partial_x & \frac{\partial_{yz}}{\hat{\mu}} \end{bmatrix} + \frac{\partial s}{\partial y} \begin{bmatrix} \frac{1}{\hat{\sigma}} & 0 \\ 0 & \frac{1}{\hat{\mu}} \end{bmatrix} \right) \begin{bmatrix} J_z \\ M_z \end{bmatrix} \qquad (5.60)$$

and continuity of currents normal to the interface, viz

$$\begin{bmatrix} J_z \\ M_z \end{bmatrix} - \frac{\partial s}{\partial x}\begin{bmatrix} J_x \\ M_x \end{bmatrix} - \frac{\partial s}{\partial y}\begin{bmatrix} J_y \\ M_y \end{bmatrix} = \tag{5.61}$$

$$\left[\underline{I} + \frac{\frac{\partial s}{\partial x}}{\partial_x^2+\partial_y^2}\begin{bmatrix} \partial_{xz} & \partial\partial_y \\ \beta\partial_y & \partial_{xz} \end{bmatrix} + \frac{\frac{\partial s}{\partial x}}{\partial_x^2+\partial_y^2}\begin{bmatrix} \partial_{xz} & \partial\partial_y \\ \beta\partial_y & \partial_{xz} \end{bmatrix}\right]\begin{bmatrix} J_z \\ M_z \end{bmatrix}$$

Any two of the three boundary conditions are sufficient to uniquely determine field quantities, but using all three in different combinations provides a check for catching algebraic errors.

Enforcing the boundary conditions along the interface s(x,y) creates a set of equations linking $\underline{J_{z1}}$ and $\underline{J_{z2}}$. The equations can be reduced to a form which can be solved algebraically for $\underline{R_{nq}}$ and $\underline{T_{nq}}$ by making the same simplifying approximations used to solve the two-dimensional problem. The field representations established in equations 5.57 and 5.58 are inserted into the boundary condition operators (equations 5.59 through 5.61). Terms multiplied by $\frac{\partial s}{\partial x}$ or by $\frac{\partial s}{\partial y}$ can be represented by a zero-order approximation. For a zero-order approximation, $e^{\pm u_{ijk}s(x,y)}$ terms are expanded into a one-term Taylor series. All other terms are represented by a first-order approximation. For a first-order approximation, $e^{\pm u_{ijk}s(x,y)}$ terms are expanded into a two-term Taylor series. Considering terms with the same e^{ik_jx} e^{ik_ky} dependence leads to sets of equations which

can be solved algebraically for the coefficients in $\underline{R_{nq}}$ and $\underline{T_{nq}}$. The field representations and boundary conditions are slightly more complex for three-dimensions rather than two, but the methodology for obtaining a solution is the same.

For $e^{ik_m x}\, e^{ik_p y}$ dependence, first-order reflection and transmission coefficients are the same as for a horizontal plane, viz

$$\underline{R_{mp}} = \begin{bmatrix} \frac{K_{1mp}-K_{2mp}}{K_{1mp}+K_{2mp}} & 0 \\ 0 & \frac{N_{1mp}-N_{2mp}}{N_{1mp}+N_{2mp}} \end{bmatrix} \tag{5.62}$$

$$\underline{T_{mp}} = \begin{bmatrix} \frac{2K_{1mp}}{K_{1mp}+K_{2mp}} & 0 \\ 0 & \frac{2N_{1mp}}{N_{1mp}+N_{2mp}} \end{bmatrix} \tag{5.63}$$

where

$$K_{ijk} = \frac{u_{ijk}}{\partial_i}$$

and

$$N_{ijk} = \frac{u_{ijk}}{\mu_i}$$

For oblique reflection and refraction, $e^{ik_n x}\, e^{ik_q y}$ dependence, first-order coefficients for an interface with three-dimensional undulations are similar in form to the two-dimensional results. $\underline{R_{nq}}$ reduces to

$$R_{11nq} = A\ T_{mp}\left[B(\Delta\beta + K_{2nq}K_{2mp}\Delta\theta) + C\right] \tag{5.64}$$

$$R_{21nq} = A^{*}T_{mp}D(N_{2nq}\Delta\beta - K_{2mp}\Delta\theta) \tag{5.65}$$

$$R_{12nq} = A\ T^{*}_{mp}D(K_{2nq}\Delta\theta - N_{2mp}\Delta\beta) \tag{5.66}$$

$$R_{22nq} = A^{*}T^{*}_{mp}\left[B(\Delta\theta + N_{2nq}N_{2mp}\Delta\beta) + C^{*}\right] \tag{5.67}$$

While solving for $\underline{T_{nq}}$ results in

$$T_{11nq} = A\ T_{mp}\left[B(\Delta\beta - K_{1nq}K_{2mp}\Delta\theta) + C\right] \tag{5.68}$$

$$T_{21nq} = A^{*}T_{mp}D(-N_{1nq}\Delta\beta - K_{2mp}\Delta\theta) \tag{5.69}$$

$$T_{12nq} = A\ T^{*}_{mp}D(-K_{1nq}\Delta\theta - N_{2mp}\Delta\beta) \tag{5.70}$$

$$T_{22nq} = A^{*}T^{*}_{mp}\left[B(\Delta\theta - N_{1nq}N_{2mp}\Delta\beta) + C^{*}\right] \tag{5.71}$$

where

$$A = \frac{d_{n-m}f_{q-p}}{K_{1nq} + K_{2nq}} \qquad B = \frac{k_m k_n + k_p k_q}{k_m^2 + k_p^2} \qquad C = \frac{k_n^2 + k_p k_q}{k_m^2 + k_p^2}\left(\frac{1}{\theta_1} - \frac{1}{\theta_2}\right)$$

$$A^{*} = \frac{d_{n-m}f_{q-p}}{N_{1nq} + N_{2nq}} \qquad D = \frac{k_n k_p - k_m k_q}{k_m^2 + k_p^2} \qquad C^{*} = \frac{k_n^2 + k_p k_q}{k_m^2 + k_p^2}\left(\frac{1}{\beta_1} - \frac{1}{\beta_2}\right)$$

$$\Delta\theta = \theta_2 - \theta_1 \qquad \Delta\beta = \beta_2 - \beta_1$$

First-order reflection and transmission coefficients for an interface with three-dimensional undulations are only slightly more complex than for an interface with two-dimensional undulations. However, due to oblique scattering in both x and y for the three-dimensional case, $\underline{R_{nq}}$ and $\underline{T_{nq}}$ couple both k_x and k_y source coefficients. The

three-dimensional case is much more cumbersome computationally. For a Fourier transform representation of electromagnetic fields, N basis functions along the k_x axis and N basis functions along the k_y axis represent computation of N^2 elements for the evaluation of each field component. Computing fields for horizontal plane layers does not couple the basis functions and thus represents an N^2 effort. Interface undulations are described by Fourier series with M terms. Adding two-dimensional undulations to one interface increases the computational effort to N^2M.

An implementation of the first-order perturbation solution with N = 40 and M =20 requires 11.3 minutes for evaluation on a personal computer using an Intel 8088-2 CPU chip and a 8087 math coprocessor running at 8MHz. The model had three layers with one undulating interface. The computer program spent 60 percent of its time in the subroutine which evaluates downward transmission, reflection, and upward transmission. A numerical approach to the same problem would be much more time consuming. For the Rayleigh-FFT approach, Jiracek (1972) reports a computation time for each plane-wave source component which is proportional to $M^{2.75}$. Generalizing Jiracek's method to include a three-dimensional source and a single interface with two-dimensional undulations would imply a computational

effort which is proportional to $N^2M^{2.75}$. Based on Jiracek's reported times, an extension of the Rayleigh-FFT approach to evaluate a three-dimensional source and three layers with one undulating interface would take roughly 12 hours on a CDC 6400.

Adding three-dimensional undulations to one interface increases the computational effort to N^2M^2. Each additional interface with two-dimensional undulations increases the amount of work needed to evaluate a model by a factor of M. Each additional interface with three-dimensional undulations increases the amount of work by a factor of M^2. To evaluate models with multiple, non-planar interfaces, either source fields must be smooth, to limit the size of N, or undulations must be smooth, to limit the size of M. Adding interfaces with three-dimensional undulations to a layered model quickly increases the amount of computation needed per model beyond reasonable limits. For the three-dimensional sources of interest in CSAMT, models limited to two-dimensional undulations are the most practical.

Multiple Layers

Evaluating models with multiple non-planar interfaces is possible, but each additional interface adds a significant amount of computational effort. A simple, yet

useful model which can be evaluated on a personal computer is one non-planar interface in a stack of horizontal layers. Allowing just one non-planar interface simplifies the interaction between layers, while including any number of planar interfaces adds flexibility with little additional numerical effort.

The interaction of vertical components of electric and magnetic current is described in chapter 4. The reflection function g_m (equation 4.23) provides a convenient recursive form. The compact recursive form for g_m can be re-written to more clearly show the geometric organization of plane-wave reflection from plane layers. Expanding the first three terms of g_0 for a N layer earth gives

$$g_0 = \qquad (5.72)$$

$$R_0 + \frac{T_0^{\downarrow}T_0^{\uparrow}}{1+R_0g_1}\, e^{-2u_1h_1}\left[R_1 + \frac{T_1^{\downarrow}T_1^{\uparrow}}{1+R_1g_2}\, e^{-2u_2h_2}\left[R_2 + \frac{T_2^{\downarrow}T_2^{\uparrow}g_3^{*}}{1+R_2g_3}\right]\right]$$

where

$$g_m = \frac{R_m + g_{m+1}}{1 + R_mg_{m+1}}\, e^{-2u_mh_m} = \left[R_m + \frac{T_m^{\downarrow}T_m^{\uparrow}}{1 + R_mg_{m+1}}\right]e^{-2u_mh_m}$$

and

$$g_m^{*} = \frac{R_m + g_{m+1}}{1 + R_mg_{m+1}}$$

The same relationship holds for g_0^{*}. Equation 5.72 provides a clear separation between contributions from each layer. If a first-order perturbation is added to R_2 in equation

5.72, the change to g_0 is

$$\Delta g_0 = \left[\frac{T_0^{\downarrow}T_0^{\uparrow}}{1+R_0g_1}\, e^{-2u_1h_1}\right]\left[\frac{T_1^{\downarrow}T_1^{\uparrow}}{1+R_1g_2}\, e^{-2u_2h_2}\right]\Delta R_2 \qquad (5.73)$$

The factors in equation 5.73 represent transmission down to interface two, the perturbation to R_2 and transmission back to the surface. The downward transmission coefficient is

$$T^{\downarrow} = \left[\frac{T_0^{\downarrow}\, e^{-u_1h_1}}{1 + R_0g_1}\right]\left[\frac{T_1^{\downarrow}\, e^{-u_2h_2}}{1 + R_1g_2}\right] \qquad (5.74)$$

the perturbation to R_2 is ΔR_2 and transmission back to the surface is

$$T^{\uparrow} = \left[T_0^{\uparrow}\, e^{-u_1h_1}\right]\left[T_1^{\uparrow}\, e^{-u_2h_2}\right] \qquad (5.75)$$

Equations 5.73 through 5.75 deal with a perturbation to the TM mode reflection coefficient R_2. A perturbation caused by an interface undulation couples J_z and M_z components with the reflection angle not equal to the angle of incidence. Equation 5.74 can be generalized to include the perturbation caused by an undulation on the M'th interface in a stack of N layers. The downward transmission has a matrix form and e^{ik_mx} dependence, viz

$$\underline{T}_m^{\downarrow} = \begin{bmatrix} T_m^{\downarrow} & 0 \\ 0 & T_m^{\downarrow *} \end{bmatrix} \tag{5.76}$$

where

$$T_m^{\downarrow} = \prod_{j=0,M-1} \frac{T_{jm}^{\downarrow} \, e^{-u_{j+1m}h_{j+1}}}{1 + R_{jm}g_{j+1m}}$$

and

$$T_m^{\downarrow *} = \prod_{j=0,M-1} \frac{T_{jm}^{\downarrow *} \, e^{-u_{j+1m}h_{j+1}}}{1 + R_{jm}^{*}g_{j+1m}^{*}}$$

with

$$T_{mj}^{\downarrow} = \frac{2K_{jm}}{K_{jm} + K_{jm+1}}$$

and

$$T_{mj}^{\downarrow *} = \frac{2N_{jm}}{N_{jm} + N_{jm+1}}$$

while $R_{jm} = T_{mj}^{\downarrow} - 1$ and $R_{jm}^{*} = T_{mj}^{\downarrow *} - 1$. g_{jm} and g_{jm}^{*} are from equation 4.23 with $e^{ik_m x}$ dependence and K_{jm} and N_{jm} are defined for equation 5.22. The perturbation reflection matrix will be $\underline{R}_n$, $n \neq m$, (equations 5.34 through 5.37). Upward transmission has $e^{ik_n x}$ dependence and is given by

$$\underline{T}_n^{\uparrow} = \begin{bmatrix} T_n^{\uparrow} & 0 \\ 0 & T_n^{\uparrow *} \end{bmatrix} \tag{5.77}$$

where

$$T_n^{\uparrow} = \prod_{j=0,M-1} T_{jn}^{\uparrow} \, e^{-u_{j+1n} h_{j+1}}$$

and

$$T_n^{\uparrow *} = \prod_{j=0,M-1} T_{jn}^{\uparrow *} \, e^{-u_{j+1n} h_{j+1}}$$

with

$$T_{nj}^{\uparrow} = \frac{2K_{jn+1}}{K_{jn} + K_{jn+1}}$$

and

$$T_{nj}^{\uparrow *} = \frac{2N_{jn+1}}{N_{jn} + N_{jn+1}}$$

while $R_{jn} = T_{nj}^{\uparrow} + 1$ and $R_{jn}^{*} = T_{nj}^{\uparrow *} + 1$. g_{jn} and g_{jn}^{*} are from equation 4.23 with $e^{ik_n x}$ dependence. The matrix equation description of the interaction is

$$\underline{J}_r = \underline{T}_n^{\uparrow} \, \underline{R}_n \, \underline{T}_m^{\downarrow} \, \underline{J}_s \tag{5.78}$$

where $\underline{J}_r$ is the perturbation of J_z and M_z due to an undulation on interface M. The result can be extended to three-dimensions by recognizing that the downward transmission leg will have $e^{ik_m x} \, e^{ik_p y}$ dependence, $\underline{R}_n$ will become $\underline{R}_{nq}$ (equations 5.64 through 5.65), and that the upward transmission leg will have $e^{ik_n x} \, e^{ik_q y}$ dependence.

For computation, half-space fields should be computed using the exact, closed-form solutions published by

Wait (1961). The modification to half-space fields caused by multiple plane layers is best computed using the hybrid solution developed in chapter 4. The hybrid algorithm involves analytical expressions which approximate the layered earth contribution and a correction term which requires the evaluation of a Hankel transform integral. Only the perturbation contribution from undulations on interface M must be evaluated by the double integration required for an inverse Fourier transform. Convergence of the undulation perturbation integrations is accelerated by exponential attenuation in $\underline{T}_n^{\downarrow}$ and $\underline{T}_n^{\uparrow}$ for increasing values of k_x and k_y.

Error Analysis

The goal of this dissertation is to provide a useful extension to existing theory which will help in understanding data collected by the CSAMT method. The theoretical results derived in the previous sections for two-dimensional undulations were implemented in a computer program. An immediate concern is to establish the validity of the theory and its computer program implementation. Computing boundary-condition errors provides a check on the many links in the chain of theoretical development. In addition to verifying the correctness of the theory,

computing errors allows the estimation of bounds on the range of permissible model parameters. The reflection and transmission coefficients derived in preceding sections are not exact. They are first-order approximations which are valid if the amplitude of s(x) is small in terms of skin depths in the surrounding media and if the maximum slope of s(x) is small. How big can the maximum values of s(x) and ds/dx be? A series of tests were run to evaluate the correctness of the theory and to check its computer program implementation. The tests also establish conservative bounds on maximum amplitudes of s(x) and ds/dx for a given level of error in matching boundary conditions across an undulating interface.

Errors introduced by approximating exponentially varying field behavior with a two-term Taylor series are detected in matching boundary conditions. The individual plane-wave components are exact solutions of the Helmholtz equation. For an undulating interface, the first-order solutions (equations 5.34 through 5.41) match the first-order boundary conditions (equations 5.28 through 5.33) exactly. The solutions were checked algebraically and numerically. A more rigorous test is to compute field components in the space domain. The actual field values predicted by the algorithm can be compared along the

undulating interface. Errors from all sources are present in the computation. Besides the approximate nature of the reflection and transmission coefficients, additional error is accumulated from the representation of a continuous Fourier spectrum by a discrete finite series and from numerical round-off in finite precision arithmetic.

The error introduced by using finite Fourier series and single precision arithmetic was checked by computing field components for a plane-layered earth using the double Fourier transform representation. By comparison with results from Anderson's (1974) program EMFIN, the field components were found to be accurate to within 0.1 percent. Computing field values for a plane-layered earth provides a check on the superstructure of the computer program. Model input routines, source representation, plane-layer reflection coefficients, electromagnetic field component computation, and integration routines must all be working correctly to duplicate independent results for plane-layered earth models. An accuracy of 0.1 percent is more than sufficient for comparison with field data. The error introduced by using finite Fourier series and single precision arithmetic is not significant in the computer program implemented for this project.

The error introduced by using first-order reflection and transmission coefficients is more significant. Tangential field components were computed in the space domain at a series of points along an undulating interface. For each boundary condition an average relative measure of error was defined to be

$$\varepsilon_{1j} = \frac{|e_{y1}[x_j,0,s(x_j)] - e_{y2}[x_j,0,s(x_j)]|}{|e^{\downarrow}_{y1}(x,0,s(x_j))|} \tag{5.79}$$

$$\varepsilon_{2j} = \frac{|e_{t1}[x_j,0,s(x_j)] - e_{t2}[x_j,0,s(x_j)]|}{|e^{\downarrow}_{x1}(x,0,s(x_j))|} \tag{5.80}$$

$$\varepsilon_{3j} = \frac{|h_{y1}[x_j,0,s(x_j)] - h_{y2}[x_j,0,s(x_j)]|}{|h^{\downarrow}_{y1}(x,0,s(x_j))|} \tag{5.81}$$

$$\varepsilon_{4j} = \frac{|h_{t1}[x_j,0,s(x_j)] - h_{t2}[x_j,0,s(x_j)]|}{|h^{\downarrow}_{x1}(x,0,s(x_j))|} \tag{5.82}$$

where

$e_t = e_x + \frac{ds}{dx} e_z$

$h_t = h_x + \frac{ds}{dx} h_z$

$e^{\downarrow}_{y1}$, $e^{\downarrow}_{t1}$, $h^{\downarrow}_{y1}$, $h^{\downarrow}_{t1}$ are down-going fields in region

and

$x_j = \Delta j$, $j = -N,N$

For the purpose of evaluating the effect of different model parameters on boundary-condition error, a simple "standard" model was chosen. The effect of model parameters on boundary-condition error was investigated by varying

parameter values from the "standard". The standard source was composed of normally incident TE and TM mode plane-waves with a frequency of 100 Hz. An undulating interface separated a 100 ohm-meter half-space from an underlying 1000 ohm-meter half-space. The cosinusoidal undulations were described by the function

$$s(x) = a \cos(b\, x) \qquad (5.83)$$

where $a = 0.2\delta$, $b = \Pi/8\delta$, and the skin depth, δ, is computed using the $\min(\rho_1,\rho_2)$. Boundary condition errors were computed at a series of equally spaced points along the interface, providing a point-matching estimate of actual error.

The inexactness in first-order reflection and transmission coefficients comes from linear approximations to exponential terms. When the maximum amplitude of s(x) is the dominate source of error, boundary-condition errors along an interface should correlate with the amplitude of s(x). This is shown to be true for the standard model in Figure 5.3. Average relative boundary-condition error (the average of equations 5.79 through 5.82) is plotted as a function of x in Figure 5.3a for the standard model, plotted in Figure 5.3b. The boundary-condition error reaches a maximum value of 10 percent and correlates in amplitude with the amplitude of s(x). Although the amplitude of s(x)

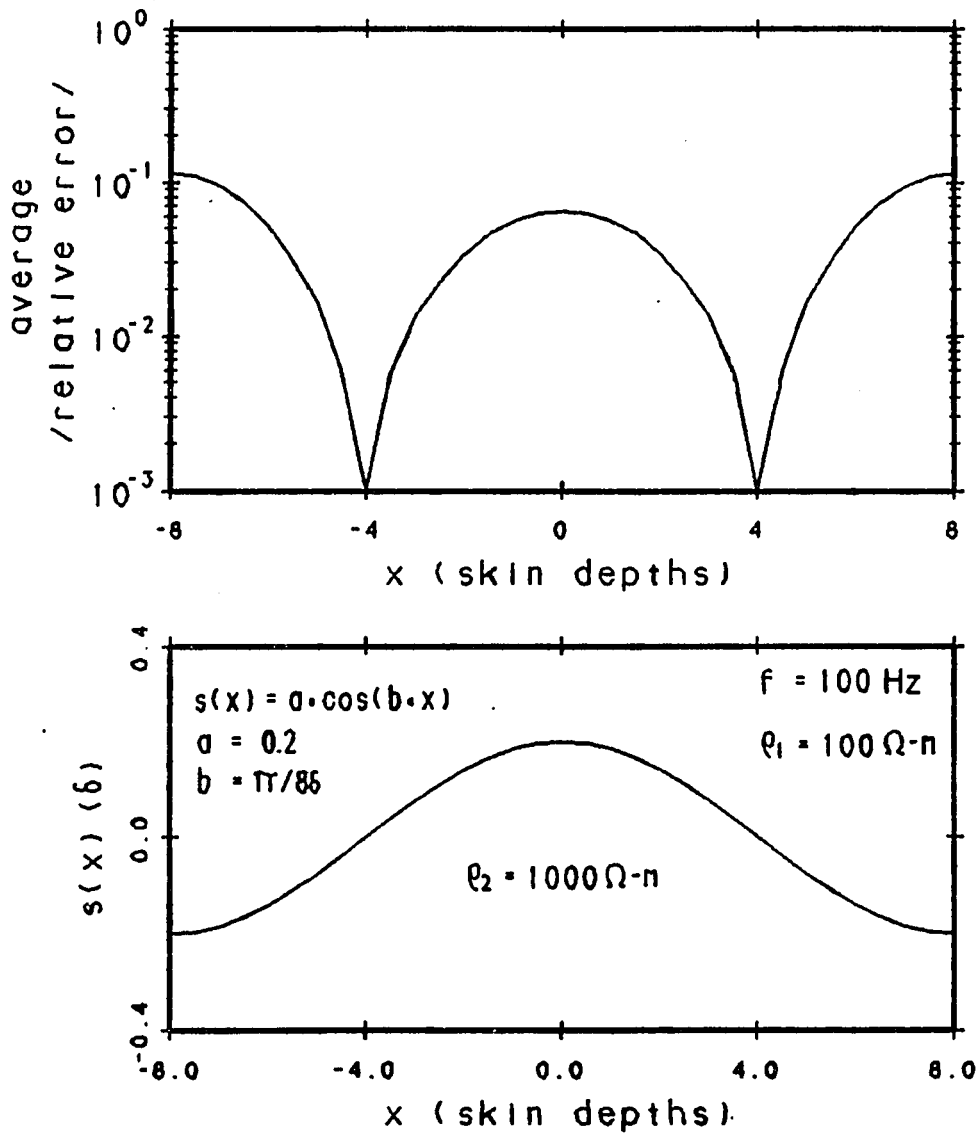

Figure 5.3 Relative Boundary-condition Error vs x

A plot of $\log_{10}|\text{relative error}|$ vs x shows a maximum where s(x) is greatest. The contribution to error of |s(x)| is not significant for this model.

creates the dominate error in Figure 5.3, the error does not go to zero when s(x) goes to zero. The boundary-condition error includes effects from slope as well as amplitude. For this model, however, the effects of slope are minor and become apparent only at small amplitudes.

Boundary condition error can be analyzed as a function of the maximum amplitude of s(x) when slope effects are small. Since the approximation is first-order, boundary-condition errors should be second-order. Figure 5.4 shows this to be true. All four error measures are averaged along the standard model interface. The average error is plotted as a function of the maximum value of s(x). Figure 5.4 is a plot of $\log_{10}$(average error) vs $\log_{10}(|s(x)|_{max})$. As expected the error is second order. A dashed line in Figure 5.4 is a log-log plot of relative error in a linear approximation to $e^{u_1 s}$ vs s. The error in the exponential approximation is second order and is somewhat smaller than the average boundary-condition error. The errors in the first-order reflection coefficients are related to a linear approximation of an exponential, but can not be directly predicted by calculating errors in exponential terms. The plot in Figure 5.4 provides a guide to how large s(x) can be for a given maximum acceptable boundary-condition error. A maximum |s(x)| of 0.28 skin depths creates an average

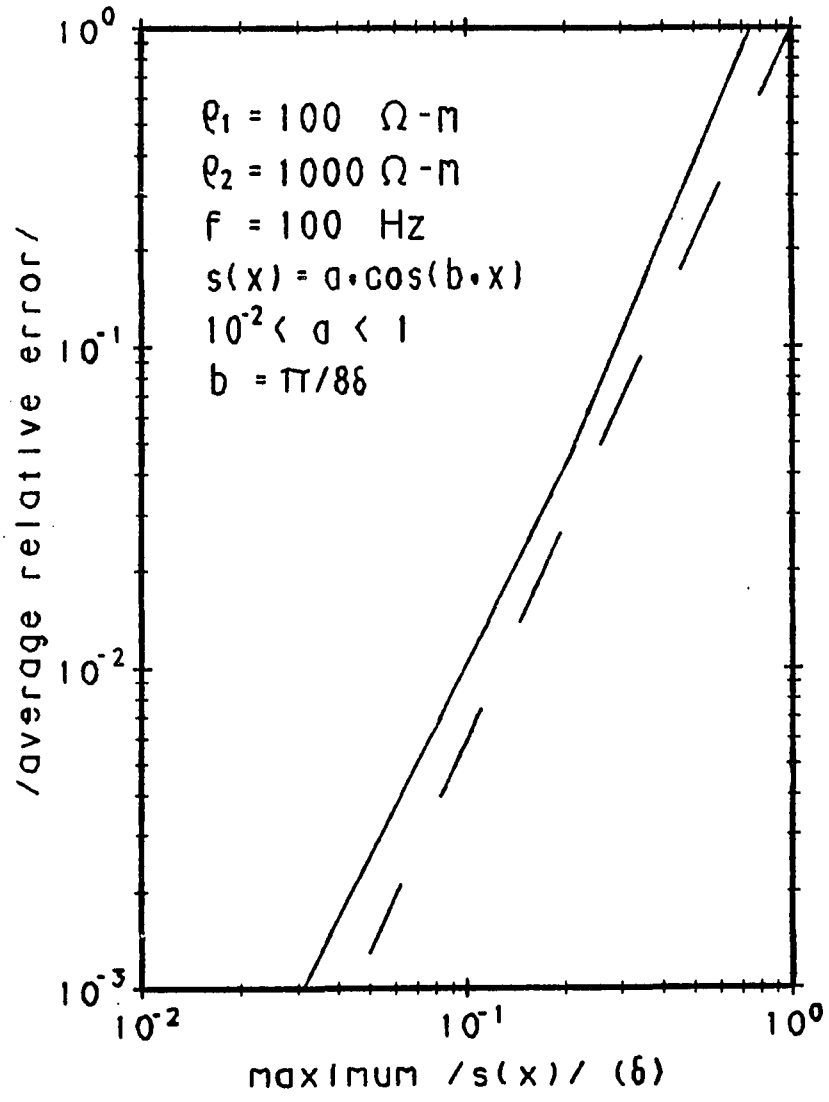

Figure 5.4 Boundary-condition Error vs Maximum |s(x)|

A log-log plot of average relative error vs maximum |s(x)| shows that boundary-condition error is second-order. Maximum |ds/dx| is much less than maximum |s(x)/δ| for this model.

relative error of 10 percent in the boundary conditions for a model with gentle slopes. For models with slopes which are comparible in magnitude with maxmimum amplitude, relative boundary-condition error is proportional to $|s(x)/\delta|^2_{max} + |ds/dx|^2_{max}$.

The effects of slope become significant when the amplitude of ds/dx exceeds the amplitude of s(x). By holding the amplitude of the standard model constant and shortening the wavelength of the cosinusoidal undulations, the contribution of steeper slopes to boundary-condition error can be determined. Figure 5.5 shows log-log plots of average relative error vs maximum slope for models with different maximum undulation amplitudes. The relative error is proportional to $|s(x)/\delta|^2_{max} + |ds/dx|^2_{max}$. To keep boundary-condition errors below 10 percent, $\left[|s(x)/\delta|^2_{max} + |ds/dx|^2_{max}\right]^{0.5}$ should be limited to a maximum of 0.28.

Another factor which affects boundary-condition error is the contrast between the resistivities of the two half-spaces. Average boundary-condition error is plotted as a function of resistivity contrast in Figure 5.6. The error is smallest for contrasts near one. For a resistivity contrast of exactly one ($\rho_1 = \rho_2$), the interface disappears and boundary-condition error is zero. For resistivity

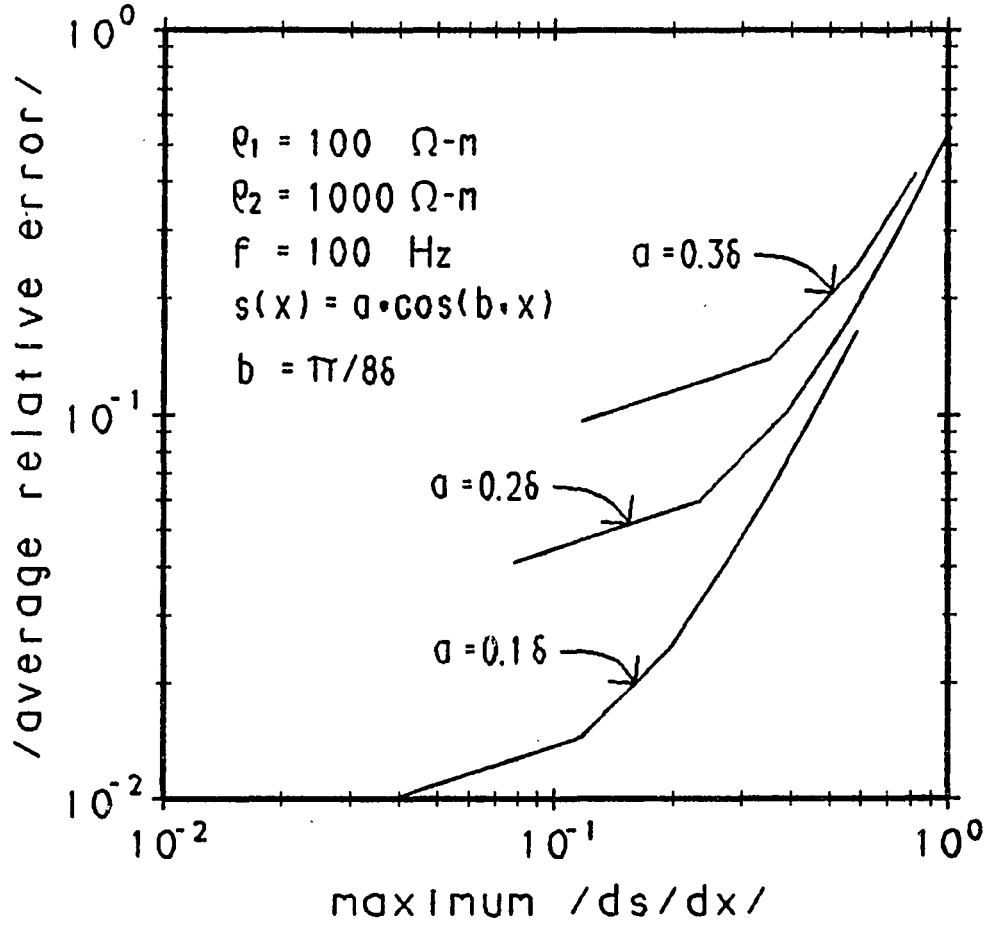

Figure 5.5 Boundary-condition Error vs Maximum |ds/dx|

Log-log plots of average relative error vs maximum |ds/dx| show that boundary-condition error is proportional to $|s(x)/\delta|^2_{max} + |ds/dx|^2_{max}$.

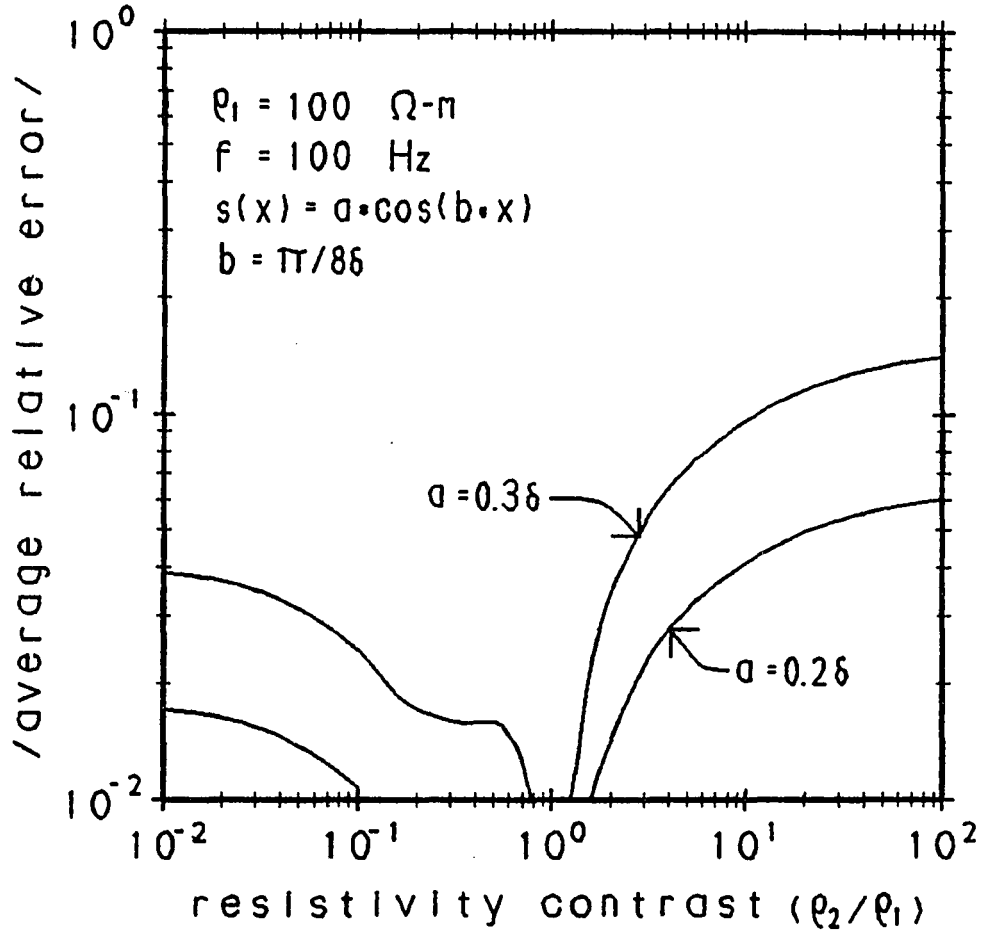

Figure 5.6 Boundary-condition Error vs Resistivity Contrast

A log-log plot of average relative error vs resistivity contrast shows that boundary-condition error reaches asymptotic limits for very large and very small resistivity contrasts.

contrasts greater than one, a low resistivity over high resistivity geometry, the boundary-condition errors rise smoothly to an asymptotic value. For resistivity contrasts less than one, a high over low geometry, boundary-condition error approach an asymptotic value, a value which is lower than the asymptotic limit for low over high resistivity contrasts. The significant information in Figure 5.6 is that errors are bounded for large resistivity contrasts. Although there is no formal limit on allowable resistivity contrasts, there is a practical limit. Increasing the conductivity in a layer implies decreasing the skin depth. A very conductive layer will have a very small skin depth and consequently, a very restrictive bound on the maximum amplitude of s(x). Large boundary-condition error in perturbation solutions to reflection from a perfectly conducting half-space with an undulating boundary is noted by Jiracek (1972, 1973). Restrictive bounds on undulations are a concern when modeling extreme high over low resistivity contrasts.

A final concern in analyzing boundary-condition error is the functional relationship between the angle of incidence and average relative error. Figure 5.7 is a perspective plot of $\log_{10}$(average error) vs k_x and k_y. The error surface has a complicated shape, but generally, error increases for increasing values of k_x and k_y. Increasing

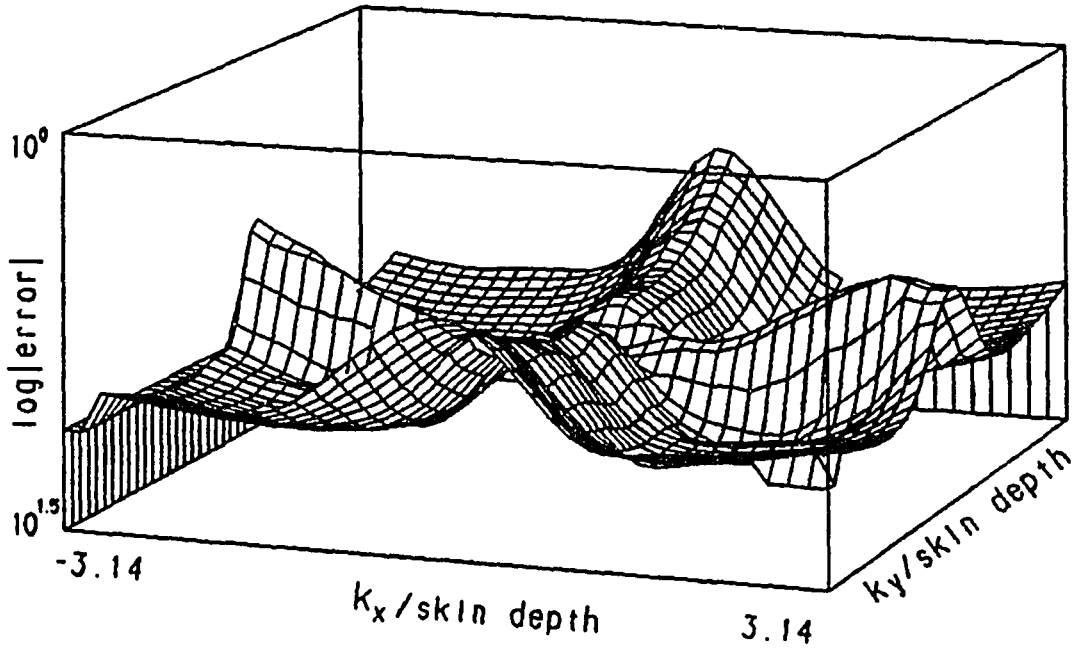

Figure 5.7 Boundary-condition Error vs Angle of Incidence

Oblique angles of incidence increase boundary-condition error. In computation of field components, the increase is more than offset by exponential attenuation in transmission coefficients.

error for larger values of k_x and k_y is to be expected. The vertical propagation factors $u_1(k_x,k_y)$ and $u_2(k_x,k_y)$ get larger as k_x and k_y increase. Larger u_1 and u_2 increase the error in approximating $e^{\pm u_j s}$ for a given s. The larger error for nonzero values of k_x and k_y is not a major concern. Exponential attenuation in the transmission coefficients $\underline{T}_m^{\downarrow}$ and $\underline{T}_n^{\uparrow}$ more than offset the increase in boundary-condition error for large $k_x^2 + k_y^2$.

The relationship between boundary-condition error and errors in surface electromagnetic field components or in apparent resistivities depends upon both the source spectrum and upon the media in which the undulating interface is embedded. The relationship between boundary-condition error and errors in other quantities of interest can be estimated for specific geometries by computing the effect of perturbations in plane-layer reflection coefficients.

This error analysis shows that the theory developed for reflection and transmission from undulating interfaces is accurate to first order in $|s(x)/\delta|$ and $|ds/dx|$. Average relative boundary-condition error is proportional to $|s(x)/\delta|^2_{max} + |ds/dx|^2_{max}$, allowing estimates of relative error for all values of $|s(x)/\delta|_{max}$ and $|ds/dx|_{max}$. If a average relative error of 10 percent in satisfying the boundary conditions can be tolerated, then

$\left[|s(x)/\delta|^2_{max} + |ds/dx|^2_{max}\right]^{0.5}$ must be less than 0.28. The programs used to compute boundary-condition error provide assurance that the theory has been derived and implemented correctly. The next step is to evaluate models which can be compared with physical measurements.

CHAPTER 6

MODELING APPLICATIONS

Application of the theory developed in the preceding chapters completes verification of the theory's correctness and demonstrates the utility of the modeling algorithm. By comparing results from the undulating interface model with data from independent sources both the theoretical development and its computer program implementation can be checked.

For a check against other numerical methods, the undulating interface model can be used to predict the effects of surface topography. A recent paper by Wannamaker, Stodt, and Rijo (1986) analyzes the effects of topography on magnetotelluric measurements. The numerical computations presented by Wannamaker, et al. (1986) include results from Rayleigh scattering and finite element models. Modeling using the theory developed in this paper are compared with a figure from Wannamaker, et al's, (1986) paper. The plane-wave source used by Wannamaker is a special case for the modeling algorithm developed here. To show how the undulating interface model developed in this dissertation is an extension to previous work, the effects of topography are evaluated for a horizontal loop-loop

system. Comparison with published results for magnetotelluric sources is a check on the correctness of the modeling algorithm, while extending previous work from a plane wave source to a loop source illustrates the originality of the theory developed here.

As a further check on the computer program implementation of the undulating interface model, numerical calculations are compared with physical measurements made over a scale model by Villegas-Garcia (1979). Villegas-Garcia (1979) measured the response of a horizontal loop-loop system over topography in a resistive basement overlain by a conductive overburden. Numerical evaluations of a non-planar, layered models closely match anomaly shapes observed in scale-model measurements. Modeling the response of a loop-loop system highlights the general applicability of the theoretical results as well as confirming the accuracy of the modeling algorithm.

To show the applicability of the undulating interface model to CSAMT measurements, a case study from Avra Valley, Arizona is presented. CSAMT data reported by Zonge, Ostrander, and Emer (1980) shows "transmitter overprint". To measure the influence of geologic structure near the transmitter, Zonge, et al. (1980) made two sets of frequency soundings. The first soundings were made with the

transmitter over shallow overburden. Without changing receiver site locations, a second set of soundings was made with the transmitter located over much thicker overburden. The two sets of sounding curves are radically different at low frequencies, a result which can not be explained by a plane-layered model. A layered model which includes the effects of changes in depth-to-bedrock, however, matches the observed data well. The transmitter overprint test provides an excellent example of the utility of the undulating interface model.

Topography Modeling

One application of the undulating interface model is in predicting the effects of subsurface topography on electromagnetic systems. For a normally incident plane-wave source, several methods of computing topographic effects are possible. An extensive literature addresses the similar problem of scattering from ocean waves. The theoretical development of the perturbation method for reflection of TE and TM mode plane waves from undulating interfaces can be applied to magnetotelluric topography modeling (Rayleigh, 1907; Rice, 1951; Barrick, 1971; Wait, 1971; Hughes, 1973, 1974, Hughes and Wait, 1975a, 1975b, Wait and Chang , 1976;, Rosich and Wait, 1976; and Hill and Wait, 1982). Wannamaker

, Stodt, and Rijo (1986) include figures of magnetotelluric topographic effects computed by the Rayleigh scattering method and cites Jiracek (1973) and Reddig and Jiracek (1984). For comparison with known results, magnetotelluric apparent resistivities were computed for the two-dimensional topography shown in Figure 6.1. Apparent resistivities are plotted in Figure 6.1 for TE mode and TM mode excitation calculated by Rayleigh scattering and by finite elements, as reported by Wannamaker, et al. (1986). Numerical results from the modeling algorithm developed here show excellent agreement with Wannamaker, et al's (1986) data.

In an extension to plane-wave source modeling, topographic effects can be computed over the same model with excitation by a three-dimensional source. Figure 6.2 is a profile for a horizontal loop-loop system over the topographic model evaluated in Figure 6.1. The source-receiver geometry is shown in Figure 6.2, the transmitter and receiver coils are 100 meters apart and 120 meters above a 100 ohm-meter earth. The coils move in tandem at a constant height. In passing over the 100 meter high ridge shown in Figure 6.2, the mutual impedance between the coils is disturbed by 50 percent. The topographic effect is appreciable for the modeled configuration.

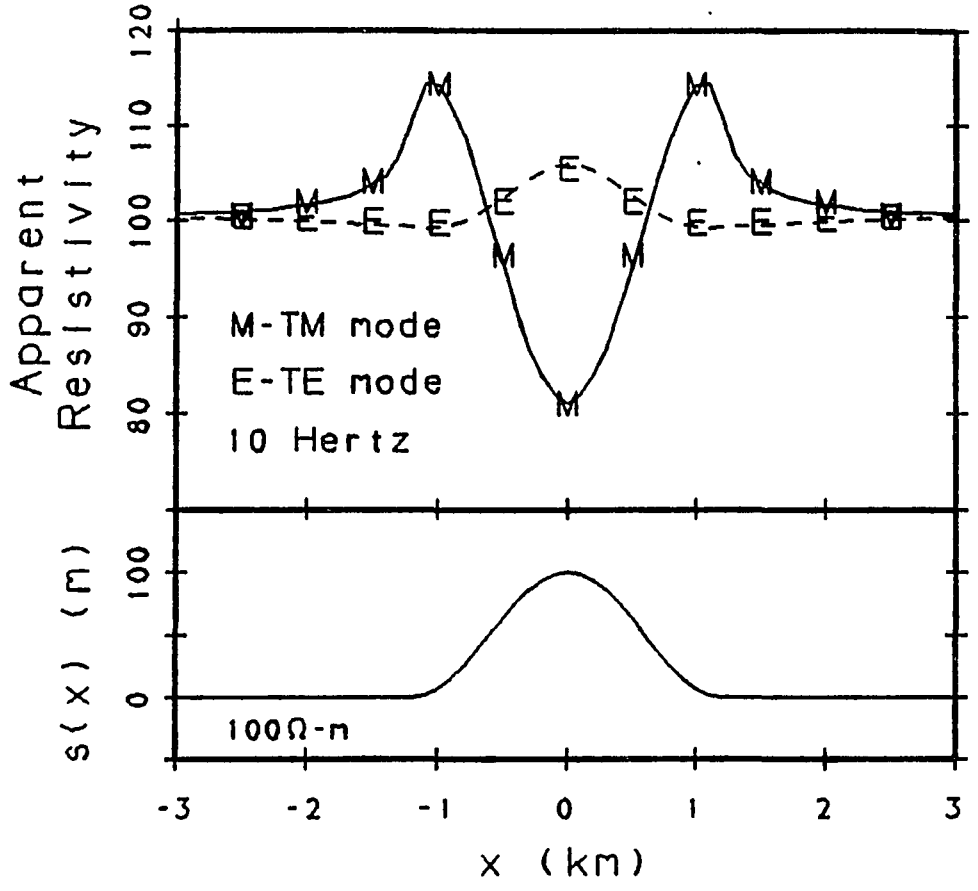

Figure 6.1 Topographic Effects on Magnetotelluric Data

Numerical results from the first-order perturbation analysis (solid line) compared with finite element and finite difference results from Wannamaker, et al. (1986).

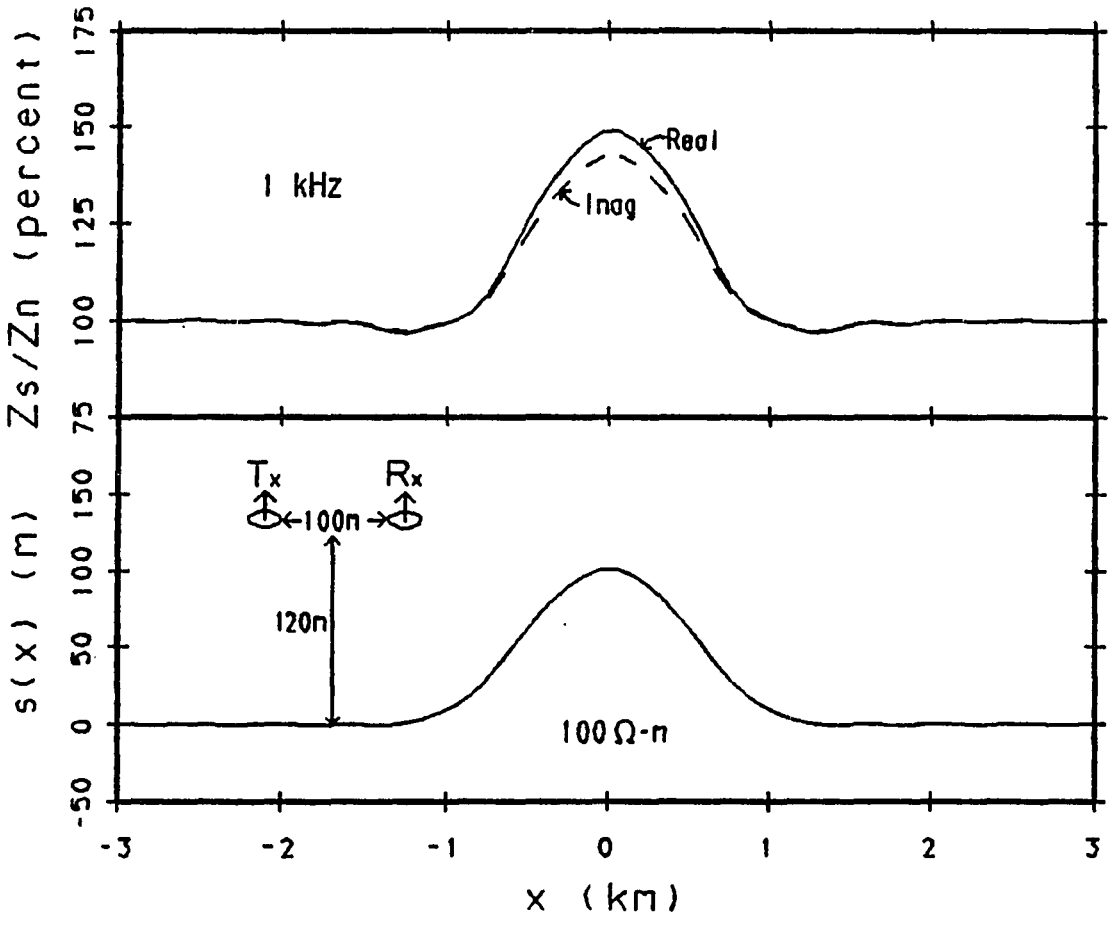

Figure 6.2 Topographic Effects on Loop-loop System

The mutual impedance between horizontal loops is perturbated by traversal over a ridge.

Modeling topographic effects is an important application of the undulating interface model. Topographic relief is easily measured, and having a practical way to predict its effect on electromagnetic measurements allows the routine use of topographic correction algorithms.

Horizontal Loop-loop Modeling

A convenient check on the validity of the undulating interface model is provided by comparison with scale modeling results from a thesis by Villegas-Garcia (1979). Villegas-Garcia (1979) measured the response of scaled-down horizontal loop-loop systems over a conductive overburden of varying thickness underlain by a resistive basement.

The geometries of Villegas-Garcia's scale models are depicted in Figure 6.3. Two small, horizontal loops are kept at a constant height, h, a constant separation, R, and are moved in tandem over the scale models shown in Figure 6.3. The four scale models represent a uniform basement, a basement step, a basement ridge, and a basement valley. The overburden layers were made from slabs of graphite with an average conductivity of 9.7×10^4 mhos/meter. The graphite's coefficient of anisotropy was less than 1.2.

To measure the effects of finite slab size, data from frequency sounding measurements over a graphite slab

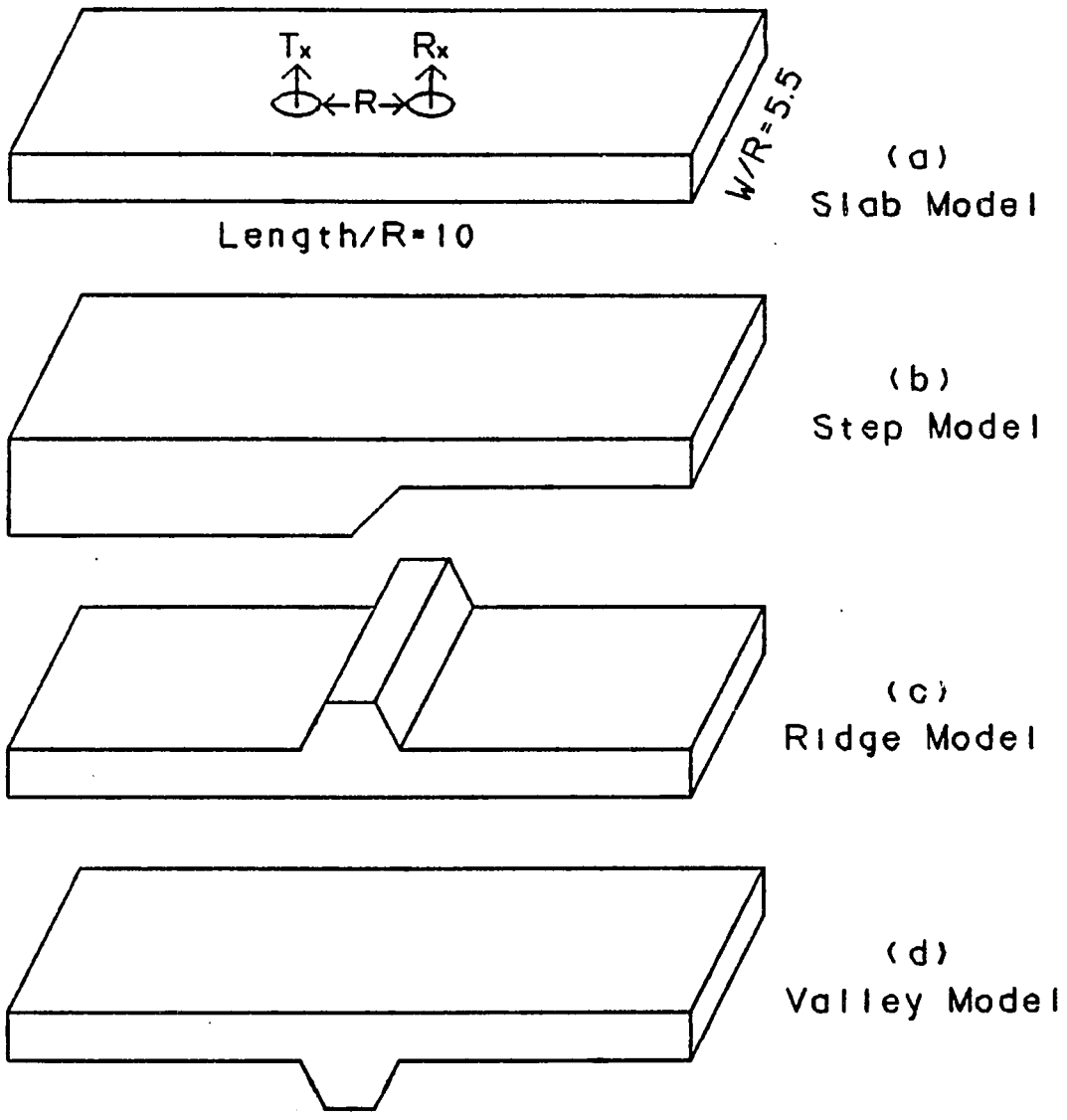

Figure 6.3 HLEM Scale Model Shapes

Scale model measurements for a horizontal loop (HLEM) configuration were made over graphite slabs milled into shapes representing a uniform layer, a basement step, a basement ridge, and a basement valley. Adapted from Villegas-Garcia (1979, Fig. 2)

with uniform thickness were compared with the theoretical results for a slab with uniform thickness and infinite horizontal extent. Scale model measurements were made with the loop configuration oriented across the width of the slab and with the loop configuration oriented along the length of the slab. The results of the frequency soundings are shown in Figure 6.4. The scale-model measurements are effected by the finite size of the graphite slabs. The curves marked A (across) and L (along) bracket the theoretical results, marked by T in Figure 6.4. Figure 6.4 shows a five to ten percent difference at 888 Hz between the scale-model measurements and the results expected for an infinite-width slab. The presence of edge effects in the scale-model measurements weakens their utility as a check on theoretical results. The scale model profiles over basement topography should have the right anomaly shape, but anomaly amplitudes are not exact. Profiles were run perpendicular to strike over the remaining three cross sections shown in Figure 6.3. In-phase and quadrature measurements of the vertical component of the secondary magnetic field are reported as a percentage relative to the primary field.

For comparison with the scale-model results the CSAMT modeling program was modified to compute horizontal loop-loop responses. The accuracy of the program's

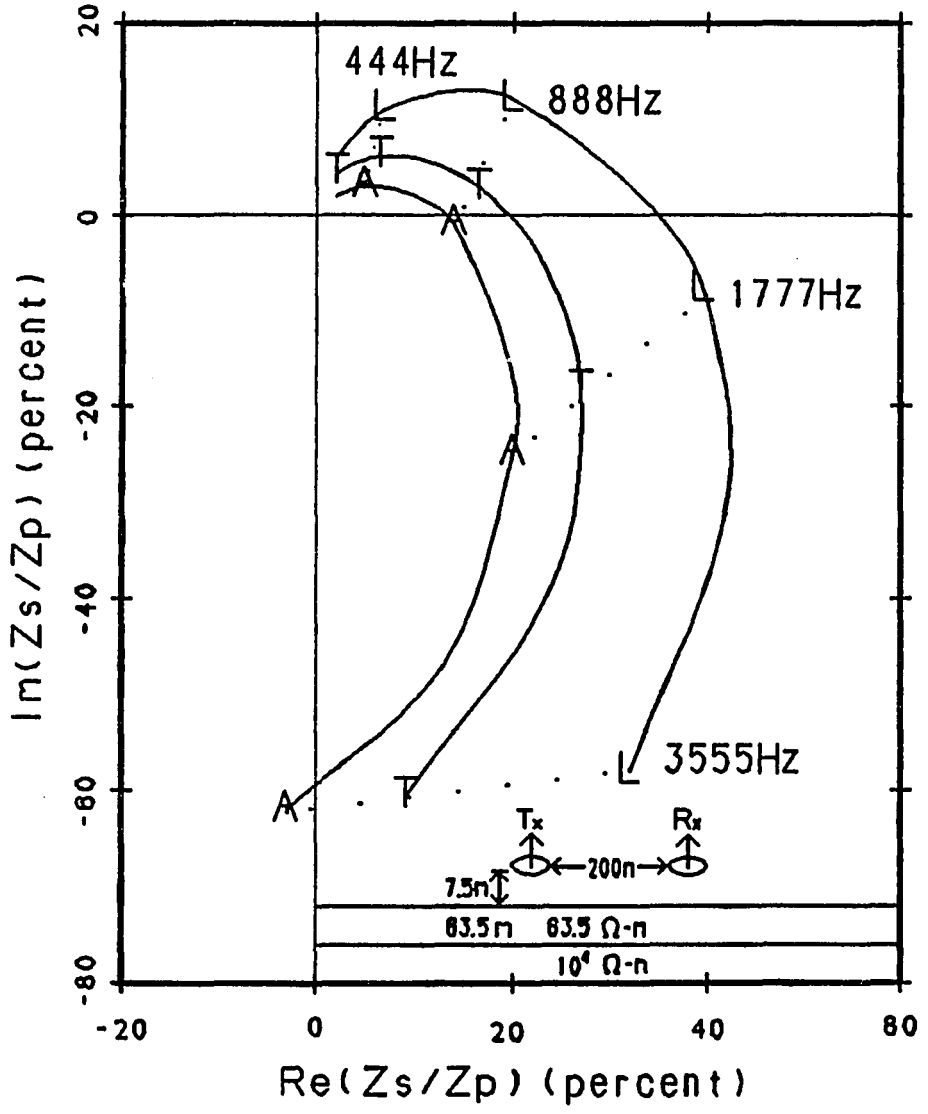

Figure 6.4 Scale Model Results for a Plane Layer

A comparison of scale model measurements with theoretical results for plane layers shows the effects of finite slab size. Measurements along the slab, L, and measurements across the slab, A, differ from the theoretical results, T, because of the slab's finite size. Profiles over basement topography were made with the along-the-slab orientation, L. Adapted from Villegas-Garcia (1979, Fig. 1).

integration routines was tested by comparing flat-layer responses computed using a double Fourier transform with the responses computed using Hankel transforms. Both methods of model evaluation agreed to within one percent. For the evaluation of undulating interface models, the Hankel transform method was used for computation of the plane-layer contribution and double Fourier transforms were used to compute the perturbing effects of undulations.

The results of a profile over a step model are shown in Figure 6.5. The solid lines mark the numerical results from the undulating interface model while the letters show the results of Villegas-Garcia's (1979) scale modeling. The scale-model results and the numerical calculations produce profiles with the same shape, but with different anomaly amplitudes. The anomaly predicted by the numerical model is lower in amplitude than the anomaly resulting from scale model measurements. Asymptotic values for plane layers are marked by the small letters "ai" and "ar" at the ends of the profiles. The numerical results approach the correct asymptotic values more closely than the results from scale-model measurements. The presence of edge effects distorts anomaly amplitudes in the scale-model measurements.

A second model geometry is a profile over a basement ridge, shown in Figure 6.6 . Again, the agreement between

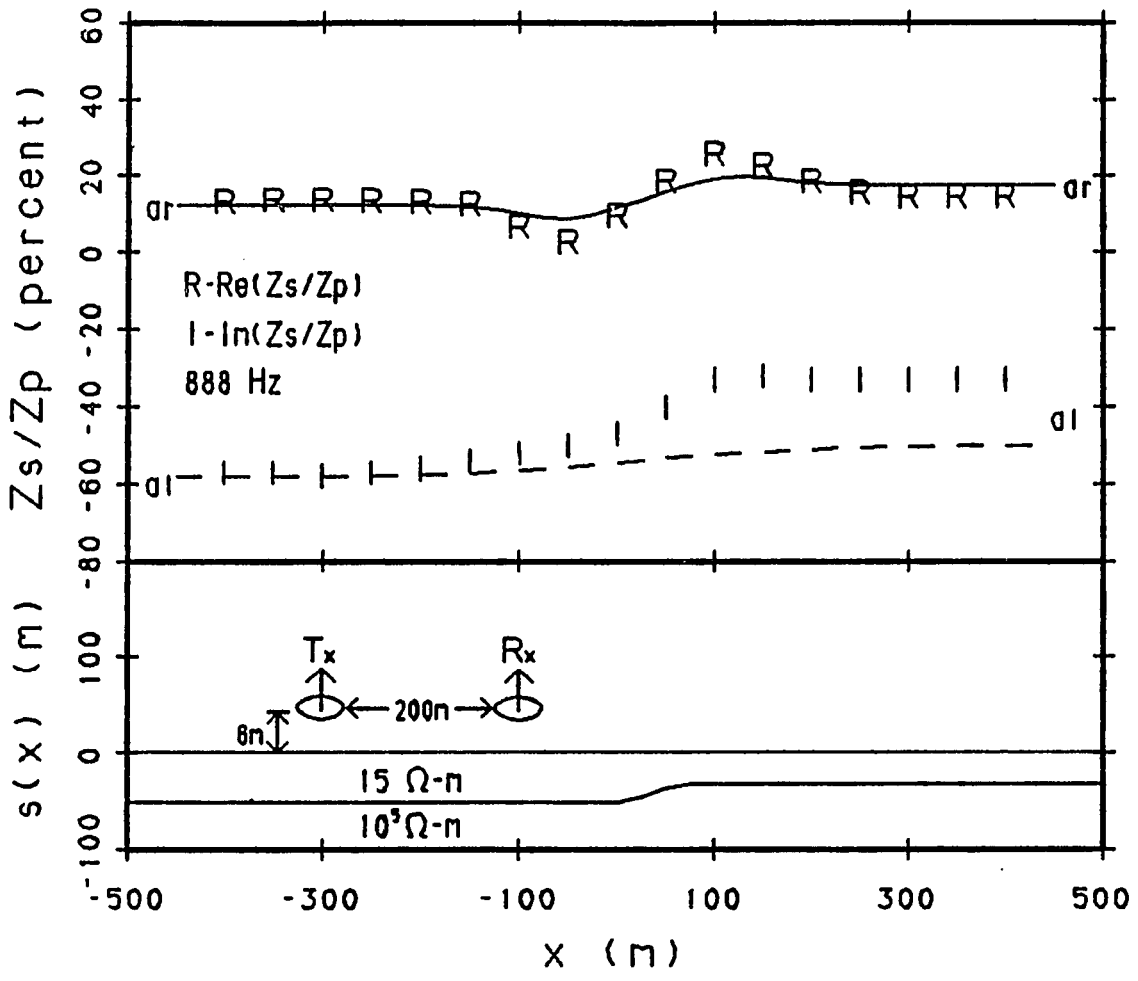

Figure 6.5 HLEM Response over a Step Model

Lines show numerical results from perturbation analysis, letters "R" and "I" mark scale model results, and letters "ar" and "ai" indicate asymptotic values for plane layers. Scale-model results are shifted by (-25,-11) percent to match asymptotic limits. Adapted from Villegas-Garcia (1979, Fig. 3).

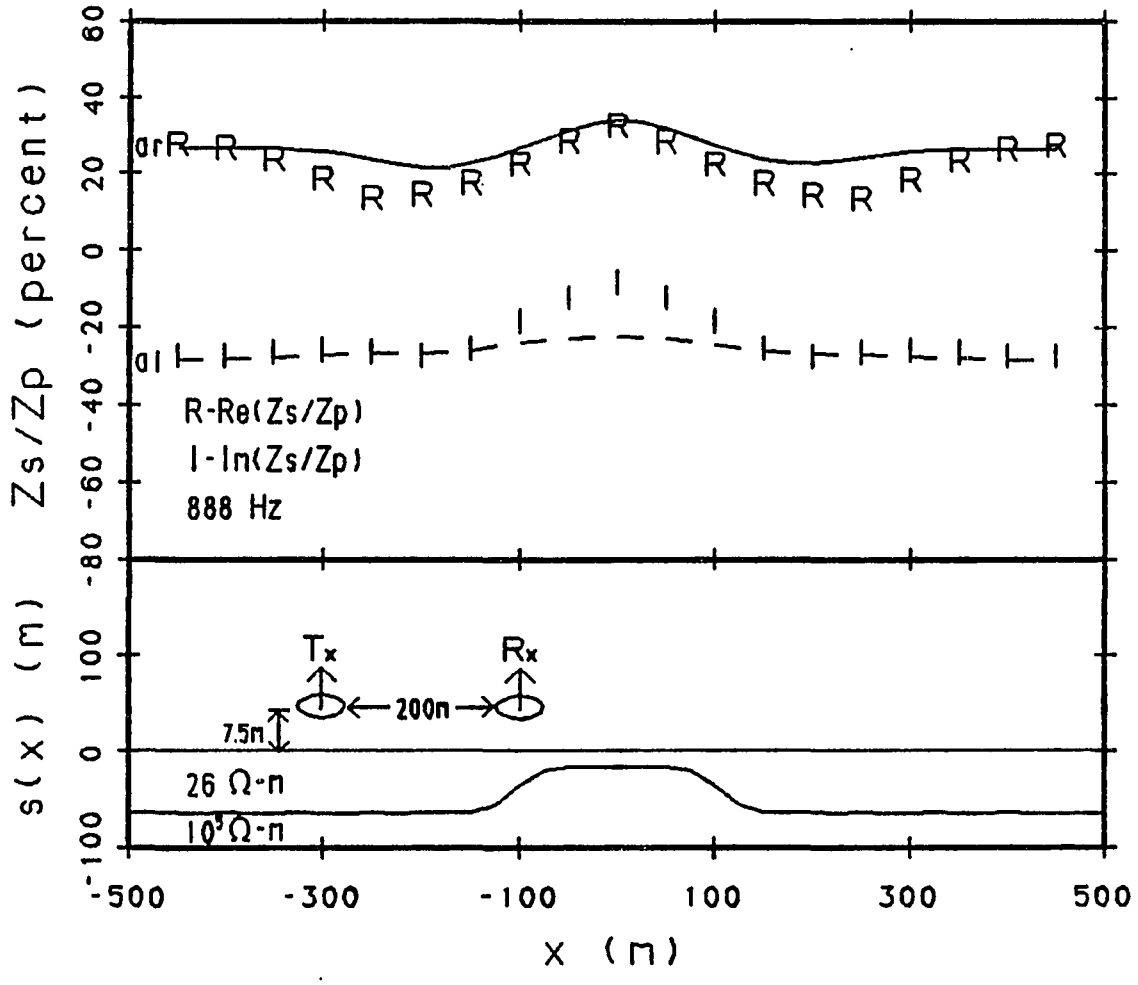

Figure 6.6 HLEM Response over a Ridge Model

Lines show numerical results from perturbation analysis, letters "R" and "I" mark scale model results, and letters "ar" and "ai" indicate asymptotic values for plane layers. Scale-model results are shifted by (-20,-16) percent to match asymptotic limits. Adapted from Villegas-Garcia (1979, Fig. 9).

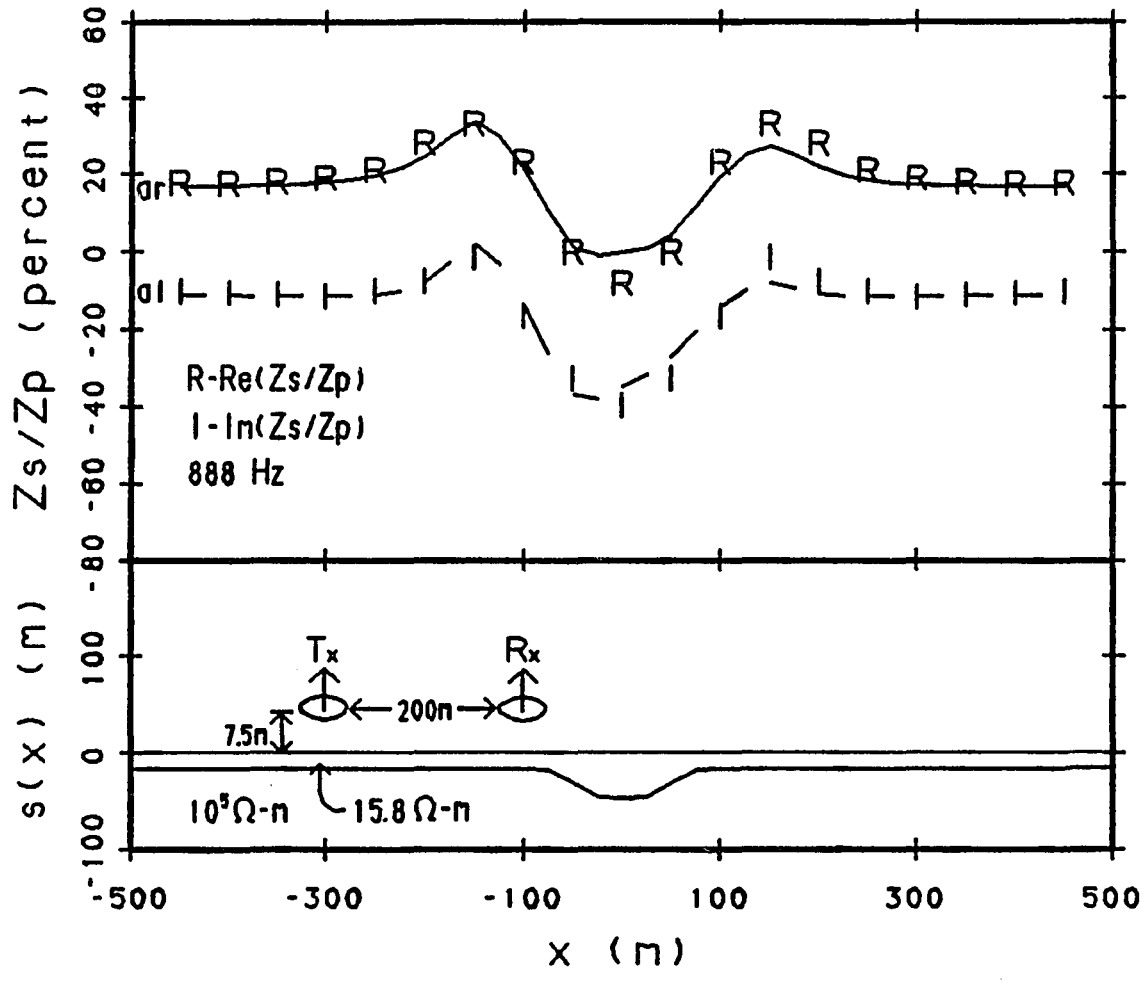

Figure 6.7 HLEM Response over a Valley Model

Lines show numerical results from perturbation analysis, letters "R" and "I" mark scale model results, and letters "ar" and "ai" indicate asymptotic values for plane layers. Scale-model results are shifted by (-12,-16) percent to match asymptotic limits. Adapted from Villegas-Garcia (1979, Fig. 13).

numerical computation and scale-model measurements is good with regard to anomaly shape, but results differ in amplitude. The numerical results are less dramatic than the scale-model results. A final profile is over a basement valley model, shown in Figure 6.7. For the basement valley model, the numerical modeling closely matches physical measurements. Comparison with scale-model results provides assurance that the numerical modelling is correct. The versatility of the theoretical undulating interface model in accommodating many source types is demonstrated in the computing the response of a loop-loop system.

Transmitter Overprint

A recurring problem in CSAMT surveys is the effect that geologic structure near the transmitter has on frequency sounding curves. The effect of near-transmitter geologic structure has been termed "transmitter overprint" (Zonge, Ostrander, and Emer, 1980). A dramatic example of transmitter overprint is provided by a set of CSAMT measurements make in Avra Valley, Arizona (Zonge, et al. 1980).

The geometry of the survey reported by Zonge, et al. (1980) is shown in Figure 6.8. Two transmitter sites were used to make frequency soundings at the same receiver

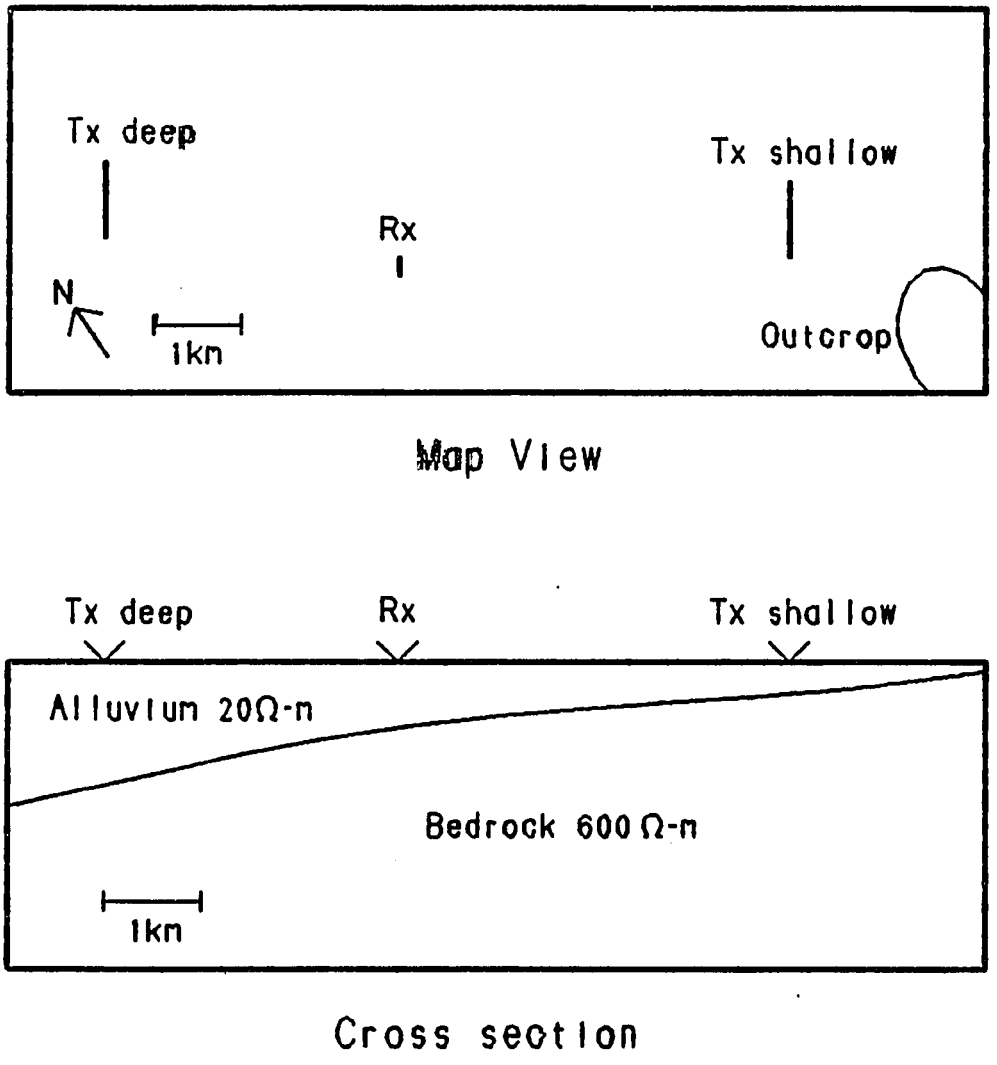

Figure 6.8 Transmitter Overprint Geometry

Two CSAMT soundings were made at the same receiver site. One sounding was made with the transmitter placed over shallow overburden and a second sounding was made with the transmitter placed over deep overburden.

locations. As shown by cross section in Figure 6.8, depth-to-bedrock in the area increases dramatically from right to left. A fairly conductive overburden of approximately 20 ohm-meters overlies a resistive basement of about 600 ohm-meters. Plane-layer theory predicts that frequency soundings made at a particular receiver site should be the same regardless of transmitter siting.

For this situation, the plane-layer paradigm fails. Two frequency soundings made at one receiver site are not the same, as is shown in Figure 6.9. Apparent resistivities plotted for a transmitter sited over deep overburden, marked by D's in Figure 6.9, show a smooth trend from high to low resistivity. In contrast, apparent resistivities plotted for the transmitter sited over shallow overburden, marked by S's in Figure 6.9, make a dramatic rise at low frequencies. The steep upward rise at low frequencies is characteristic of "near-field" measurements. For CSAMT measurements in the near-field, static current patterns are a much more accurate model than the plane-wave source assumed in magnetotellurics. At high frequencies, apparent resistivities for both transmitter sites are coincident, indicating that the magnetotelluric model is valid and that near-transmitter geology is not affecting the measurements. The discrepancy at low frequencies, however, can only be

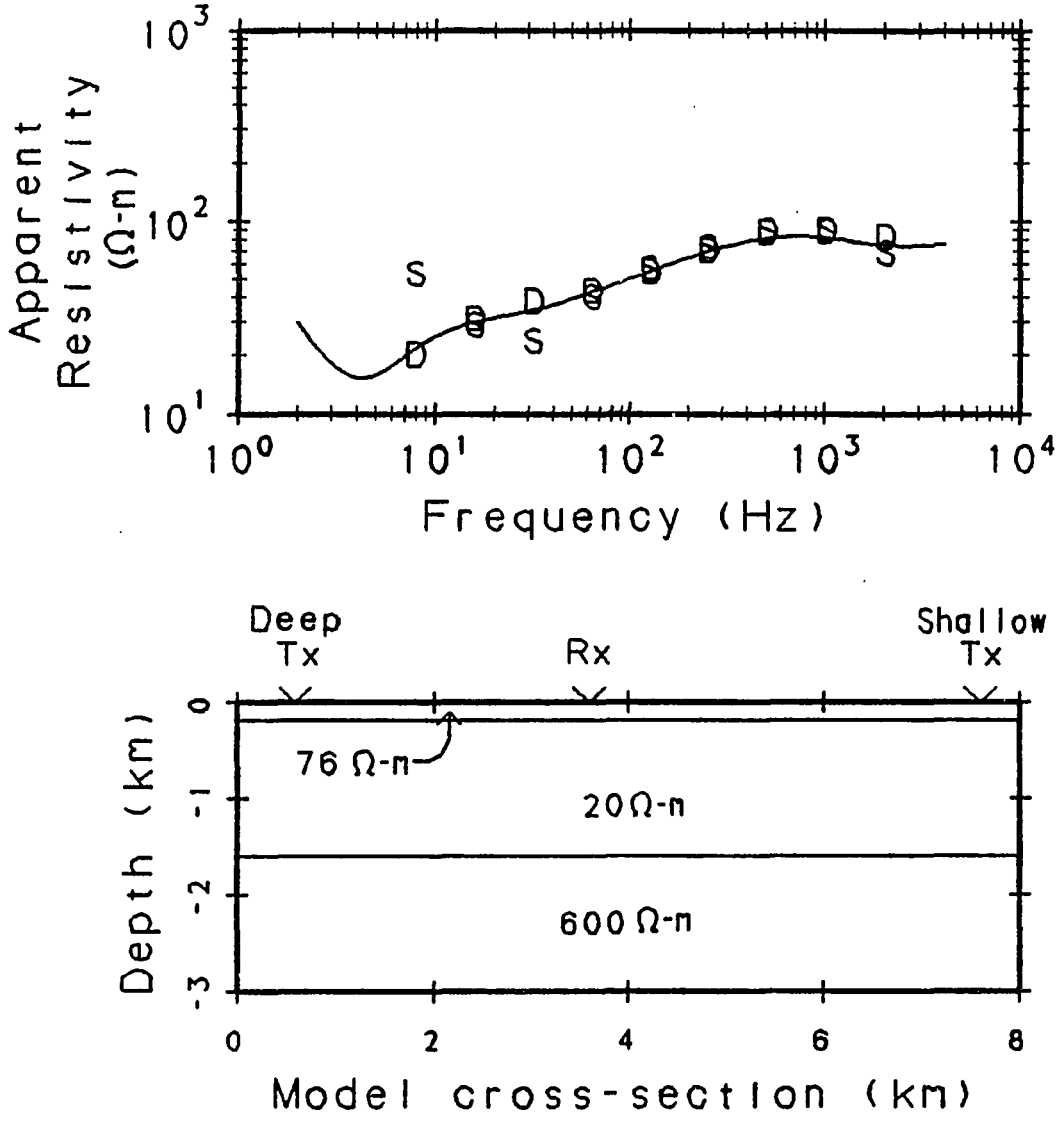

Figure 6.9 Transmitter Overprint Sounding Curves

A log-log plot of apparent resistivity vs frequency for the area shown in Figure 6.8. Data from the sounding with the transmitter over deep overburden is marked with "D" and data from the sounding with the transmitter over shallow overburden is marked with "S". The solid line is the result from evaluation of the plane-layered model shown in cross section.

explained by models with a variable depth-to-basement.

Conventional wisdom holds that the frequency sounding for data collected with the transmitter over thick overburden should give accurate results when interpreted with plane-layer models. The result of inversion of the deep transmitter data into a plane-layer model is shown in Figure 6.9. The solid line in log-log plot results from evaluation of the three-layer model shown in cross section. The plane-layered model matches the observed data for a transmitter sited over deep overburden. The plane-layered inversion predicts a depth of 1.6 km to the resistive basement. Conventional interpretation would discount the data collected with the transmitter sited over shallow overburden as contaminated by "transmitter overprint" and accept the data collected with the transmitter sited over deep overburden as equivalent to measurements over a plane-layered earth. The validity of the plane-layered model can be tested against results which include a variable depth-to-basement.

Including the effects of varying depth-to-basement allows an accurate match to both sets of data with the same model. Figure 6.10 compares modeling results for a sloping basement with the transmitter overprint data from Avra Valley. The match is excellent. A cross section of model

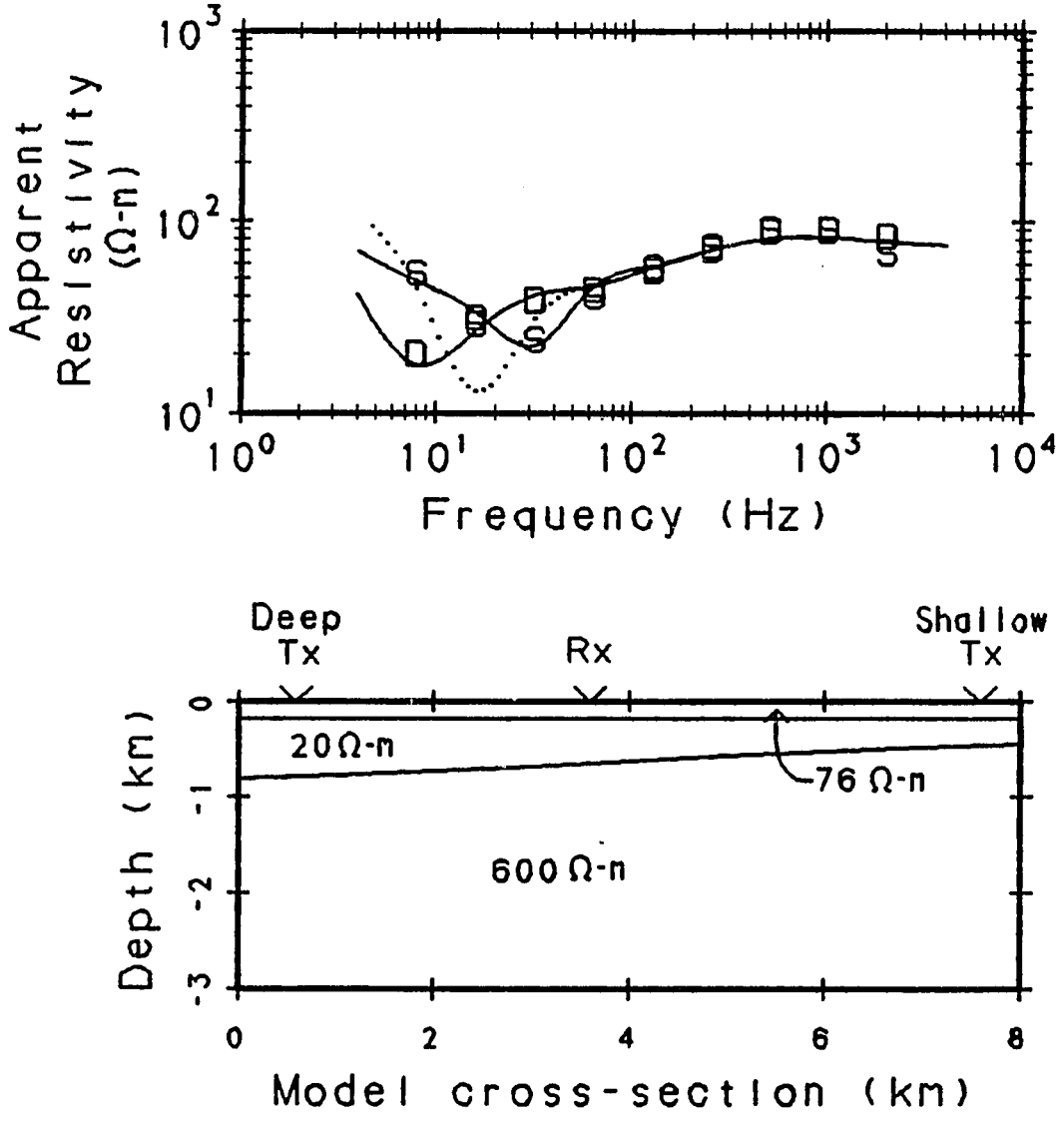

Figure 6.10 Transmitter Overprint Modeling Results

The results of matching the transmitter overprint data with a model which includes a sloping interface. The solid lines are the result of evaluating the model shown in cross section. The dotted line is from the evaluation of a plane-layered model which matches layer thicknesses under the receiver site.

geometry in Figure 6.10 shows the sloping basement. The depth-to-basement predicted by the sloping interface model is much less than the depth predicted by a plane-layered model using the frequency sounding made with the transmitter over deep overburden. Ignoring the effects of sloping basement results in an inaccurate interpretation. Using a model which includes the effects of basement topography allows a match to frequency soundings for both transmitter sites and gives a more accurate depth-to-basement estimate.

The model of a sloping depth-to-basement is supported by gravity measurements. Oppenheimer (1980a, 1980b) estimated depth-to-bedrock in Arizona's basin and range province by inverting gravity data. Oppenheimer's (1980b) depth-to-bedrock map shows a sloping alluvium-bedrock interface in the Avra Valley study area, an interpretation which is in agreement with the results of CSAMT modeling.

Lateral variations in layer thicknesses can have a significant effect on CSAMT measurements, an effect which is not predicted or explained by plane-layered models. The undulating interface algorithm successfully models CSAMT data from Avra Valley, data which can not be matched by plane-layer models.

CHAPTER 7

CONCLUSIONS

The effects of lateral changes in geology on CSAMT data can be significant. The effects are most pronounced at lower frequencies. Interpretation of transition zone and near field data requires an explicit representation of the three dimensional source used in CSAMT. When lateral variations are present, both the three-dimensional source and geology between the transmitter and receiver must be represented in models. The application of plane-layered models in cases where lateral variations are present leads to inaccurate estimates of geological parameters.

The theory developed here extends the plane-layered model to include the effects of lateral variation in layer thickness. A first-order perturbation solution is developed for reflection from and transmission through an interface with two- or three-dimensional undulations. The theoretical formulation incorporates three-dimensional source excitation. A numerical analysis of error indicates that the first-order perturbation solution is accurate to within 10 percent for smooth undulations with a maximum amplitude of 0.28 skin depths.

Evaluation of the undulating interface model agrees with results from finite element modeling of topographic features for the special case of excitation by a plane-wave source. The capability of including both a three-dimensional source and interface undulations is an extension to previous work.

The utility of the theoretical result extends beyond modeling CSAMT data. A more general application of the theory is illustrated by comparison of numerical modeling with data form physical scale models of a horizontal loop electromagnetic system.

Application of the undulating interface model to CSAMT data from Avra Valley highlights a situation where plane-layered models are inadequate. CSAMT measurements made over a sloping basement can not be interpreted accurately using models with uniform layer thicknesses. Allowing lateral variation in layer thickness produces model responses which agree with physical measurements and a model geometry which coincides with what is known about the geology at the case study area.

Lateral variations in layer thickness is only one possible extension to the plane-layered model. More complicated effects are observed over areas where the geology varies laterally both in layer thickness and in

resistivity. A natural extension of the theory developed here would be to derive a first-order perturbation solution for variations in layer resistivity. The development would be similar to the analysis of an undulating interface. The ability to model lateral variations in resistivity would advance the theoretical understanding of electromagnetic exploration techniques closer to an accurate representation of nature.

CSAMT remains a popular exploration tool. The difficulties associated with the interpretation of low frequency data can be attacked with theoretical models which include the effects of lateral variation. The development and application of a model which includes the effects of changes in layer thickness provides a useful extension to existing theory.

SELECTED BIBLIOGRAPHY

Aguirre, G., 1986, An appraisal of the electrically thin conductive sheet model in geophysical probing: Unpublished M.S. thesis, University of Arizona.

Aleksandrova, A.A., and Khizhnyak, N.A.,1975, Diffraction of electromagnetic waves by a dielectric wedge: Sov. Phys. Tech. Phy., v.19, 1385-1389.

Alterman, Z., and Nathaniel, R., 1975, Seismic waves in a wedge: Bull. of the Seism. Soc. of America, v.65, 1697-1719.

Anderson, J.B., and Solodukhow, V.V., 1978, Field behavior near a dielectric wedge: IEEE Tran. on Antennas and Propagation, v.AP-26, 598-602.

Anderson, W.L., 1974, Electromagnetic fields about a finite electric wire source: U.S. Dept. Comm. Natl. Tech. Inf. Service report, PB 238199.

Anderson, W.L., 1982, Fast Hankel transforms using related and lagged convolutions: ACM Trans. on Math. Software, v.8, 344-368.

Anderson, W.L., 1984, Computation of Green's tensor integrals for three-dimensional electromagnetic problems using fast Hankel transforms: Geophysics, v.49, 1754-1759.

Assal, H.M., and Mahmoud, S.F., 1987, A new inversion technique for apparent resistiviy measurements: IEEE Tran. on Geoscience and Remote Sensing, v.GE-25, 7-10.

Bannister, P.R., 1966, Quasi-static fields of dipole antennas at the earth's surface: Radio Science, v.1, 1321-1330.

Banos, A., 1966, Dipole radiation in the presence of a conducting half-space: Pergamon Press, New York.

Barashkov, A.S., 1985, Interpretation of magntotelluric sounding data in the class of quasi-one-dimensional models: Izvestiya, Earth Physics, v.21, 767-774.

Barrick, D.E., 1971, Theory of HF and VHF propagation across the rough sea: Radio Science v.6, 517-533.

Barthes, V., and Vasseur, G., 1978, An inverse problem for electromagnetic prospecting: in Applied Inverse Problems, Ed. P.C. Sabatier, Lecture notes in Physics, v.85, 325-329.

Bates, R.H.T., 1975, Analytic constraints on electromagnetic field computations: IEEE Transactions on Microwave Theory and Techniques, v.MT-23, 605-623.

Bates, R.H.T., and Wall, D.J.N., 1977, Null field approach to scalar diffraction I: General method., II: Approximate methods: Phil. Trans. Roy. Soc. London, v.A287, 45-95.

Belyavskiy, V.V., Vollkovich, V.E., and Panich, I.M., 1985, The possibility of studying telluric anomalies in the lower half-space: Izvestiya, Earth Physics, v.21, 279-284.

Berdichevskiy, M.N., Dmitriyev, V.J., Barashlov, I.S., Mershchikova, N.A., and Kobzova, V.M., 1982, On magnetotelluric sounding of conducting layers in the Earth's crust and upper mantle: Izvestiya, Earth Physics, v.18, 520-530.

Best, M.E., Duncan, P., Jacobs, F.J., and Scheen, W.K., 1985, Numerical modeling of three-dimensional conductors in a layered earth: Geophysics, v.50, 665-676.

Bobrovnikov, M.S., and Kislitsyna, V.N., 1964, Diffraction of a uniform plane electromagnetic wave at an impedance step discontinuity: Radio Engineering and Electronic Physics, v.9, 1401-1404.

Bojarski, N.N., 1982a, Low frequency inverse scattering: IEEE Transactions on Antennas and Propagation, v.AP-30, p775-778.

Bojarski, N.N., 1982b, A survey of the near-field far-field inverse scattering source integral equation: IEEE Trans. on Antennas and Propagation, v.AP-30, 975-979.

Bojarski, N.N., 1984, Scattering by a cylinder: a fast exact numerical solution: J. Acoust. Soc. Am., v.75, 320-323.

Bostrom, A.G., Kristensson, G., and Strom, 1983, Transformation properities of plane, spherical and cylindrical scalar and vector functions: Handbook on Acoustic Electromagnetic and Elastic wave scattering.

Bowerman, J.J., Senior, B.A., and Uslenghi, P.L., 1969, Electromagnetic and acoustic scattering by simple shapes: North Holland Publishing Co., Amsterdam, Wiley and Sons, New York.

Bracewell, R.N., 1978, The Fourier transform and its applications, McGraw-Hill, New York.

Brebbia, C.A., Telles, J.C.F., and Wrobel, L.C., 1984, Boundary element techniques: Springer-Verlag Publishing Co., New York.

Campbell, G.A., and Foster, R.M., 1948, Fourier integrals for practical applications: Van Nostrand, New York.

Chang, D.C., and Wait, J.R., 1974, Extremely low frequency (ELF) propagation along a horizontal wire located above or buried in the earth: IEEE Tran. on Communications, v.COM-22, 421-426.

Chen, P.F., and Fung, P.C.W., 1986, The frequency response of two-dimensional anomalies revisited: J. Geomag. Geoelectr., v.38, 873-881

Chuang, S.L., and Kong, J.A., 1981, Scattering of waves from periodic surfaces: Proceedings of the IEEE, v.69, 1132-1144.

Chuang, S.L., and Kong, J.A., 1982, Wave scattering from a periodic dielectric surface for a general angle of incidence: Radio Science: v.17, 545-557.

Clemmow, P.C., 1966, The plane wave spectrum representation of electromagnetic fields: Pergamon Press, Oxford.

Das, U.C., 1982, Designing digital linear filters for computing resistivity and electromagnetic sounding curves: Geophysics, v.47, 1456-1459.

Das, U.C., and Parasnis, D.S., 1987, Resistivity and induced polarization responses of arbitrary shaped 3D bodies in a two-layered earth, Geophys. Prosp., v.35, 93-109.

Davies, B., 1978, Integral transforms and their applications: Applied mathematical sciences, v.25, Springer-Verlang, New York.

Dawson, T.W., 1983, E-polarization induction in two thin half-sheets: Geophys. J. Roy. Astr. Soc., v.73, 83-107.

Dawson, T.W., and Weaver, J.T., 1979a, H-polarization induction in two thin half-sheets: Geophys. J. Roy. Astr. Soc, v.56, 419-438.

Dawson, T.W., and Weaver, J.T., 1979b, Three-dimensional induction in a non-uniform thin sheet at the surface of a uniformily conducting earth: Geophys. J. Roy. Astr. Soc., v.59, 445-462.

Devaney, A.J., and Wolf, E., 1974, Multipole expansions and plane wave representations of the electromagnetic field: J. Math. Physics, v.15, 234-244.

Dmitriev, V.I., and Zakharov, E.V., 1970, A method for solving problems in the electrodynamics of inhomogeneous media: USSR Comp. Math. Phys., v.10, 144-151.

D'Yakonov, B.P., 1959, The diffraction of electromagnetic waves by a circular cylinder in a homogeneous half-space: Bull. Acad. Sci., USSR, Geophys. Ser., (4), 950-955.

Edwards, R.N., Lee, H., and Nabighian, M.N., 1978, On the theory of magnetometric resistivity (MMR) methods: Geophysics, v.43, 1176-1203.

Erdelyi, A., Magnus, W., Oberhettinger, F., and Tricomi, F.G., 1954, Tables of integral transforms, vols I and II: McGraw-Hill, New York.

Felsen, L.B., 1984, Progressing and oscillatory waves for hybrid synthesis of source-excited propagation in layered media: Geophys. J. Roy. Astr. Soc., v.79, 11-33.

Fisher, G., and LeQuang,B. 1981, Topography and minimization of the standard deviation in one-dimensional magnetotelluric modeling: Geophys. J. Roy. Astr. Soc, v.67, 279-282.

Fisher, G., and Schnegg, P.A., 1986, Modeling active audio-magnetotelluric data: J. Geophysics, v.59, 49-55.

Geyer, R.G., 1972, The effect of a dipping contact on the behavior of the electromagnetic field: Geophysics, v.37, 337-350.

Geyer, R.G., 1976, Magnetotelluric probing for buried geologic structures: IEEE Tran. on Geoscience Electronics, v.GE-14, 223-230.

Green, V.R., and Weaver, J.T., 1978, Two-dimensional induction in a thin sheet of variable integral conductivity at the surface of a uniformly conducting earth: Geophys. J. Roy. Astr. Soc., v.55, 721-736.

Goldstein, M.A., and Strangway, D.W., 1975, Audio-frequency magnetotellurics with a grounded electric dipole source: Geophysics, V. 40, 669-683.

Gunderdson, B.M., Newman, G.A., and Hohmann, G.W., 1986, Three-dimensional transient electromagnetic reponses for a grounded source: Geophysics, v.51, 2117-2130.

Habashy, T.M., Kong, J.A., and Tsang, L., 1985, Quasi-static electromagnetic fields due to dipole antennas in bounded conducting media: IEEE Tran. on Geoscience and Remote sensing, GE-23, 325-333.

Harrington, R.F., 1961, Time-harmonic electromagnetic fields: McGraw-Hill Book Co., New York.

Heikka, J., Zhamaletdinov, A.A., Hjedt, S.E., Demidova, T.A., and Velikhov, Ye.P., 1984, Preliminary results of MHD test registrations in northern Finland: J. Geophysics, v.55, 199-202.

Hermance, J.F., 1973, Processing of magnetotelluric data: Physics of Earth and Planetary Interiors, v.7, 349-364.

Hermance, J.F., 1978, Electromagnetic induction in the Earth by moving ionospheric current systems: Geophysic. J. Roy. Astr. Soc., v.55, 557-576.

Hermance, J.F., 1982a, Refined finite-difference simulations using local integral forms: Application to telluric fields in two-dimensions: Geophysics, v.47, 825-831.

Hermance, J.F., 1982b, The asymptotic response of three-dimensional basin offsets to magnetotelluric fields at long periods: The effects of current channeling: Geophysics, v.47, 1562-1573.

Hibbs, R.D., and Jones, F.W., 1976, The calculation of the electromagnetic fields of a sheet current source with an arbitrary spatial intensity distribution over a layered half space - I, The general method and results.: Geophys. J. Roy. Astr. Soc, v.46, 433-452.

Hill, D.A., and Wait, J.R., 1973a, Subsurface electromagnetic fields of a grounded cable of finite length: Can. J. Phys., v.51, 1534-1540.

Hill, D.A., and Wait, J.R., 1973b, Subsurface electric fields of a grounded cable of finite length for both frequency and time domain: Pageoph, v.111, 2324-2332.

Hill, D.A., and Wait, J.R., 1982, Theoretical noise and propagation models for through-the-earth communication: Final Report to Bureau of Mines (contract JO113058).

Howard, A.Q., 1972, Electromagnetic fields of a subterranean cylindrical inhomogeneity excited by a line source: Geophysics, v.37, 975-984.

Howard, A.Q., 1975a, A canonical solution to the three-dimensional electromagnetic prospecting problem: Radio Science, v.10, 461-471.

Howard, A.Q., 1975b, On approximating Fourier integral transforms by their discrete counterparts in certain geophysical applications: IEEE Tran. on Antennas and Propagation, v.AP-23, 264-266.

Howard, A.Q., ed., 1984, Electromagnetic methods in applied geophysics: IEEE Tran. on Geoscience and Remote Sensing, special issue, v.GE-22.

Hudson, J.A., 1982, The diffraction of an acoustic wave by an embedded quarter-space: IMA J. Appl. Math, v.28 (1).

Hughes, W.J., 1973, The effect of two periodic conductivity anomalies on geomagnetic micropulsation measurements: Geophys. J. Roy. Astr. Soc., v.31, 407-431.

Hughes, W.J., 1974, The polarization of micropulsations and geo-electric structure, Geophys. J. Roy. Astr. Soc., v.38, 95-117.

Hughes, W.J., and Wait, J.R., 1975a, Effective wave tilt and surface impedance over a laterally inhomogeneous two-layer Earth: Radio Science, v.10, 1001-1008.

Hughes, W.J., and Wait, J.R., 1975b, Electromagnetic induction over a two-layer earth with a sinusoidal overburden: Pageoph, v.113, 591-599.

Ikuno, H., and Yasuura, K., 1973, Improved point-matching method with application to scattering from a periodic surface: IEEE Tran. on Antennas and Propagation, v.AP-21, 657-662.

Izadian, J.S., Peters, L., and Richmond, J.H., Computation of scattering from penetrable cylinders with improved numerical efficiency: EM methods in applied geophysics: IEEE Tran. on Geoscience and Remote Sensing, v.GE-22, 52-61.

Jiracek, G.R., 1972, Geophysical studies of electromagnetic scattering from rough surfaces and from irregularly layered structures: unpublished Ph.D. Thesis, Univ. of California, Berkeley.

Jiracek, G.R., 1973, Numerical comparisons of a modified Rayleigh approach with other rough surface EM scattering solutions: IEEE Trans. on Antennas and Propagation, 393-396.

Jiracek, G.R., Reddig, R.P., and Kojima, R.K., 1986, Application of the Rayleigh-FFT technique to magnetotelluric modelling and correction: Physics of Earth and Planetary Interiors, special issue, 8th induction workshop, Neuchatel, Swizerland.

Johansen, H.K, Sorenson, K., 1979, Fast Hankel transforms: Geophys. Prospecting, v.27, 876-901.

Jones, F.W., 1973, Induction in laterally non-uniform conductors, Theory and numerical models: Physics of Earth and Planetary Interiors, v.7, 282-293.

Jones, F.W., and Price, A.T., 1971, Geomagnetic effects of sloping and shelving discontinuities of earth conductivity: Geophysics, v.36, 58-66.

Jupp, D.L.B., 1978, Estimation of the magnetotelluric impedance functions: Physics Earth and Planetary Interiors, v.17, 75-82.

Kan, T., and Clay, C.S., 1979, Hybrid-ray approximation in electromagnetic sounding: Geophysics, v.44, 1846-1861.

Karlsson, A., 1981, Scattering from inhomogeneities in layered structures: J. Acoust. Soc. Am., v.71, 1083-1092.

Karlsson, A., and Kristensson, G., 1983, Electromagnetic scattering from subterranean obstacles in a stratified ground: Radio Science, v.18, 345-356.

Kartashov, Yu.A., Parantayev, G.V., and Yakhno, Yu.L., 1985, Approximate boundary conditions on quasiplanar conducting layers in geomagnetic and geoelectric problems: Izvestiya, Earth Physics, v.21, 689-692.

Kao, D., and Rankin, D., 1980, Magnetotelluric response on inhomogeneous layered earth: Geophysics, v.45, 1793-1802.

Kauahikaua, J., 1978, Electromagnetic fields about a horizontal electric wire source of arbitrary length: Geophysics, v.43, 1019-1022.

Keceli, A., 1983, The direct method of interpretation in the magnetotelluric method: Geoexploration, v.21, 65-71.

King, W.P., Owens, M., and Wu, T.T., 1986, Properties of lateral electromagnetic fields and their application: Radio Science, v.21, 13-23.

Klem-Musatov, K.D., Klem-Mustava, G.A., 1980, Scattering on a wedge: Sov. Geol. Geophysics, v.21(4), 97-108.

Koefoed, O., 1979, Geosounding Principles, 1: Resistivity sounding measurements: Elsevier Scientific Publishing Co., New York.

Kojima, R.K., 1985, Application of the Raleigh-FFT technique to magnetotelluric modeling: M.S. thesis, San Diego State University, San Diego, California.

Kristensson, G., 1983, The electromagnetic field in a layered earth induced by an arbitrary stationary current distribution: Radio Science, v.18, 357-368.

Kristensson, G., 1984, Influence of inhomogeneites in a stratified ground on the field of a circular loop antenna: EM methods in applied geophysics, IEEE Tran. on Geos. and remote sensing, v.GE-22, 29-33.

Kristensson, G., and Strom, S., 1978, Scattering from buried inhomogeneities - a general three-dimensional formalism: J. Acoust. Soc. Am., v.64, 917-936.

Kristensson, G., and Strom, S., 1982, Electromagnetic scattering from geophysical targets by means of the T-matrix approach: A review of some recent results: Radio Science, v.17, 903-912.

Kristensson, G., and Waterman, P.C., 1982, The T-matrix for acoustic and electromagnetic scattering by circular discs: J. Acoust. Soc. Am., v.72, 1612-1625.

Ku, C.C., Hsieh, M.S., and Lim, S.H., 1973, The topographic effect on EM fields: Can. J. Earth Sci., v.10, 645-656.

Kuznetzov, A.N., 1982, Distorting effects during electromagnetic sounding of horizontally non-uniform media using an artificial field source: Izvestiya, Earth Physics, v.18, 130-137.

Kuznetov, A.N., 1985, The features of an electromagnetic field from multiple-frequency sounding and transient sounding over a horst structure: Izvetiya, Earth Physics, v.21, 524-530.

Lajoie, J.J., Alfonso-Roche, J., and West, G.F., 1975, EM response of an arbitrary source on a layered earth: A new computational approach: Geophysics, v.40, 773-789.

Lajoie, J., and West, G.F., 1976, The electromagnetic response of a conductive inhomogeneity in a layered earth: Geophysics, v.41, 1133-1156.

Lam, H.L., Jones, F.W., and Hibbs, R.D., 1982, The response of perturbation and induction arrows to a three-dimensional buried anomaly: Geophysics, v.47, p51-59.

Langer, R.E., 1962, Electromagnetic waves: University of Wisconsin Press, Madison, Wisconsin.

Lebedev, N.N., 1965, Special functions and their applications: Prentice-Hall Inc., New York.

Lebedev, N.N., and Skal'skaya, I.P., 1963, A new method for solving the problems of diffraction of electromagnetic waves by a wedge with finite conductivity: Sov. Phy. - Tech. Phy., v.7, 867-874.

Lee, K.H., and Morrison, H.F., 1985a, A numerical solution for the electromagnetic scattering by a two-dimensional inhomogeneity, Geophysics, V50, 466-472.

Lee, K.H., and Morrison, H.F., 1985b, A solution for TM-mode plane waves incident on a two-dimensional inhomogeneity: Geophysics, v.50, 1163-1165.

Lee, K.H., Pridmore, D.F., and Morrison, H.F., 1981, A hybrid three-dimensional modeling scheme: Geophysics, v.46, 796-805.

Lee, T., 1983, The transient electromagnetic response of a conducting sphere in an imperfectly conducting half-space: Geophys. Prospecting, v.31, 766-781.

Lee, T., and Lewis, R., 1974, Transient EM response of a large loop on a layered ground: Geophys. Prospecting, v.22, 430-444.

Lienert, B.R., 1980, The effect of source field polarization on estimates of the magnetotelluric impedance tensor: Geophysics, v.45, 1803-1812.

Mahmoud, S.F., Botros, A.Z., and Wait, J.R., 1979, Transient electromagnetic fields of a vertical magnetic dipole on a two-layer earth: Proc. of the IEEE, v.67, 1022-1029.

Mangus, W., Oberhettinger, F., and Soni, R.P., 1966, Formulas and theorems for the special functions of mathematical physics, v.52, Springer-Verlag Publishing Co., New York.

Mann, J.E., 1964, Magnetotelluric theory of the sinusoidal interface: J. G. R., v.69, 3517-3524.

Mann, J.E., 1970, A perturbation technique for solving boundary value problems arising in the electrodynamics of conducting bodies: Appl. Sci. Res., v.22, 113-126.

Mareschal, M., and Vasseur, G., 1984, Bimodel induction in non-uniform thin sheets, do the present algorthms work for regional studies?: J. Geophys., v.55, 203-213.

Martin, S.P., 1982, Computing scattering amplitudes for arbitrary cylinders under incident plane waves: IEEE Tran. on Antennas and Propagation, v.AP-30, 1045-1049.

Maurer, S.J., and Felson, L.B., 1967, Ray-optical techniques for guided waves: Proceedings of the IEEE, v.55, 1718-1729.

McKirdy, D.McA., and Weaver. J.T., 1984, Induction in a thin sheet of variable conductance at the surface of a stratified earth - I. Two dimensional theory: Geophys. J. R. Astr. Soc., v.78, 93-103.

McKirdy, D. McA., Weaver, J.T., and Dawson, T.J., 1985, Induction in a thin sheet of variable conductance at the surface of a stratified earth - II. Three dimensional theory: Geophys. J. Roy. Astr. Soc., v.80, 177-194.

Meixner, J., 1972, The behavior of electromagnetic fields at edges: IEEE Tran. Antennas and Propagation, v.AP-20, 442-446.

Millar, R.F., 1973, The Rayleigh hypothesis and a related least squares solution to scattering problems for periodic surfaces and other scatterers: Radio Science, v.8, 785-796.

Mittra, R., 1973, Computer techniques for electromagnetics: Pergamon, New York.

Mittra, R., and Lee, S.W., 1971, Analytical techniques in the theory of guided waves: Macmillian, New York.

Mohsen, A., 1982, On the asymptotic diffraction of scalar waves by a wedge: J. Phys. A: Math Gen., v.15, 1965-1969.

Nabighian, M.N., Oppliger, G.L., Edwards, R.N., Lot, B.B.H., and Cheesman, S.J., 1984, Cross-hole magnetometric resistivity (MMR): Geophysics, v.49, 1313-1326.

Newman, G.A., Hohmann, G.W., and Anderson, W.L., 1986, Transient electromagnetic response of a three-dimensional body in a layered earth: Geophysics, v.51, p1608-1627.

Ogunade, S.O., and Ramaswamy, V. and Dosso, H.W., 1974, Electromagnetic response of a conducting sphere buried in a conducting earth: J. Geomag. Geoelectr., v.26, 417-427.

Ogunade, S.O., and Dosso, H.W., 1980, The inductive response of a horizontal conducting cylinder buried in a uniform earth for a uniform inducting field: Geophys. Prospecting, v.28, 601-609.

Ogunade S.O., 1981, Electromagnetic response of an embedded cylinder for line current excitation: Geophysics, v.46, 45-52.

Olsson, O., 1978, Scattering of electromagnetic waves by a perfectly conducting half-plane below a stratified overburden: Radio Science, v.13, 391-397.

Olsson, O., 1980, VLF anomalies from a perfectly conducting half-plane below an overburden: Geophys. Prospecting, v.28, 415-434.

Olsson, O., 1983, Computation of VLF response over half-plane and wedge models: Geophys. Prospecting, v.31, 171-191.

Oppenheimer, J.M., 1980a, Gravity modeling of the alluvial basins, southern Arizona: unpublished Master's thesis, University of Arizona, Tucson.

Oppenheimer, J.M., and Sumner, J.S., 1980b, Depth-to-bedrock map, basin and range province, Arizona: Laboratory of Geophysics, University of Arizona, Tucson.

Pao, Y.H., and Varatharajulu, V., 1976, Huygen's principle, radiation conditions, and integral formulas for the scattering of elastic waves: J. Acoust. Soc. Am., v.59, 1361-1371.

Park, S.K., 1985, Distortion of magnetotelluric sounding curves by three-dimensional structures: Geophysics, v.50, 785-797.

Park, S.K., Orange, A.S., and Madden, T.R., 1983, Effects of three-dimensional structure on magnetotelluric sounding curves: Geophysics, v.48, 1402-1405.

Patella, D., 1987, Tutorial interpretation of magnetotelluric measurements over an electrically dispersive one-dimensional earth: Geophys. Prospecting, v.35, p1-11.

Patra, H.P., and Mallick, K., 1980, Geosounding principles, 2: Time varying geoelectric soundings: Elsevier, New York.

Pearson, C.E., 1983, Handbook of applied mathematics, selected methods and results, 2nd ed., Van Nostrand Reinhold Co., New York.

Perkis, C.L., 1940, Direct method of interpretation in resistivity prospecting: Geophysics, v.5, 31-46.

Peterson, B.A., Varadan, V.V., and Varadan, V.K., 1983, T-matrix approach to study the vibrational frequencies of elastic bodies in fluids: J. Acoust. Soc. Am., v.74, 1051-1056.

Poruchikov, V.B., 1981, Exact solutions of three-dimensional problems of the diffraction of plane elastic waves by a wedge: Sov. Phys. Dokl., v.26, 626-627.

Price, A.T., 1949, The induction of electric currents in non-uniform thin sheets and shells: Quart. J. Mech. Appl. Math., v.2, 282-310.

Pridmore, D.F., Hohmann, G.W., Ward, S.H., and Sill, W.R., 1981, An investigation of finite-element modeling for electrical and electromagnetic data in three dimensions: Geophysics, v.46, 1009-1024.

Quon, C., Vozoff, K., Hoversten, M., Morrison, H.F., and Lee, K.H., 1979, Source effects on magnetotelluric apparent resistivities: J. Geophysics, v.46, 291-299.

Raiche, A.P., 1978, Green's functions for modeling the electromagnetic response of a target near a dipping contact: Geophy. J. Roy. Astr. Soc., v.55, 507-511.

Ranganayaki, R.P., and Madden, T.R., 1980, Generalized thin sheet analysis in magnetotellurics: an extension of Price's analysis: Geophys. J. Roy. Astr. Soc., v.60, 445-457.

Rawlins, A.D., 1977, Diffraction by a dielectric wedge: J. Inst. Maths. Applics., v.19, 231-279.

Rayleigh, Lord (J.W. Strutt), 1896, The theory of sound: v.2, 2nd ed., Macmillan, London.

Rayleigh, Lord (J.W. Strutt), 1907, On the dynamical theory of gratings, Proc. Roy. Soc. London, v.A79(532), 399-416.

Reddig, R.P., 1984, Application of the Rayleigh-FFT technique to topographic corrections in magnetotellurics: M.S. Thesis, San Diego State University, San Diego, California.

Reddig, R.P., and Jiracek, G.R., 1984, Topographic modeling and correction in magnetotellurics: Presented at the 54th Ann. Internat. Mtg. Soc. Explor. Geophys.; abstracts and biographies, 44-47.

Reddy, I.K., Rankin, D., and Phillips, R.J., 1977, Three-dimensional modeling in magnetotellurics and magnetic variational sounding, Geophys. J., v.51, 313-326.

Rice, S.O., 1951, Reflection of electromagnetic waves from slightly rough surfaces: in Theory of Electromagnetic Waves, edited by M. Kline, 351-378, Interscience, New York.

Robertson, R.C., 1986, The magnetotelluric field for a two-dimensional Earth modeled by a non-uniform buried thin sheet: IEEE Tran. on Geoscience and Remote Sensing, v.GE-24, 204-211.

Robertson, R.C., 1987, The electromagnetic response of thin sheets buried in a uniformly conducting half-space: Geophysics, v.52, 108-117.

Rosich, R.K., and Wait, J.R., 1977, A general perturbation solution for reflection from two-dimensional periodic surfaces: Radio Science, v.12, 719-729.

San Filipo, W.A., and Hohmann, G.W., 1985, Integral equation solution for the transient electromagnetic response of a three-dimensional body in a conductive half-space: Geophysics, v.50, 798-809.

Sandberg, S.K., and Hohmann, G.W., 1982, Controlled source audiomagnetotellurics in geothermal exploration: Geophysics, v.47, 100-116.

Schegg, P.A., and Fischer, G., 1984, A new pulsed audiomagnetotelluric technique: J. Geophysics, v.55, 191-198.

Schlak, G.A., and Wait, J.R., 1967, Electromagnetic wave propagation over a nonparallel stratified conducting medium: Canadian J. of Physics, v.45, 3697-3720.

Schmucker, U., 1971, Interpretation of induction anomalies above non-uniform surface layers: Geophysics, v.36, 156-165.

Sedelnikov, E.S., 1983, The effects of terrain relief on the field of remote sources of a variable electromagnetic field: Izvestiyia, Earth Physics, v.19, 575-579.

Shaub, Yu.B., and Terentlev, S.A., 1982, Characteristics of the structure of the electromagnetic field due to a stationary and moving linear source: Izvestiya, Earth Physics, v.18, 150-153.

Stefancescu, S.S., 1929, Etudes theoriques sur la prospection electrique du sous-sol: Studii Technice si Economice, v.14, No. 1.

Stefancescu, S.S., 1963, The magnetic field lines of a point electrode in a layered media (in Rumanian): Probleme de Geofizica, v.2, 135-1345, Bucharest.

Stodt, J.A., Hohmann, G.W., and Ting, S.C., 1981, The telluric-magnetotelluric method in two- and three-dimensional environments: Geophysics, v.46, 1137-1147.

Strangway, D.W., Swift, C.M., and Holmer, R.C., 1973, The application of audio-frequency magnetotellurics (AMT) to mineral exploration: Geophysics, v.38, 1159-1175.

Stratton, J.A., 1941, Electromagnetic theory: McGraw-Hill Book Co., New York.

Sumner, J., Jones, G., MacInnes, S., Flaccus, C., and Greenes, K., 1980, A report on geophysical surveys in the Avra Valley area, Pima County, Arizona. unpublished report submitted to U.S.G.S., Tucson, Arizona.

Tabbagh, A., 1985, The response of three-dimensional magnetic and conductive body in shallow depth electromagnetic prospecting: Geophys. J. Roy. Astr. Soc., v.81, p215-230.

Tarlowski, C.Z., Raiche, A.P., and Nabighian, M.N., 1984, The use of summary representation for electromagnetic modeling: Geophysics, v.49, 1506-1516.

Thomson, D.J., and Weaver, J.T., 1975, The complex image approximation for induction in a multilayered earth: J.G.R., v.80, 123-129.

Tygel, M., and Hubral, P., 1984, Transient representation of the Summerfeld-Weyl integral with application to the point source response from a planar acoustic interface: Geophysics, v.49, 1495-1505.

Tsubota, K., and Wait, J.R., 1980, The frequency and time-domain responses of a buried axial conductor: Geophysics, v.45, 941-951.

Uflyand, Y.S., and Yushkova, E.A., 1976, Harmonic fields in a composite truncated wedge: Soviet Phys. Tech. Phy., v.21, 247-250.

Van den Berg, P.M., and Dehoop, A.T., 1984, Reflection and transmission of electromagnetic waves at a rough interface between two different media: IEEE Tran. on Geoscience and Remote Sensing, v.GE-22, 42-51.

Varadan, V.K., Varadan, V.V., and Pao, Y.H., 1978, Multiple scattering of elastic waves by cylinders of arbitrary cross-section I. SH-waves: J. Acoust. Soc. Am., v.63, 1310-1319.

Varadan, V.V., and Varadan, V.K., 1980, Acoustic electromagnetic and elastic wave scattering - focus on the T-matrix approach: Pergamon Press, New York.

Varadan, V.V., and Varadan, V.K., 1981, Configurations with finite numbers of scatterers - a self-consistent T-matrix approach: J. Acoust. Soc. Am., v.70, 213-217.

Varatharajulu, V., and Pao, Y.H., 1976, Scattering matrix for elastic waves: I Theory: J. Acoust. Soc. Am. v.60, 556-567.

Varentsov, I.M., 1983, Modern trends in the solution of forward and inverse 3D electromagnetic induction problems: Geophys. Surveys, v.6, p55-78.

Vasseur, G., and Weidelt, P., 1977, Bimodal electromagnetic induction in non-uniform thin sheets with an application to the northern Pyrenean induction anomaly: Geophys. J. Roy. Astr. Soc., v.51, 669-690.

Villegas-Garcia, C.J., 1979, On the electromagnetic response of non-uniform overburden layers: scale model experiments: Research in Applied Geophysics #10, University of Toronto, Toronto, Canada.

Vozoff, K., 1972, The magnetotelluric method in the exploration of sedimentary basins: Geophysics, v.37, 98-141.

Wait, J.R., 1953, Propagation of radio waves above statified ground: Geophysics, v.18, 416-422.

Wait, J.R., 1954, On the relation between telluric currents and the earth's magnetic field: Geophysics, v.19, 281-289.

Wait, J.R., 1959, Electromagnetic radiation from cylindrical structures, Pergamon Press, Oxford.

Wait, J.R., 1960, On the electromagnetic response of a conducting sphere to a dipole field: Geophysics, v.25, 649-658.

Wait, J.R., 1961, The electromagnetic fields of a horizontal dipole in the presence of a conducting half-space: Can. J. Phys., v.39, 1017-1028.

Wait, J.R., 1966, Fields of a horizontal dipole over a stratified anisotropic half-space: IEEE Tran. on Antennas and Propagation, v.AP-14, 790-792.

Wait, J.R., 1970, Electromagnetic waves in stratified media: Pergamon Press, New York.

Wait, J.R., 1971, Perturbation analysis for reflection from two-dimensional periodic sea waves: Radio Science, v.6, 387-391.

Wait, J.R., 1972, The effect of a buried conductor on the subsurface fields for line source excitation: Radio Science, v.7, 587-591.

Wait, J.R., 1974, A wave-optical field solution for a line source over nonparallel stratified earth: Radio Science, v.9, 593-597.

Wait, J.R., 1977, Multiple scattering between a buried line conductor and the earth's surface: Geophysics, v.42, 1470-1472.

Wait, J.R., 1980a, Electromagnetic surface impedance for a layered earth for general excitation: Radio Science, v.15, 129-134.

Wait, J.R., 1980b, Exact surface impedance for a spherical conductor: Proceedings of the IEEE, v.68, 279-281.

Wait, J.R., 1981, Wave propagation theory: Pergamon Press, New York.

Wait, J.R., 1982, Geo-electromagnetism, Academic Press, New York.

Wait, J.R., 1985, Electromagnetic wave theory: Harper and Row Publishers, New York.

Wait, J.R., 1986, Introduction to Antennas and Propagation: Peter Peregrinus Ltd., London, United Kingdom.

Wait, J.R., and Chang, D.C., 1976, Theory of electromagnetic scattering from a layered medium with a laterally varying substrate: Radio Science, v.11, 221-229.

Wait, .J.R., and Hill, D.A., 1973, Excitation of a homogeneous conductive cylinder of finite length by a prescribed axial current distribution: Radio Science, v.8, 1169-1176.

Wait, J.R., and Hill, D.A., 1980, Fields of a horizontal loop of arbitrary shape buried in a two-layer earth: Radio Science, v.15, 903-912.

Wait, J.R., and Spies, K.P., 1973a, Range dependence of the surface impedance and wave tilt for a line-source excited two-layer earth: IEEE Tran. on Antennas and Propagation, v.AP-21, 905-907.

Wait, J.R., and Spies, K.P., 1973b, Source-to-observer distance dependance of the surface impedance and wave tilt for a line-source excited two-layer earth: Off. U.S. Naval Res. Tech. Rep. No. 6, NA-ONR-15-71, (4 Sept. 1973) [available from U.S. Dept. Comm. Natl. Tech. Inf. Service under AD767089].

Wait, J.R., and Spies, K.P., 1974, Magnetotelluric fields for a segmented overburden: J. Geomag. Geoelectr., v.26, 449-458.

Wannamaker, P.E., Hohmann, G.W., and San Filipo, W.A., 1984, Electromagnetic modeling of three-dimensional bodies in layered earths using integral equations: Geophysics, v.49, 60-74.

Wannamaker, P.E., Stodt, J.A., and Rijo, L., 1986, Two-dimensional topographic responses in magnetotellurics modeled using finite elements, Geophysics, v.51, 2131-2144.

Ward, S.H., 1983, Controlled source electrical methods for deep exploration: Geophys. Survey, v.6, 137-152.

Waterman, P.C., 1969, New formulation of acoustic scattering: J. Acoust. Soc. Am., v.45, 1417-1429.

Waterman, P.C., 1975, Scattering by periodic surfaces: J. Acoust. Soc. Am., v.57, 791-802.

Waterman, P.C., 1976, Matrix theory of elastic wave scattering: J. Acoust. Soc. Am. v.60, 567-580.

Weaver, J.T., 1970, The general theory of electromagnetic induction in a conducting half-space: Geophys. J. Roy. Astr. Soc., v.22, 83-100.

Weaver, J.T., 1973, Induction in a layered plane-earth by uniform and non-uniform sources: Physics of Earth and Planetary Interiors, v.7, 266-281.

Weaver , J.T., Le Quang, B.V., and Fischer, G., 1985, A comparison of analytical and numerical results for a two-dimensional control model in electromagnetic induction-I. B-polarization calculations: Geophys. J. Roy. Astr. Soc., v.82, 263-277.

Weaver, J.T., LeQuang, B.V., Fischer, G., 1986, A comparison of analytical and numerical results for a two-dimensional control model in electromagnetic induction - II. E - polarization calculations: Geophy. J. Roy. Astr. Soc., v.87, 917-948.

Weidelt, P., 1971, The electromagnetic induction in two thin half-sheets: Z. Geophys., v.37, 649-665.

Weidelt, P., 1975, Electromagnetic induction in three-dimensional structures, Geophysics, v.41, 85-109.

Weidelt, P., 1983, The harmonic and transient EM response of a thin dipping dike: Geophysics, v.48, 934-952.

Weyl, 1919, Ausbreitung elektromagnetischer Wellen uber einem ebenen Leiter: Ann. Physik, v.60, 481-500.

Zonge, K.L., Ostrander, A.G., and Emer, D.F., 1980, Controlled source audio-magnetotelluric measurements, Technical Papers, 50th Ann. Internat. Soc. Explor. Geophys. Mtg. and Exhibition, v.5, 2491-2521.